

**THEORETICAL AND MASS SPECTROMETRIC STUDIES OF N-
HETEROCYCLIC COMPOUNDS AND THEIR ROLES IN REACTIONS**

by

YUAN TIAN

A Dissertation submitted to the

Graduate School-New Brunswick

Rutgers, The State University of New Jersey

in partial fulfillment of the requirements

For the degree of

Doctor of Philosophy

Graduate Program in Chemistry and Chemical Biology

Written under the direction of

Professor Jeehiun K. Lee

And approved by

New Brunswick, New Jersey

[OCTOBER 2015]

ABSTRACT OF THE DISSERTATION

THEORETICAL AND MASS SPECTROMETRIC STUDIES OF N-HETEROCYCLIC COMPOUNDS AND THEIR ROLE IN REACTIONS

By YUAN TIAN

Dissertation Director:

Professor Jeehiun K. Lee

This dissertation focuses on the gas phase properties and reactivity of two types of N-heterocyclic compounds: N-heterocyclic carbenes (NHCs) and nucleobase derivatives.

Imidazole-2-ylidene and imidazolidin-2-ylidene are stabilized carbenes widely applied in organometallics and organocatalysis. The only structural difference between the two is the degree of unsaturation on their heterocyclic backbone. Imidazole-2-ylidene is unsaturated (denoted as unsatNHCs) while imidazolidin-2-ylidene is saturated (denoted as satNHC). Our studies focused on the proton affinities comparison between unsatNHCs and satNHCs. The results indicate that satNHCs are more basic than their unsaturated counterparts. They are both more basic than the first generation Grubbs catalyst ligand tricyclohexylphosphine.

N-Heterocyclic carbenes (NHCs) catalyze Umpolung condensation reactions of carbonyl compounds, including the benzoin condensation and Stetter reaction. These

types of reactions have not been examined in the gas phase. We explored the feasibility of examining these reactions in the absence of solvent. Charge-tagged thiazolylidene catalysts were used to track the reactions by mass spectrometry. We found that the addition of the NHC catalysts to a carbonyl compound to form the "Breslow intermediate" can only be accessed by introducing acylsilanes, which takes advantage of Brook rearrangement. The second step addition, with another aldehyde or a Michael acceptor, does not occur under our gas phase conditions. The differential reactivity between the condensed and gas phases was discussed.

A light-responsive NHC was to have different electronic properties between its two isomers. We conducted a series of molecular orbital calculations to clarify the electronic structure difference between the two isomers.

The DNA glycosylase MutY repairs the DNA damage by removing adenine from mismatched adenine:8-oxoguanine base pair. To help understand the mechanism of MutY, gas phase proton affinities and acidities of four MutY substrates were measured. The measurement matches calculated values by our group. The tautomerization of protonated 6-methyl-1-deazaadenine was also discussed.

It is hypothesized that nicotinamide adenine dinucleotide (NAD^+) can initiate *in vitro* DNA transcription catalyzed by *E.coli* RNA polymerase (RNAP). To prove this hypothesis, a mixture of DNA template, *E.coli* RNAP, CTP and NAD^+ were made, aiming to find the 5'- NAD^+ modified RNA sequence NAD^+pC . An LC-MS method was developed to analyze NAD^+pC .

DEDICATION

To my parents, Xuelong Tian and Binglian Zhu, for their love.

ACKNOWLEDGEMENTS

First, I would like to express my deepest appreciation to my research advisor Dr. Jeehiun K. Lee, for her mentoring and support during my graduate career. She not only provides guidance to my research, but also taught me how to face difficulties and pressure.

I would like to thank my colleagues in Lee group, Dr. Min Liu, Dr. Anna Michelson, Dr. Mu Chen, Dr. Kai Wang, Dr. Landon Greene, Sisi Zhang, Hao Zeng and Yijie Niu for their great help to my research and the profound friendship. I would like to thank Yijie Niu especially for his encouragement during 2014 to 2015, the most stressful time during the last five years. Thanks to Dr. Alexei Ermakov for his wonderful expertise on mass spectrometry.

I also want to thank my committee members Dr. Ralf Warmuth, Dr. Karsten Krogh-Jespersen and Dr. Brian Buckley for their valuable time, attention and help for my research.

I would like to thank Dr. Brian Buckley and Dr. Ill Yang at EOHSI of Rutgers for their precious instrument time. I would also like to thank our collaborators Dr. Bryce Nickels from Rutgers University and Dr. Christopher W. Bielawski from University of Texas at Austin.

Last but not least, I want to thank my family and all my friends to their love and support.

TABLE OF CONTENTS

ABSTRACT OF THE DISSERTATION	ii
DEDICATION.....	iv
ACKNOWLEDGEMENTS	v
TABLE OF CONTENTS	vi
LIST OF FIGURES	x
LIST OF TABLES	xiv
Chapter 1 Introduction.....	1
1.1 Overview.....	1
1.1.1 N-heterocyclic carbenes	1
1.1.2 Damaged nucleobase and DNA repair	4
1.1.3 DNA transcription initiation.....	6
1.2 Instrumentation	8
1.2.1 Electrospray ion source (ESI)	8
1.2.2 Quadrupole and ion trap mass spectrometry	8
1.2.3 Fourier transform ion cyclotron resonance mass spectrometry (FT-ICR)	11
1.3 Methodology.....	14
1.3.1 Gas phase reactions	14
1.3.2 Bracketing method	14
1.3.3 Cooks kinetic method.....	16
1.3.4 Computational method	17
Chapter 2 Characterization of N-heterocyclic Carbenes – Saturated Vs.	
Unsaturated Rings	18

2.1. Introduction	18
2.2. Experimental section	21
2.2.1. NHC preparation	21
2.2.2. LCQ bracketing	22
2.2.3. Hetero dimer dissociation experiments	23
2.2.4. Calculation	23
2.3. Results and discussion	23
2.3.1 Calculations for Carbene Site.....	23
2.3.2 Proton Affinity Measurement by Bracketing Method.....	24
2.3.3 Proton Affinity Comparison Between unsaturated carbene 1 and the saturated counterpart 2 by proton bond heterodimer dissociation experiment	27
2.3.4 Carbene-phosphine Complex Dissociation	28
2.4. Conclusion	33
 Chapter 3 Gas Phase Stetter Reaction catalyzed by Charged Handle Thiazolium	
Catalysts.....	34
3.1. Introduction	34
3.2. Experimental section	37
3.2.1 Gas phase reaction monitoring	37
3.2.2 Calculation	38
3.3. Results and discussion	38
3.3.1 Preparation of charge handle thiazolium pre-catalyst	38
3.3.2 Formation of Breslow intermediate.....	39
3.3.3 Second step addition.....	45
3.3.3 Calculation results	48
3.4. Conclusion	55

Chapter 4 Computational Study of Photoswitchable Carbenes	56
4.1 Introduction	56
4.2. Computational Methods.....	57
4.3. Results and disscussion	58
4.3.1 ¹³ C NMR of photoswitchable carbenes	58
4.3.2 Molecular orbitals of photoswitchable carbenes	58
4.4. Conclusion	61
 Chapter 5 Gas Phase Studies of Adenine Analogs: Implications for Adenine	
Removal by MutY	62
5.1. Introduction	62
5.2. Experimental section	63
5.2.1 Bracketing method	64
5.2.2 Cook's kinetic method	64
5.2.3 Calculations.....	64
5.3. Results.....	64
5.3.1 Calculation of MutY substrates proton affinities and acidities	65
5.3.2 7-Deazaadenine (Z, 1) measurements	66
5.3.3 1-Deazaadenine (Z1, 2) measurements	67
5.3.4 "6-Methylated" 1,3-Deazaadenine (B, 3).....	68
5.3.5 "6-Methylated" 1-Deazaadenine (Q, 4) measurement	69
5.4. Discussion	71
5.5. Conclusions	77
 Chapter 6 Identification Of Key Species In the <i>In-vitro</i> DNA Transcription via	
HPLC-MS/MS	78
6.1. Introduction	78

6.2 Experimental section	80
6.2.1 experiment materials and instrumental specification	80
6.2.2 sample preparation protocol (from Dr. Jeremy Bird).....	81
6.2.3 sample analysis protocol	81
6.3 Results and discussion	83
6.3.1 Fragmentation of NAD ⁺ and CTP	83
6.3.2 LC-UV analysis of CTP standard, NAD standard, and transcription reaction samples.....	85
6.3.3 LC-MS/MS of CTP standard, NAD standard, and transcription reaction samples	87
6.4 Conclusion	93
References	94

LIST OF FIGURES

Figure 1.1 various N-heterocyclic carbene backbones	1
Figure 1.2 The electronic structure of ground state NHC.....	2
Figure 1.3 First-generation (left) and second-generation (right) Grubbs catalyst.	2
Figure 1.4 Examples of NHC attack on carbonyl groups	3
Figure 1.5 Base pairs in DNA.....	5
Figure 1.6 Base excision by DNA glycosylase via stepwise S _N 1 type reaction	6
Figure 1.7 DNA transcription process.	7
Figure 1.8 Process of electrospray ionization (adapted from ref ³⁷).....	8
Figure 1.9 Quadrupole with hyperbolic rods	9
Figure 1.10 Ion trap diagram	10
Figure 1.11 The house-made leak valves on the He buffer gas line	10
Figure 1.12 Diagram of an ion cyclotron resonance instrument.....	12
Figure 1.13 Finnigan 2001 FT/MS duel cell setup	12
Figure 1.14 Ion transfer process in Finnigan 2001 FT/MS duel cell	13
Figure 2.1 The TEP (ν_{co}) of phosphine compounds and NHCs.....	19
Figure 2.2 NHCs studied in this chapter.	19
Figure 2.3 Structures of carbene-phosphine complexes studied herein.....	28
Figure 3.1 Breslow mechanism of benzoin condensation (right) and the mechanism of Stetter reaction (left) proposed according to Breslow mechanism	25
Figure 3.2 Dimer mechanisms of Benzoin condensation. Blue: proposed by Lemal; Red: proposed by Castells.	36
Figure 3.3 Charge handle thiazolyliidines and carbonyl substrates used in this study	40

Figure 3.4 Substrates used to test the second step addition	45
Figure 3.5 The energy profile of the simulated gas phase Stetter reactions shown in Scheme 3.8. Calculations were conducted at B3LYP/6-31+G(d) [ΔH at 298 K in kcal mol ⁻¹].	49
Figure 3.6 The energy profile of the formation of (silyl)Breslow intermediates via 1a. (Corresponding to Scheme 3.9) Calculations were conducted at B3LYP/6-31+G(d) [ΔH at 298 K in kcal mol ⁻¹].	51
Figure 3.7 Proton affinity of thiazolium carbene site.	51
Figure 3.8 The energy profile of second step Michael addition. Red: silyl Stetter reaction. Blue: normal Stetter reaction. Calculations were conducted at B3LYP/6-31+G(d) [ΔH at 298 K in kcal mol ⁻¹].	52
Figure 3.9 Possible pathways for the sila-Stetter. [1,4] O to C trimethylsilyl migration is in red and [1,6] O to O trimethylsilyl migration is in blue. Transition structures for the [1,4] and [1,6] migrations were not calculated. Calculations were conducted at B3LYP/6-31+G(d) [ΔH at 298 K in kcal mol ⁻¹].	54
Figure 4.1 Photoswitchable carbene switching between two forms by UV or visible light	57
Figure 4.2 model photoswitchable carbene studied herein	58
Figure 4.3 HOMO (bottom) and LUMO (top) visualization of Me _o and ring-closed analogue Me _c . Molecular orbitals were generated with an isovalue of 0.02.	60
Figure 4.4 HOMO (bottom) and LUMO (top) visualization of Ar _o and ring-closed analogue Ar _c . Molecular orbitals were generated with an isovalue of 0.02.	60
Figure 5.1 The normal G:C base pair and the mismatch OC:A base pair	62

Figure 5.2 Adenine and synthetic analogs studied herein.....	63
Figure 5.3 The most stable tautomers of MutY substrates and the thermodynamic values. Proton affinities are labeled in blue; acidities in red. The most basic sites and most acidic sites are in bold.....	65
Figure 5.4 Structures of 4a, 4b, 4aH ⁺ , and 4bH ⁺ and calculated proton affinities. Relative stabilities of the two neutral tautomers are shown in parentheses. Calculations were conducted at B3LYP/6-31+G(d) [ΔH at 298 K in kcal mol ⁻¹].....	73
Figure 5.5 Structure of deprotonated 4a and 4b and calculated acidities. Calculations were conducted at B3LYP/6-31+G(d) [ΔH at 298 K in kcal mol ⁻¹].....	74
Figure 5.6 Structures of 4a and 4b and calculated acidity of the most acidic site. Relative stabilities of the two neutral tautomers are shown in parentheses. Calculations were conducted at B3LYP/6-31+G(d) [ΔH at 298 K in kcal mol ⁻¹].....	75
Figure 5.7 Reaction coordinate for the base-catalyzed tautomerization of 4b to 4a. Values in red are B3LYP/6-31+G(d) calculated ΔH_{acid} values (298 K).	76
Figure 6.1 Chemical structure of nicotinamide adenine dinucleotide. Left: oxidized form; Right: reduced form.	78
Figure 6.2 Chemical structure of NAD ⁺ pC.....	79
Figure 6.3 Fragmentation of NAD ⁺ in positive mode.....	84
Figure 6.4 Fragmentation of (NAD ⁺ -2H) ⁻ in negative mode.....	84
Figure 6.5 Fragmentation of (CTP-H) ⁻ in positive mode.....	85
Figure 6.6 LC-UV chromatograms of NAD ⁺ (top) and CTP (bottom) standards.	86

Figure 6.7 LC-UV chromatograms of four samples. Red: Sample 1. experimental; Green: Sample 2. control (no NAD ⁺); Purple: Sample 3. control (no CTP); Black: Sample 4. control (no RNA polymerase).....	86
Figure 6.8 The injection vs. peak area linearity for NAD ⁺ (left) and CTP (right). The trend lines were generated without the outlier (40 pmol injection).	87
Figure 6.9 CID of <i>m/z</i> 967 detected in sample 1(experimental).....	88
Figure 6.10 LC-MS/MS chromatograms of sample 1 (experimental). Top: analysis of NAD ⁺ pC, isolating <i>m/z</i> 967, detecting <i>m/z</i> 845; Middle: analysis of CTP, isolating <i>m/z</i> 482, detecting <i>m/z</i> 384; Bottom: analysis of NAD ⁺ pC, isolating <i>m/z</i> 662, detecting <i>m/z</i> 540	90
Figure 6.11 LC-MS/MS chromatograms of sample 2 (control, no CTP). Top: analysis of NAD ⁺ pC, isolating <i>m/z</i> 967, detecting <i>m/z</i> 845; Middle: analysis of CTP, isolating <i>m/z</i> 482, detecting <i>m/z</i> 384; Bottom: analysis of NAD ⁺ pC, isolating <i>m/z</i> 662, detecting <i>m/z</i> 540.	91
Figure 6.12 LC-MS/MS chromatograms of sample 3 (control, no NAD ⁺). Top: analysis of NAD ⁺ pC, isolating <i>m/z</i> 967, detecting <i>m/z</i> 845; Middle: analysis of CTP, isolating <i>m/z</i> 482, detecting <i>m/z</i> 384; Bottom: analysis of NAD ⁺ pC, isolating <i>m/z</i> 662, detecting <i>m/z</i> 540.	92
Figure 6.13 LC-MS/MS chromatograms of sample 4 (control, no RNA polymerase). Top: analysis of NAD ⁺ pC, isolating <i>m/z</i> 967, detecting <i>m/z</i> 845; Middle: analysis of CTP, isolating <i>m/z</i> 482, detecting <i>m/z</i> 384; Bottom: analysis of NAD ⁺ pC, isolating <i>m/z</i> 662, detecting <i>m/z</i> 540.	93

LIST OF TABLES

Table 1.1 Examples of DNA glycosylases and their substrates ^{25,26}	6
Table 2.1 Computation results of NHCs gas phase proton affinities ^a	24
Table 2.2 Summary of results for PA bracketing of more basic site of 1a	24
Table 2.3 Summary of results for PA bracketing of more basic site of 1b	25
Table 2.4 Summary of results for PA bracketing of more basic site of 2a	26
Table 2.5 Summary of results for PA bracketing of more basic site of 2b	26
Table 3.1 Observations of thiazoylidene catalysts plus benzaldehyde	41
Table 3.2 Observations of thiazoylidene catalysts plus benzoyltrimethylsilane	44
Table 3.3 Silyl Breslow intermediates nucleophilic attack to the Michael acceptors/aldehydes	46
Table 4.1 HOMO/LUMO Coefficient of Carbenic Carbon	59
Table 5.1 Summary of results for acidity bracketing of Z (7-deazaadenine, 1)	66
Table 5.2 Summary of results for proton affinity bracketing of Z (7-deazaadenine, 1) ...	67
Table 5.3 Summary of Results for Acidity Bracketing of B (3)	68
Table 5.4 Summary of Results for Proton Affinity Bracketing of B (3)	69
Table 5.5 Summary of results for acidity bracketing of Q (4)	70
Table 5.6 Summary of results for proton affinity bracketing of Q (4)	70
Table 5.7 Calculated (B3LYP/6-31+G(d); 298 K) and experimental data	71
Table 5.8 <i>Hypothetical</i> bracketing table if only 4a were present	72
Table 6.1 <i>in vitro</i> reactions to test the NAD ⁺ initiation hypothesis	79
Table 6.2 HPLC method used in separating samples	82
Table 6.3 Typical ESI-MS/MS condition used in this project	82

Table 6.4 Intensities of NAD ⁺ and CTP in different ion modes	83
--	----

Chapter 1 Introduction

1.1 Overview

Mass spectrometry, as a powerful tool to study charged species, is widely used in identification and quantification of molecules in simple and complex mixtures.¹⁻⁶ Monitoring ion molecule reactions in the gas phase by mass spectrometry and by computation, we investigated intrinsic properties and reactivity of N-heterocyclic compounds. We also analyzed species in a complex biological sample.

1.1.1 N-heterocyclic carbenes

Since the successful isolation and characterization by Arduengo *et al.* in 1991,⁷ N-heterocyclic carbenes (NHCs), a group of stabilized carbene species, have received much attention.⁸⁻¹⁰ With different degrees of unsaturation, heteroatom stabilization, substitution, and ring size, NHCs have great structural variations (Figure 1.1). NHCs are considered as singlet ground state. The sp^2 like carbenic carbon has a lone pair and an empty p orbital. This electronic configuration is stabilized by the nitrogen atom(s) adjacent to it, as their π -electrons donate to the empty p orbital. In addition, the ring structure forces the carbenic carbon to adopt a more bent orbital shape, which favors the singlet state. (Figure 1.2) Taking Arduengo's 1,3-di-1-adamantyl-imiazol-2-ylidene as an example, the N-C-N angle at carbene center is 102.2° , quite close to that of the typical singlet carbene without constrains.¹¹

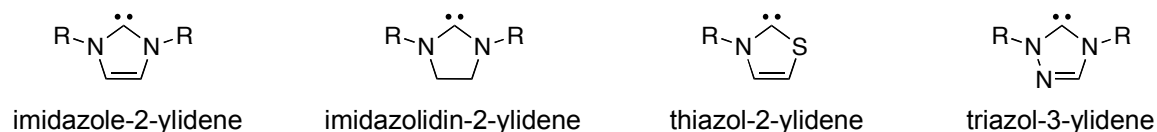


Figure 1.1 various N-heterocyclic carbene backbones

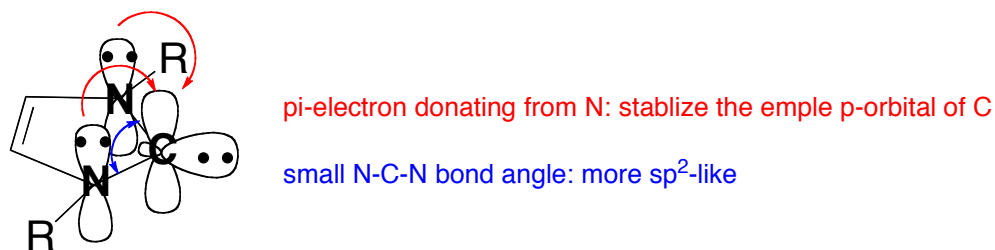


Figure 1.2 The electronic structure of ground state NHC

The singlet state nature makes NHCs a good sigma donor. The rich chemistry of the nucleophilic lone pair and its relatively high stability led to an explosion of NHC application in coordination chemistry and organocatalysis,¹²⁻²² both theoretically and experimentally. One of the most noticeable applications of NHCs in organometallics is the second-generation Grubbs catalyst. The first generation Grubbs catalyst utilized tricyclohexylphosphine as ligand, while the second generation used a bulky imidazolidin-2-ylidene. (Figure 1.3) Compared to the first-generation, the NHC-coordinated catalyst shows excellent air and water resistance and higher catalytic ability on olefin metathesis.^{23,24} Later on, more ruthenium-based heterocyclic carbene-coordinated metathesis catalysts were synthesized and studied.²⁵ Because NHCs and phosphines are both used in Grubbs catalysts, many studies have been done towards the comparison between them. The reasons for the increased activity of second-generation catalyst have also been under debate for years.

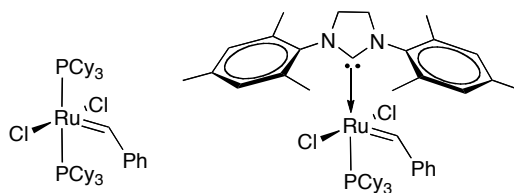


Figure 1.3 First-generation (left) and second-generation (right) Grubbs catalyst.

In addition to the role of ligands, NHCs themselves can catalyze a variety of organic transformations. In most case, the catalysis involves an attack of the NHC on a carbonyl group.²⁶ (Figure 1.4) One rapidly growing group of reactions is the NHC catalyzed umpolung reaction. First, the nucleophilic carbene attacks an aldehyde, and then this tetrahedral intermediate isomerizes to an enamine via proton transfer. This process converts the initial electrophilic carbonyl group to a nucleophilic double bond, which can further react with other substrates.

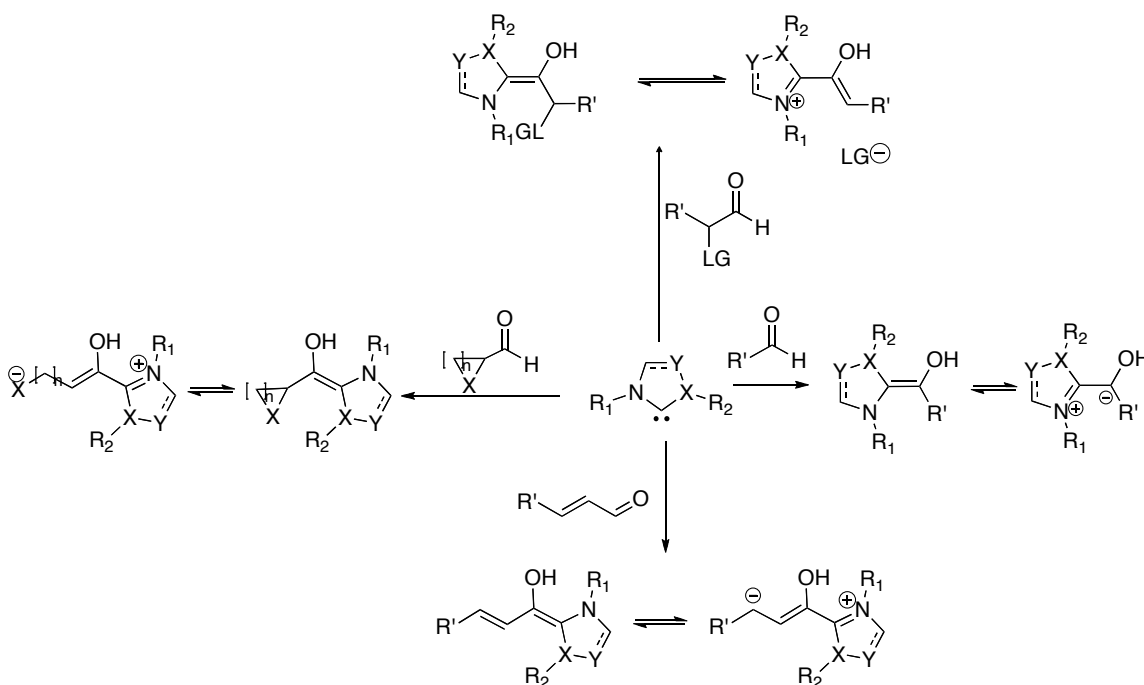


Figure 1.4 Examples of NHC attack on carbonyl groups

Recently, NHCs have also demonstrated great potential in CO₂ fixation. The electron lone pair attacks CO₂ to form NHC-CO₂ adducts, which can be used in carboxylate reactions.^{27,28} NHCs' protonated analogues, imidazoli(ni)ums, with low vapor pressure and biomass solubility, are widely used as room temperature ionic liquids.^{29,30} Due to their wide applications, the properties of NHCs are subject to study.²²

Most studies focus on the structure-property relationship and the modulation of carbene properties via steric and electronic modification. The studies are mainly conducted in the condensed phase, where solvation plays an important role. However the gas phase exploration is still limited. Due to the high vacuum environment in the gas phase, we can easily obtain the intrinsic properties of the subject. The gas phase data is a significant supplement to the solution phase studies. At the same time, by comparing the measurements in the gas phase and that in the solution phase, we can also better understand the effect of solvents. We are interested in the gas phase behavior of NHCs and their related reactions. The gas phase proton affinities of a series NHCs were examined (Chapter 2) and the gas phase NHC reactions were explored (Chapter 3) herein. Chapter 4 discusses the structure-nucleophilicity relationship of a photoswitchable NHC.

1.1.2 Damaged nucleobase and DNA repair

The double helix DNA encodes the genetic information using nucleotide sequences. As in Figure 1.5, the bases in nucleotides pair up in specific hydrogen bonding patterns. This complementary nature provides a precise mechanism of duplication and transcription. In organisms, spontaneous decay, environmental chemicals, and radiation may cause oxidation, deamination and alkylation of nucleobases. The consequent base pair mismatch leads to genetic information variation or loss. Sometimes the lesion can be fatal. Organisms thus developed a base excision repair (BER) mechanism to correct such DNA damage.

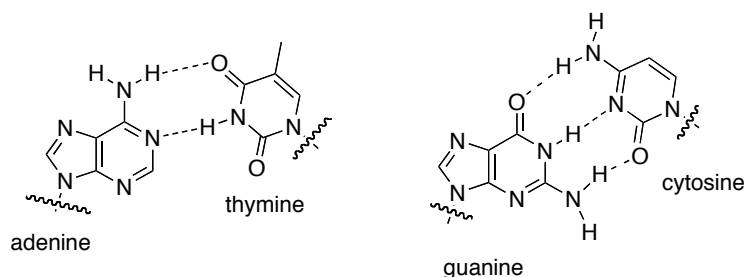


Figure 1.5 Base pairs in DNA

The discovery of BER dates back to 1974, when Thomas Lindahl found an enzyme (DNA glycosylase) that cleaves the bond between the nucleobase and the deoxyribose via hydrolysis.³¹ The resulting abasic site was then processed by the AP endonuclease that cleaves DNA at base-free sugar-phosphate residues. One of the key steps of BER is the initial damage recognition and base excision by DNA glycosylases. Several DNA glycosylase has been discovered, that cleave a wide variety of damaged bases. (Table 1.1) The kinetic isotope effect studies indicate that the hydrolysis is an S_N1 type reaction.³² The nucleobase leaves to yield an oxocarbenium ion, which is then attacked by water. (Figure 1.6) The leaving group ability of the nucleobase thus plays an important role in the excision rate. During the reaction, the leaving group ability of the nucleobase can be enhanced by protonation or hydrogen bonding with acidic residue or water molecule in the active site of the enzyme. Therefore, the acidity and basicity of the base and damaged base becomes an interesting topic. It helps to understand the enzyme-substrate recognition as well as the reaction mechanism.

Although the enzyme catalyzed reaction happens in water, the glycosylase binding pocket is hydrophobic. The gas phase provides an excellent nonpolar environment: the solvent effect is completely excluded. The examination of properties in the gas phase reveals the intrinsic reactivity of the substrates that can be correlated to

activity in the hydrophobic active sites. In Chapter 5, a series of MutY substrates are studied in the gas phase by measuring their acidity and proton affinity. The studies support a hypothesized mechanism of MutY.

Table 1.1 Examples of DNA glycosylases and their substrates^{33,34}

DNA Glycosylases	Substrates
AlkA, Mag1, MPG	3-meA, hypoxanthine
UDG, Ung1, UNG	uracil
Fpg, Ogg1, hOGG1	8-oxoG, FapyG
Nth, Nei	FapyG, urea, hoU, hoC, Tg
MutY, hMYH	A:8-oxoG

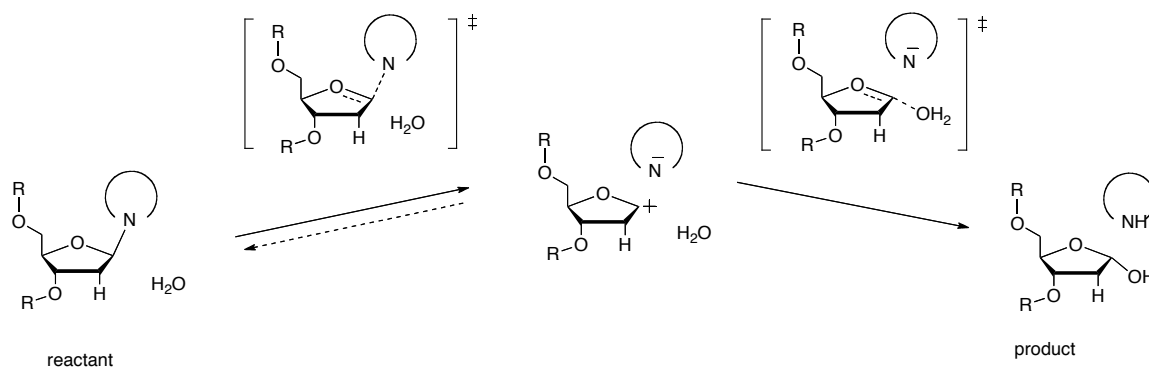


Figure 1.6 Base excision by DNA glycosylase via stepwise S_N1 type reaction

1.1.3 DNA transcription initiation

DNA transcription is the process in which messenger RNA (mRNA) is synthesized using one strand of the DNA double helix as the template. Therefore the genetic information is copied from DNA to mRNA. The whole process can be described in four steps. (Figure 1.7) First, the RNA polymerase (RNAP) binds to the promoter

DNA, unwinding the helix; then the transcription is initiated by using or synthesizing a short piece of RNA segment; after that, the RNA chain elongates until RNAP meets the terminator DNA.

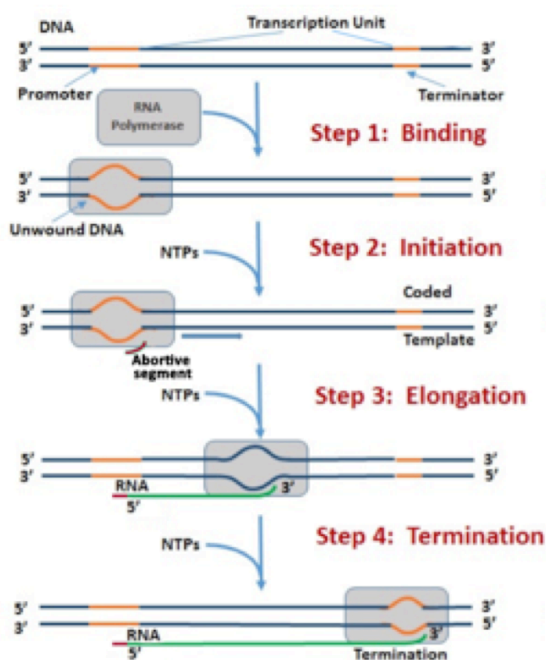


Figure 1.7 DNA transcription process.

It is proposed that the initiation step involves an abortive segment, which will be removed by other enzymes after the transcription process.³⁵ Our collaborator Dr. Bryce Nickels and his coworkers have detected the abortive transcripts *in vivo*. They recently proposed some biomolecules that can function as abortive segments in the *in-vitro* transcription reaction. In order to test their proposal, it is significant to develop a method to analyze the key species in the transcription reaction.

The coupling of HPLC and tandem mass spectrometry is a powerful tool that can separate and analyze components in a complex system. In Chapter 6, a quick HPLC-MS method for small biomolecules identification is described.

1.2 Instrumentation

1.2.1 Electrospray ion source (ESI)

The electrospray ion source (ESI) as a “soft” ion source, produces protonated molecular ions $(M + zH)^{z+}$ or deprotonated molecular ions $(M - zH)^{z-}$. (Whereas the hard ion source produces fragment ions that have mass-to-charge ratios less than that of the molecular ions. *e.g.* electron ionization) ESI happens under atmospheric pressure. (Figure 1.8) The liquid passes through a capillary tube, the end of which bears a high electric field. Under the electric field, charges accumulate at the liquid surface at the end of the capillary, and break the liquid into charged droplets. The evaporation of solvent shrinks the droplets and the increasing repelling force breaks the droplets into small ones. After cascades of this process, the solvent is dried out and ions are desorbed from the solvent.³⁶

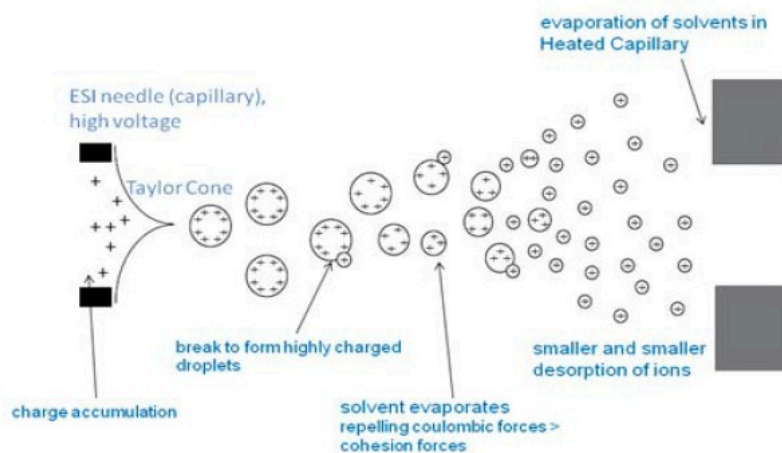


Figure 1.8 Process of electrospray ionization (adapted from ref³⁷)

1.2.2 Quadrupole and ion trap mass spectrometry

The quadrupole analyzes different mass-to-charge ratios using the stability of their trajectories. A quadrupole is made up of four hyperbolic rods (Figure 1.9). The rods next to each other have opposite polarity. An ion entering the region between the rods

will be deflected towards the rods with opposite polarity. A polarity reverse of the potential applied on the rods can change the ion travel direction before it hits the rods and discharges. The potential applied to the rods (ϕ_0) is shown in Eq. 1.1, where U is the direct potential; ω is the angular frequency of the RF field; and V is the “zero to peak” amplitude of the RF voltage. This potential selects ions with different mass-to-charge ratio by stabilizing their trajectories. By changing U linearly as a function of V , different ions are scanned as they can travel through the quadrupole.

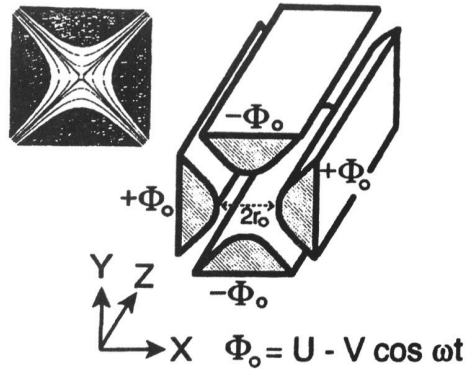


Figure 1.9 Quadrupole with hyperbolic rods

$$\pm\phi_0 = \pm(U - V \cos \omega t) \quad \text{Eq. 1.1}$$

The ion trap is conceptually a bended quadrupole. (Figure 1.10) The inner rod is reduced to a point; the outer rod is the circular electrode and the other two rods are circulated to be top and bottom caps. The ions with different masses are present together in the trap and are expelled according to their masses.

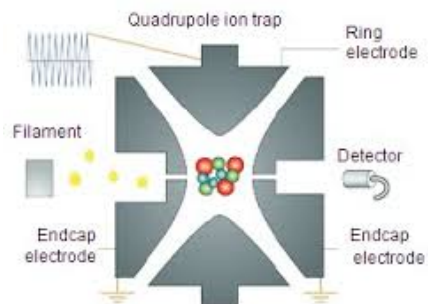


Figure 1.10 Ion trap diagram

Both the linear quadrupole and the ion trap can perform tandem mass, involving multi-stage mass selections and ion fragmentation.

A Finnigan LCQ DUO (ESI-ion trap) and a Finnigan LTQ (ESI-linear quadrupole) were used for Cooks kinetic experiments. A modified Finnigan LCQ instrument was used in bracketing and gas phase reaction experiments. Two leak valves were inserted on the buffering gas line in order to introduce the vapor of neutral compounds into the ion trap. (Figure 1.11) The two inlets can be controlled independently.

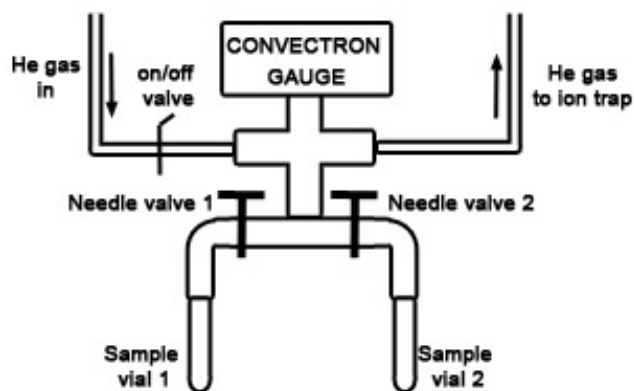


Figure 1.11 The house-made leak valves on the He buffer gas line

1.2.3 Fourier transform ion cyclotron resonance mass spectrometry (FT-ICR)

Fourier transform ion cyclotron resonance mass spectrometry (FT-ICR) analyzes mass-to-charge ratio of ions according to their cyclotron frequency (*viz.* angular velocity ω) in a magnetic field.

An ion injected into a magnetic field B with a velocity v feels the Lorentz force, (Eq. 1.2) which curves the ion trajectory, and the centrifugal force F' on the curved trajectory. (Eq. 1.3)

$$\text{Lorentz force: } \mathbf{F} = q\mathbf{v}B \quad \text{Eq. 1.2}$$

$$\text{Centrifugal force: } \mathbf{F}' = \frac{mv^2}{r} \quad \text{Eq. 1.3}$$

The ion trajectory is stabilized if the two forces are balanced:

$$qvB = \frac{mv^2}{r} \quad \text{Eq. 1.4}$$

Thus, the frequency ω and the m/z of the ion have an inverse proportional relationship, given a certain magnetic field B . (Eq. 1.5)

$$\omega = 2\pi\nu = \frac{v}{r} = \frac{q}{m}B \quad \text{Eq. 1.5}$$

Notice that, although the ion frequency is independent to its velocity, the trajectory radius is proportional to the velocity. By irradiating the ions with an electromagnetic wave that has the same frequency, we can transfer the energy to the ions via resonance absorption, which causes an increase of the trajectory radius. The energy absorbed by the ions can be measured as it correlates to the mass-to-charge ratio of the ions. And as the trajectory radius increases, the resonance ions end up hitting the detector and the resulting current is proportional to the number of ions, which can also be measured. (Figure 1.12)

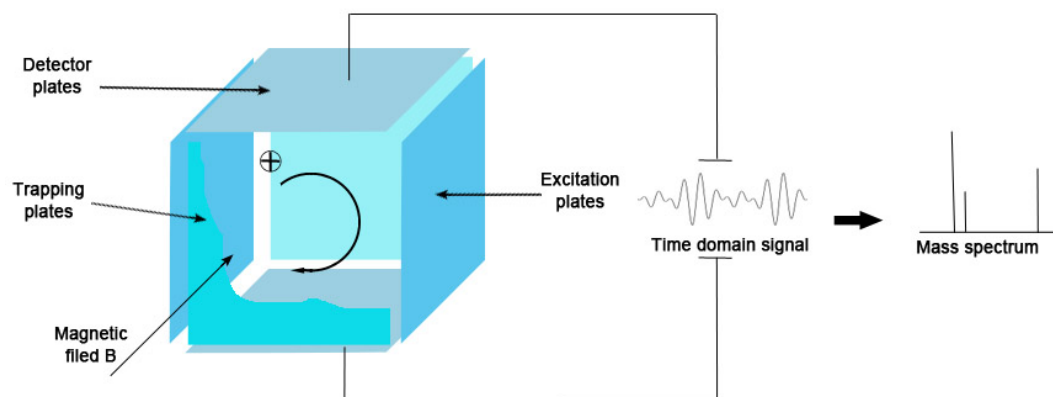


Figure 1.12 Diagram of an ion cyclotron resonance instrument

In particular, our Finnigan 2001 FT/MS instrument has a duel cell setup. (Figure 1.13) The ions are injected in either of the two adjacent 2-inch cubic cells, located in a 3.3 T magnetic field. As required by the Fourier transform technique, a high vacuum (about 10^{-8} psi) was maintained in the instrument.

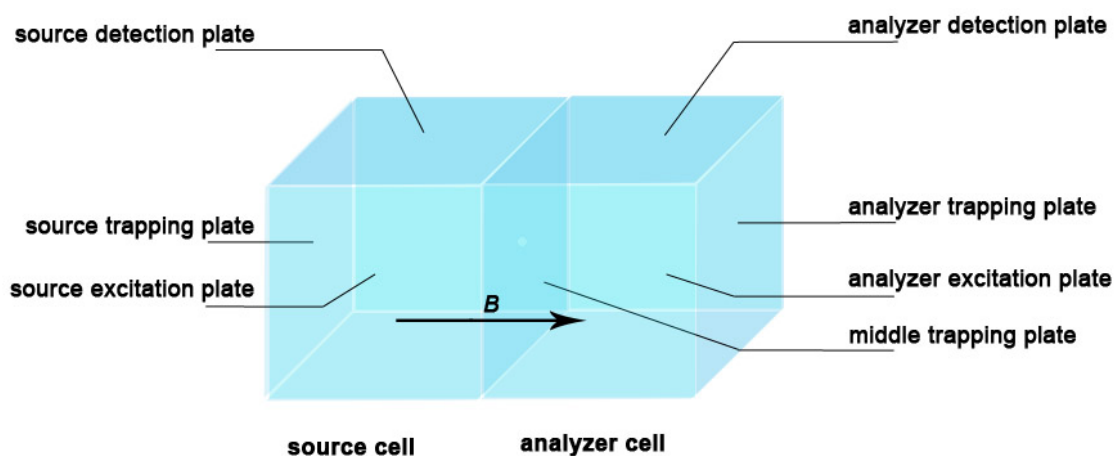


Figure 1.13 Finnigan 2001 FT/MS duel cell setup

In addition to analyzing the ion mass and abundance, it also allows ions to be selected and transferred from one cell to another via the hole on the middle plate. The electron potential of the three trapping plates (source, middle, and analyzer) are E_0 .

(Figure 1.14) During the transfer process, the electron potential of the middle plate is decreased to 0 to form an electron potential well between source and analyzer plates. The ions are allowed to oscillate between the two cells. The oscillation period correlates to the mass-to-charge ratio of the ions. (Eq. 1.6)

By setting the electric potential of the middle plate back to E_0 at time t , the oscillating ions can be partially transferred from one cell to another cell.

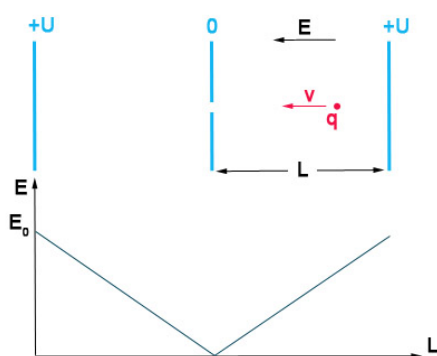


Figure 1.14 Ion transfer process in Finnigan 2001 FT/MS duel cell

$$W = \frac{1}{2} qU$$

$$E_k = \frac{1}{2} mv^2$$

$$W = E_k$$

$$v = at$$

$$F = qE = ma$$

$$\text{Oscillation period: } t = \sqrt{\frac{m}{q}} \sqrt{\frac{U}{E_0^2}} \quad \text{Eq. 1.6}$$

The Finnigan 2001 FT/MS was coupled with a chemical ionization source, in which water is used as the ionizing gas.

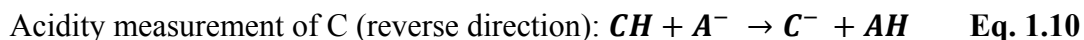
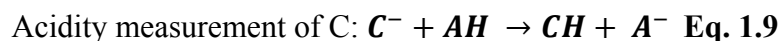
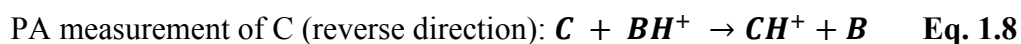
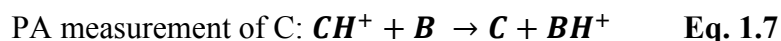
1.3 Methodology

1.3.1 Gas phase reactions

The gas phase reactions were conducted on the modified LCQ mass spectrometer. Charged species are dissolved in solution and introduced into the ion trap via ESI. Neutral substrates were added via leak valves. Reactions were tracked for up to ten seconds. Spectra were recorded as an average of ten scans.

1.3.2 Bracketing method

The bracketing method is used to measure the proton affinity (PA) or acidity of the most basic or acidic site of an analyte. By comparing the thermodynamic property (PA or acidity herein) of the analyte and a series of references, the unknown value can be bracketed in a narrow range. In practice, the proton transfer reactions between the analyte and the reference are monitored by FT-ICR. (Eq. 1.7 to Eq.1.10) The vapor of the neutral analyte was introduced into the source cell, and the vapor of the neutral reference base/acid was introduced into the analyzer cell. To generate compound/reference ions, water was pulsed into the corresponding cell and ionized by an electron beam. The neutral vapor was then protonated/deprotonated by the hydronium/hydroxide. Ions are then transferred from one cell to another as described before and cooled by a pulse of argon. Then the ions are allowed to react with the neutral species in the corresponding cell. The occurrence of proton transfer indicates an exothermic reaction.



The reaction efficiency is defined as the ratio of the reaction rate constant k_{exp} and the theoretical ion-molecule collision rate constant k_{coll} . (Eq. 1.11) k_{coll} is estimated by the ADO program, using parameterized trajectory theory.³⁸⁻⁴² The proton transfer reaction is considered as occurred when the efficiency is larger than 10%.

$$\text{Efficiency, \%} = \frac{k_{exp}}{k_{coll}} \times 100\% \quad \text{Eq. 1.11}$$

The reaction is performed under pseudo-first order conditions. The concentration of neutral species is much higher than the ionic reactant (denotes as $[ion]$ in the equations), thus can be considered as a constant. The rate of the reaction r can be expressed as Eq. 1.12 and Eq. 1.13.

$$r = k[Neutral][ion] = k_{obs}[ion] \quad \text{Eq. 1.12}$$

$$r = -d[ion]/dt \quad \text{Eq. 1.13}$$

Then,

$$\ln[ion]_t - \ln[ion]_0 = -k_{obs}t$$

The k_{obs} can be obtained from the plot of $\ln[ion]$ versus reaction time t . If the concentration of neutral reactant is known, k_{exp} can easily be obtained. We consider a fast reaction between the neutral reactant and hydronium in PA measurement. Because the PA difference between water and any basic compounds is very large, we assume the reaction has theoretical collision rate. Thus $k_{exp}' = k_{coll}'$. Taking the slope of plot of $\ln[H_3O^+]$ versus t , the concentration of the neutral reactant can be calculated by Eq. 1.14.

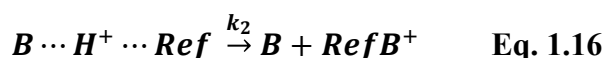
$$[Neutral] = -\text{slope} / k_{coll}' \quad \text{Eq. 1.14}$$

A similar bracketing experiment for PA measurement (Eq. 1.7) can be performed on our modified LCQ instrument. The neutral reference base is introduced into the ion trap from the leak valve and the protonated analyte is introduced from ESI. Instead of

hydronium, a weak base is chosen to measure the neutral reference concentration in the ion trap. The LCQ experiment compensates FT-ICR by handling the non-volatile analyte.

1.3.3 Cooks kinetic method

Cooks kinetic method is also used in PA and acidity measurement on mass spectrometer. This method was first described by Cooks in 1977.⁴³ This method involves the dissociation pattern of a meta-stable proton bound dimer. Taking the PA measurement as an example, the analyte (B) and reference base (Ref) are bounded by a proton. The dissociation of the dimer may undergo two different pathways: Eq. 1.15 and Eq. 1.16.



The rate constant k can be expressed as $k = \frac{RT}{h} \frac{Q^*}{Q} e^{-\epsilon_0/RT}$ Eq. 1.17, where Q is the partition function of the reactant; Q^* is the partition function the activated complex; and ϵ_0 is the activation energy.

$$k = \frac{RT}{h} \frac{Q^*}{Q} e^{-\epsilon_0/RT} \quad \text{Eq. 1.17}$$

Assuming the reverse reaction of dissociation is barrier free and the dimer is symmetric, it is easy to derive the following equation:

$$\ln\left(\frac{k_1}{k_2}\right) = \ln\left(\frac{Q_1^*}{Q_2^*}\right) + \frac{\Delta\epsilon_0}{RT} \cong \ln\left(\frac{\nu_1}{\nu_2}\right) + \frac{\Delta\epsilon_0}{RT} = \frac{PA_B - PA_{ref}}{RT} \quad \text{Eq. 1.18}$$

The ratio of rate constants can be represented by the relative abundance of two ion products. If we plot $\frac{k_1}{k_2}$ versus PA_{ref} , The T_{eff} can be obtained from the slope and PA_B can be obtained from the y-interception and T_{eff} .

The same theory can be applied in acidity measurement, in which the proton bound dimer is negatively charged.

1.3.4 Computational method

The gas phase calculations were used to predict PA/acidity and potential energy surface. All the calculations were conducted using Gaussian09⁴⁴ programs. B3LYP/6-31+G(d) method was chosen. The geometries are fully optimized and the frequencies are calculated. No scaling factor is applied. The gas phase values reported are ΔH at 298K.

Dielectric medium calculations were conducted for chemical shifts prediction. The conductor-like polarizable continuum solvent model (CPCM, full optimization; UKAS cavity) at B3LYP/6-31+G(d) as applied in Gaussian09.⁴⁴

Chapter 2 Characterization of N-heterocyclic Carbenes – Saturated Vs. Unsaturated Rings

2.1. Introduction

As discussed in Chapter 1, applications and properties of N-heterocyclic carbenes are hot topics in recent years. Among various NHC backbones, the imidazole core based NHCs are the earliest reported stable singlet carbenes as well as the most studied ones. Since 1999, when the second-generation Grubbs catalyst was reported, NHCs took the place of the phosphine ligand, yielding stronger stability and better reactivity. Plenty of work focuses on developing good organometallic catalysts using NHCs.²⁵ NHCs' excellent performance in organometallics promotes the exploration of the relationship between their structures and properties. The rich discussion includes how the N-substituents trigger the reactivity of the metal-carbene complex,⁸ and the comparison between phosphines and NHCs. The Tolman electronic parameter (TEP) is a commonly used parameter indexing the donor ability of a ligand. A lot of measurements have been performed. It was found that organophosphines have larger TEPs than NHC ligands, which indicates their weaker σ -donor nature. (Figure 2.1)⁴⁵ Interestingly, both imidazolium (unsaturated) and imidazolinium (saturated) cores are used in organometallics catalysis. Little work has been done in discussing how the degree of unsaturation affects the property of NHCs. The backbones of the two are quite similar. At first glance, the unsaturated imidazolium core seems more stable, as it takes advantage of aromaticity. However, the first discovered stable carbene is a saturated one. No experimental evidence shows the superiority of the double bond or the opposite. Regarding the possible correlation between basicity (proton affinity in gas phase) and

nucleophilicity, we decided to study NHCs in terms of PA, hoping to find an easy way to compare between NHCs and to correlate their properties and structure characteristics. We therefore chose five pairs of imidazolylidenes/imidazolinylidenes as our objects of study. (Figure 2.2)

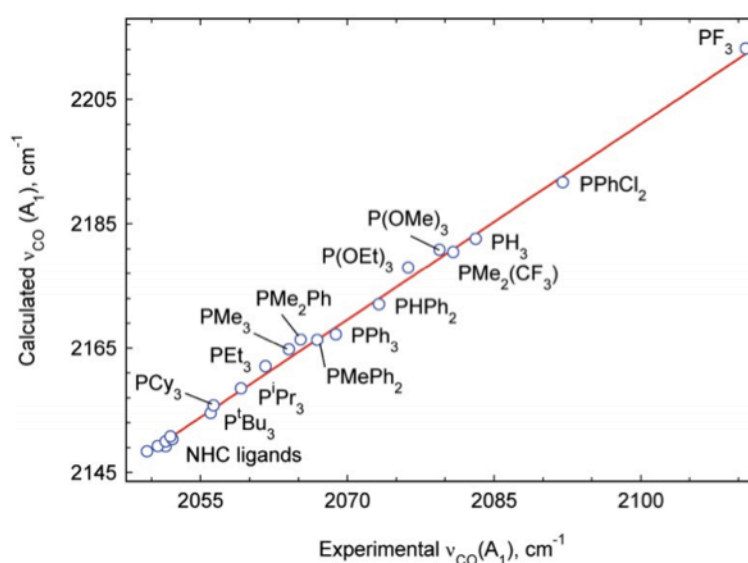


Figure 2.1 The TEP (ν_{CO}) of phosphine compounds and NHCs

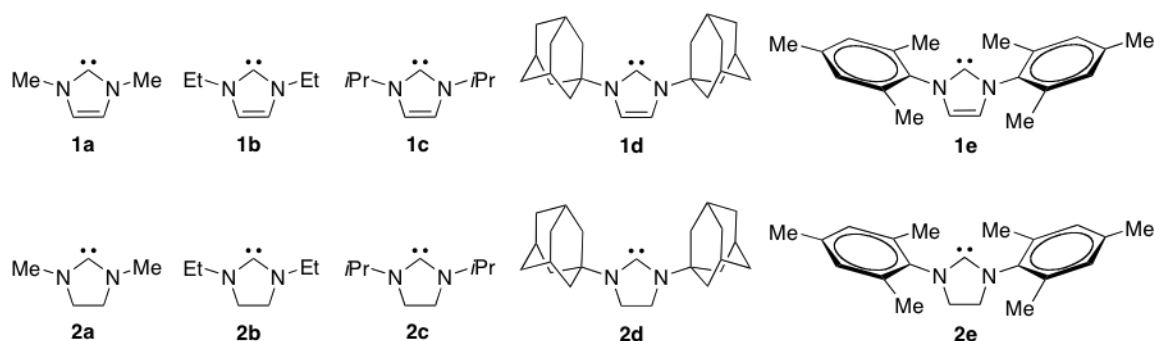
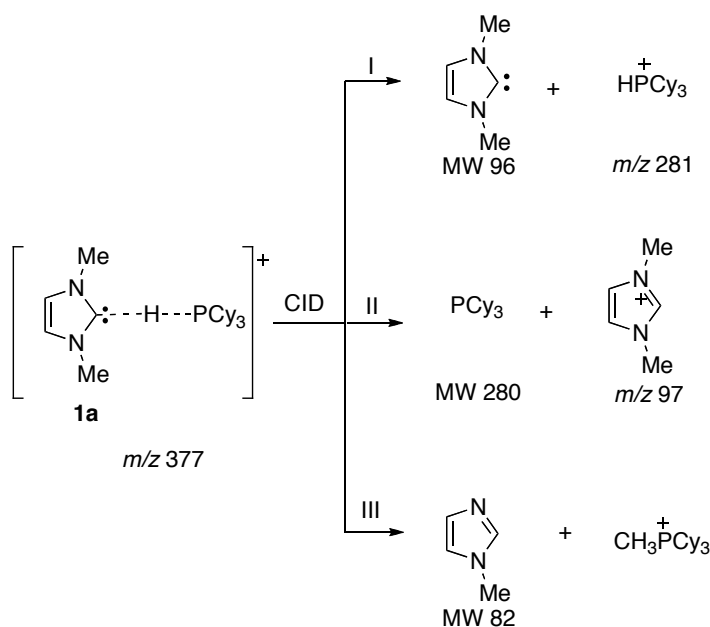


Figure 2.2 NHCs studied in this chapter.

Also, we were interested in how the saturated and unsaturated NHCs behave differently when comparing to the phosphine compounds. In our previous study, during the dissociation of $\mathbf{1a} \cdots \text{H} \cdots \text{PCy}_3^+$, a substitution pathway was also observed in addition to

the hydrogen bond breakage. Phosphine attacks the methyl group, resulting in the bond breakage between the attacked methyl group and the imidazole ring. (Scheme 2.1) This intriguing result generates a question: does $\text{NHC}\cdots\text{H}\cdots\text{PCy}_3^+$ dissociation follow certain rules or patterns? To answer this question, we tested three more carbene phosphine complexes: $\mathbf{2a}\cdots\text{H}\cdots\text{PCy}_3^+$, $\mathbf{1b}\cdots\text{H}\cdots\text{PCy}_3^+$ and $\mathbf{2b}\cdots\text{H}\cdots\text{PCy}_3^+$.



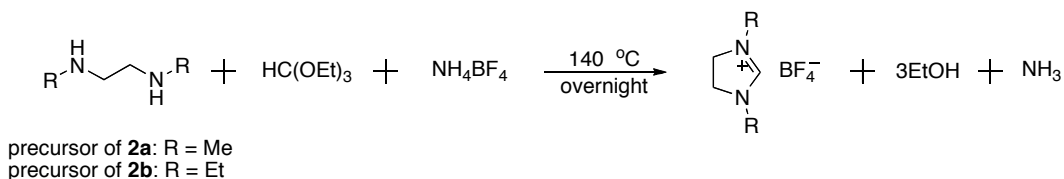
Scheme 2.1 Dissociation pathways found in $\mathbf{1a}\cdots\text{H}\cdots\text{PCy}_3^+$. Pathway A and B are the normal hydrogen bond breakage. Pathway C is the substitution in which PCy_3 attacks one of the methyl groups on 1,3-dimethylimidazolium.

2.2. Experimental section

2.2.1. NHC preparation

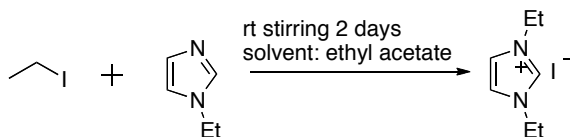
The **1b**, **2a**, and **2b** protonated precursors (imidazolium/imidazolinium salts) were synthesized according to the methods from literature. Others are used as purchased.

*Preparation of 1,3-substituted imidazolinium tetrafluoroborate (precursor of **2a** and **2b**):*⁴⁶ For the precursor of **2a**, N,N'-dimethyl-1,3-ethanediamine (5 mmol) and ammonium tetrafluoroborate (5 mmol) were dissolved in triethyl orthoformate (5mmol). The mixture was heated up to 140°C, stirring for overnight. After cooling down, the mixture was placed under vacuum for 1 h. No further workup was performed. Precursor of **2b** was prepared by the same method. (**Scheme 2.2**)



Scheme 2.2 Synthesis of 1,3-dimethylimidazolinium tetrafluoroborate (precursor of **2a**), and 1,3-diethylimidazolinium tetrafluoroborate (precursor of **2b**).

*Preparation of 1,3-diethylimidazolium iodide (precursor of **1b**):*⁴⁷ N-ethyl-imidazole (16.7 mmol) were dissolved in 20 mL ethyl ethanoate, and placed in iced water bath. Ethyl iodide (18.7mmol) was added dropwise with stirring. The solution was allowed to warm up slowly to the room temperature. After two days stirring, the mixture was placed under vacuum to remove solvent. White solid product was slowly crystallized. No further workup was performed. (Scheme 2.3)



Scheme 2.3 Synthesis of 1,3-diethylimidazolium iodide (precursor of **1a**).

2.2.2. LCQ bracketing

Proton affinities of NHCs were measured by bracketing method described as in Chapter 1. Considering the non-volatile nature of NHCs and their protonated precursors, experiments were performed on the modified LCQ instrument. Neutral reference bases were vaporized and added into the ion trap with the helium gas flow via the house-built leak valve. The analyte solutions were prepared by dissolving protonated carbene precursors in methanol. The concentration of the solutions were ~ 0.1 mM. The free ions were generated by ESI from solutions using a flow rate of 20 $\mu\text{L}/\text{min}$. The capillary temperature was 150 $^{\circ}\text{C}$. The spray voltage was 4.5 kV. The ions were isolated from full scan and allowed to react with neutral reference bases for 0.03-1000 ms. A total of 10 scans were collected and averaged.

To measure the pressure of neutral references, a protonated base of which the PA is > 5 kcal/mol lower than the reference was allowed to react with the neutral references. This reaction was assumed to be diffusion control. Then protonated NHCs were allowed to react with the neutral reference. (Eq. 2.1)



The occurrence of proton transfer indicates an exothermic reaction (“+” in the tables), therefore the proton affinities of NHCs and references can be compared.

2.2.3. Hetero dimer dissociation experiments

The dissociation experiments were performed on LCQ duo or LTQ instrument. NHCs mixture solutions or NHC-phosphine mixture solutions were prepared by dissolving each component 1:1 ratio in methanol. The final concentration of each component is 0.5 mM. Hetero proton bond dimers were generated by ESI from solutions using a flow rate of 20 μ L/min. The capillary temperature was 150 $^{\circ}$ C. The spray voltage was 4.5 kV. Ions were then isolated from full scan and then subjected to collision-induced dissociation (CID); the complexes are activated for 30 ms. A total of 20 scans were averaged for the product ions.

2.2.4. Calculation

Calculations are conducted at B3LYP/6-31+G(d) using Gaussian09.⁴⁴ The geometries are fully optimized and frequencies are calculated. No scaling factor is applied. All the values reported are ΔH at 298 K.

2.3. Results and discussion

2.3.1 Calculations for Carbene Site

The calculated results are shown in Table 2.1. All the calculated values are higher than the reported gas phase proton affinity of tricyclohexylphosphine (PCy₃),⁴⁸ the ligand used in the 1st generation Grubbs catalyst. And two clear trends can be summarized: (1) As the substituents become bulkier, the proton affinities of the lone pair increase notably; (2) The unsaturated imidazolylidene series have slightly lower proton affinities than their imidazolinylidene counterparts.

Table 2.1 Computation results of NHCs gas phase proton affinities ^a

Structures	PA (kcal/mol)	Structures	PA (kcal/mol)
1a	259.9	2a	260.3
1b	262.8	2b	263.1
1c	265.3	2c	266.1
1d	269.9	2d	269.3
1e	270.4	2e	270.5

^aCalculations were conducted at B3LYP/6-31+G(d) [ΔH at 298 K in kcal mol⁻¹].

2.3.2 Proton Affinity Measurement by Bracketing Method

Six reference bases are used for measuring PA of the unsaturated carbene **1a** (Table 2.2). This measurement was conducted by Mu Chen in our group. The protonated **1a** can be deprotonated by *tert*-butylimino tris(dimethylamino)phosphorane, but the proton transfer reaction was not observed with imino-tris(dimethylamino)phosphorane. PA of **1a** is bracketed as 259.0 ± 2.0 kcal/mol. The bracketing result is very close to our calculation value 259.9 kcal mol⁻¹.

Table 2.2 Summary of results for PA bracketing of more basic site of **1a**

Referece compound	PA/kcal mol ⁻¹	Proton transfer Ref. base
2- <i>tert</i> -butylimino-2-diethylamino-1,3-dimethylperhydro-1,3,2-diazaphosphorine	263.8 ± 2.0	+
<i>tert</i> -octylimino-tris(dimethylamino)phosphorane	262.0 ± 2.0	+
<i>tert</i> -butylimino-tris(dimethylamino)phosphorane	260.6 ± 2.0	+
imino-tris(dimethylamino)phosphorane	257.4 ± 2.0	—
7-methyl-1,5,7-triazabicyclo[4.4.0]dec-5-ene	254.0 ± 2.0	—
1,8-diazabicyclo[5.4.0]undec-7-ene	250.5 ± 2.0	—

The bracketing results of **1b** are shown in Table 2.3, which seems complicated. No proton transfer was observed for reaction with *tert*-octylimino-tris(dimethylamino)phosphorane and *tert*-butylimino-tris(dimethylamino)phosphorane, which indicates **1b** has higher PA than *tert*-octylimino-tris(dimethylamino)phosphorane. In the reaction with 2-*tert*-butylimino-2-diethylamino-1,3-dimethylperhydro-1,3,2-diazaphosphorine, proton transfer was observed three times out of six repeats. The calculated efficiencies are very close to the cutoff value. We may circumspectly conclude that the similar PA of **1b** and 2-*tert*-butylimino-2-diethylamino-1,3-dimethylperhydro-1,3,2-diazaphosphorine causes the ambiguous results. The calculated value of 262.8 kcal mol⁻¹ supports this explanation.

Table 2.3 Summary of results for PA bracketing of more basic site of **1b**

<i>Reference compound</i>	<i>PA/kcal mol⁻¹</i>	<i>Proton transfer Ref. base</i>
2- <i>tert</i> -butylimino-2-diethylamino-1,3-dimethylperhydro-1,3,2-diazaphosphorine	263.8 ± 2.0	+/- ^a
<i>tert</i> -octylimino-tris(dimethylamino)phosphorane	262.0 ± 2.0	-
<i>tert</i> -butylimino-tris(dimethylamino)phosphorane	260.6 ± 2.0	-

^a The reaction with 2-*tert*-butylimino-2-diethylamino-1,3-dimethylperhydro-1,3,2-diazaphosphorine was repeated six times. Three of them showed proton transfer, while the rest showed no reaction.

The bracketing result for **2a** is in Table 2.4. Protonated **2a** showed no proton transfer with 7-methyl-1,5,7-triazabicyclo[4.4.0]dec-5-ene, but reacted with *tert*-butylimino-tris(dimethylamino)phosphorane. When protonated **2a** was injected in to imino-tris(dimethylamino)phosphorane atmosphere, the hydrogen bonded complex of **2a** and reference are observed as the product of the reaction. We conclude this as no proton

transfer. Thus the experimental PA of **2a** was bracketed as $259 \pm 3 \text{ kcal mol}^{-1}$, in the same range as **1a**.

Table 2.4 Summary of results for PA bracketing of more basic site of **2a**

<i>Reference compound</i>	<i>PA/kcal mol⁻¹</i>	<i>Proton transfer Ref. base</i>
2- <i>tert</i> -butylimino-2-diethylamino-1,3-dimethylperhydro-1,3,2-diazaphosphorine	263.8 ± 2.0	+
<i>tert</i> -octylimino-tris(dimethylamino)phosphoranec	262.0 ± 2.0	+
<i>tert</i> -butylimino-tris(dimethylamino)phosphorane	260.6 ± 2.0	+
imino-tris(dimethylamino)phosphorane	257.4 ± 2.0	dimer
7-Methyl-1,5,7-triazabicyclo[4.4.0]dec-5-ene	254.0 ± 2.0	–
1,8-diazabicyclo[5.4.0]undec-7-ene	250.5 ± 2.0	–

The bracketing results of **2b** are shown in Table 2.5. All the reference bases showed negative reaction. **2b** has higher PA than that of 2-*tert*-butylimino-2-diethylamino-1,3-dimethylperhydro-1,3,2- diazaphosphorine ($263.8 \text{ kcal mol}^{-1}$).

Table 2.5 Summary of results for PA bracketing of more basic site of **2b**

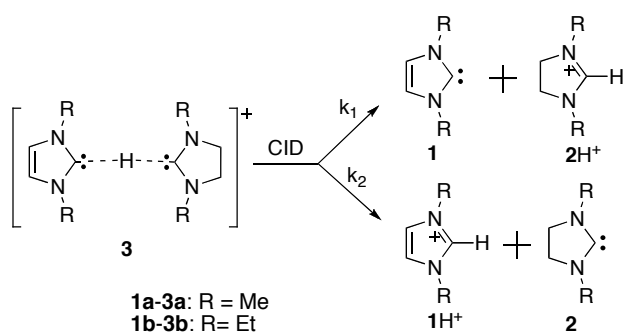
<i>Reference compound</i>	<i>PA/kcal mol⁻¹</i>	<i>Proton transfer Ref. base</i>
2- <i>tert</i> -Butylimino-2-diethylamino-1,3-dimethylperhydro-1,3,2- diazaphosphorine	263.8 ± 2.0	-
<i>tert</i> -Octylimino-tris(dimethylamino)phosphorane	262.0 ± 2.0	-
<i>tert</i> -Butylimino-tris(dimethylamino)phosphorane	260.6 ± 2.0	-

We also tried to bracket the PA of **2c**, **2d** and **2e**. Their reactions with 2-*tert*-butylimino-2-diethylamino-1,3-dimethylperhydro-1,3,2-diazaphosphorine showed

negative results (the same as the results of **2b**). This compound is the most basic reference base that may be applied in our LCQ-MS bracketing experiment. The more basic ones are not volatile enough to be introduced into the ion trap via our house-built leak valve by evaporation. We can only conclude their PA are higher than 263.8 kcal mol⁻¹ from this experiment.

2.3.3 Proton Affinity Comparison Between unsaturated carbene **1** and the saturated counterpart **2** by proton bond heterodimer dissociation experiment

According to the calculation values, saturated carbenes have a slightly higher PA than their unsaturated counterparts. We tried to measure PAs by Cooks kinetics method, but due to the nature of NHCs, proton bound dimers of NHC and reference bases could not be generated and isolated. Therefore, we decided to try a relative PA measurement using the proton bond heterodimer dissociation experiment. The theoretical foundation of the dissociation experiment is similar to Cooks kinetics method. The proton bond between weaker base and proton is more likely to break in CID, therefore generated less positively charged such fragments. (Scheme 2.4)



Scheme 2.4 CID of proton-bound complex of **1** and **2**.

In comparison between **1a** and **2a**, when the protonated complex **3a** signal (*m/z* 195) was isolated from full scan and CID was applied, the fragmentation spectrum gave

more protonated-saturated derivative **2a** than that of unsaturated **1a**, which indicated that the saturated carbene **2a** is more basic. The experimental value for $PA_{2a} - PA_{1a}$ was 1.0 kcal/mol, close to the relative calculated value 0.4 kcal/mol.

The diethyl carbenes' measurement also yielded result consistent with calculated values. (0.8 kcal/mol from experiment, and 0.3 kcal/mol from calculation for $PA_{2b} - PA_{1b}$).

2.3.4 Carbene-phosphine Complex Dissociation

As introduced in **2.1**, we studied three more carbene-phosphine complexes: $2a \cdots H \cdots PCy_3^+$, $1b \cdots H \cdots PCy_3^+$ and $2b \cdots H \cdots PCy_3^+$, (Figure 2.3) trying to understand their dissociation patterns.

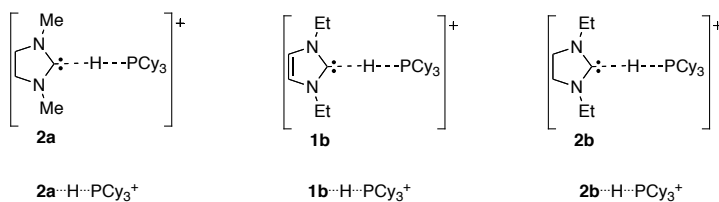
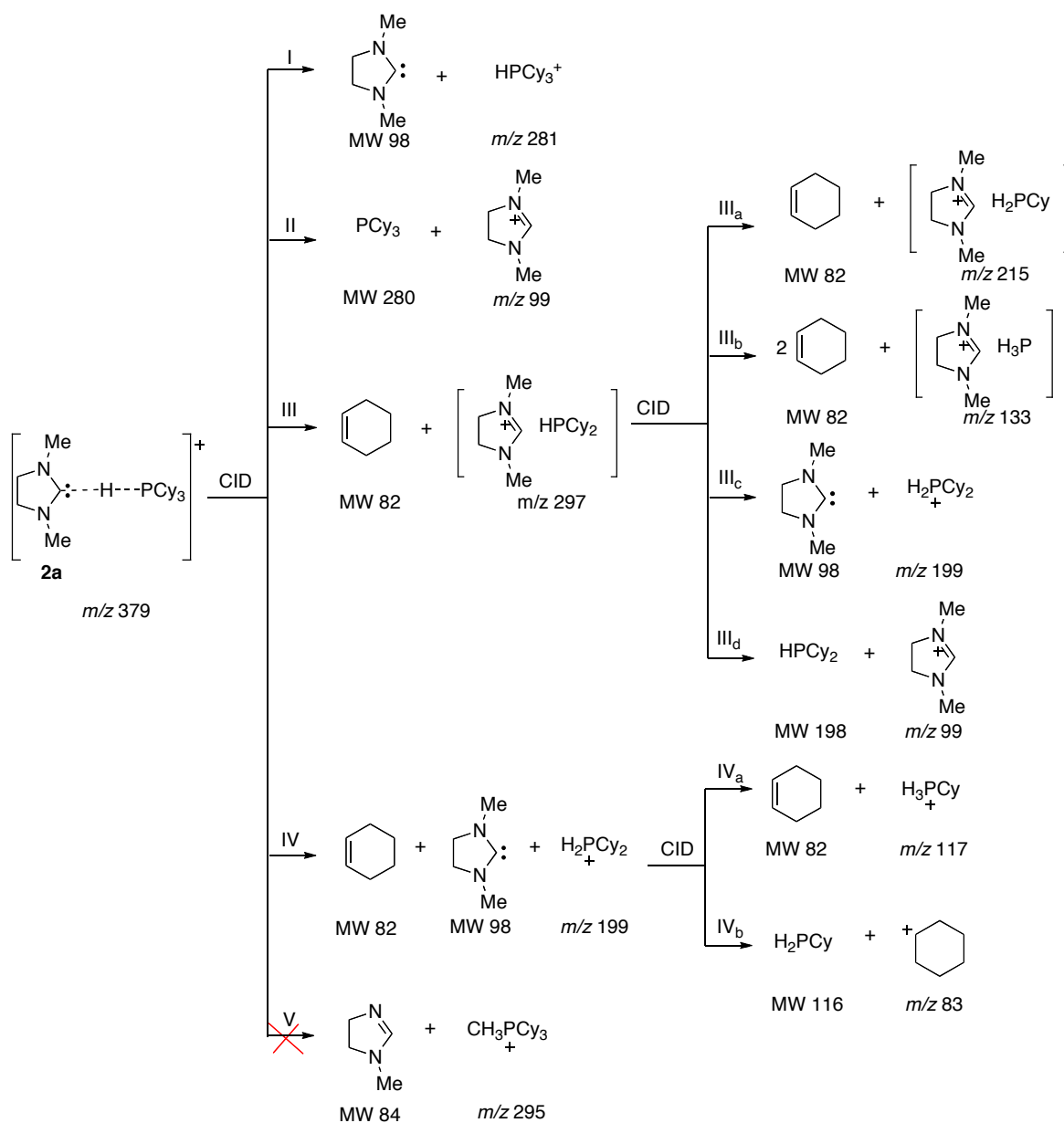


Figure 2.3 Structures of carbene-phosphine complexes studied herein.

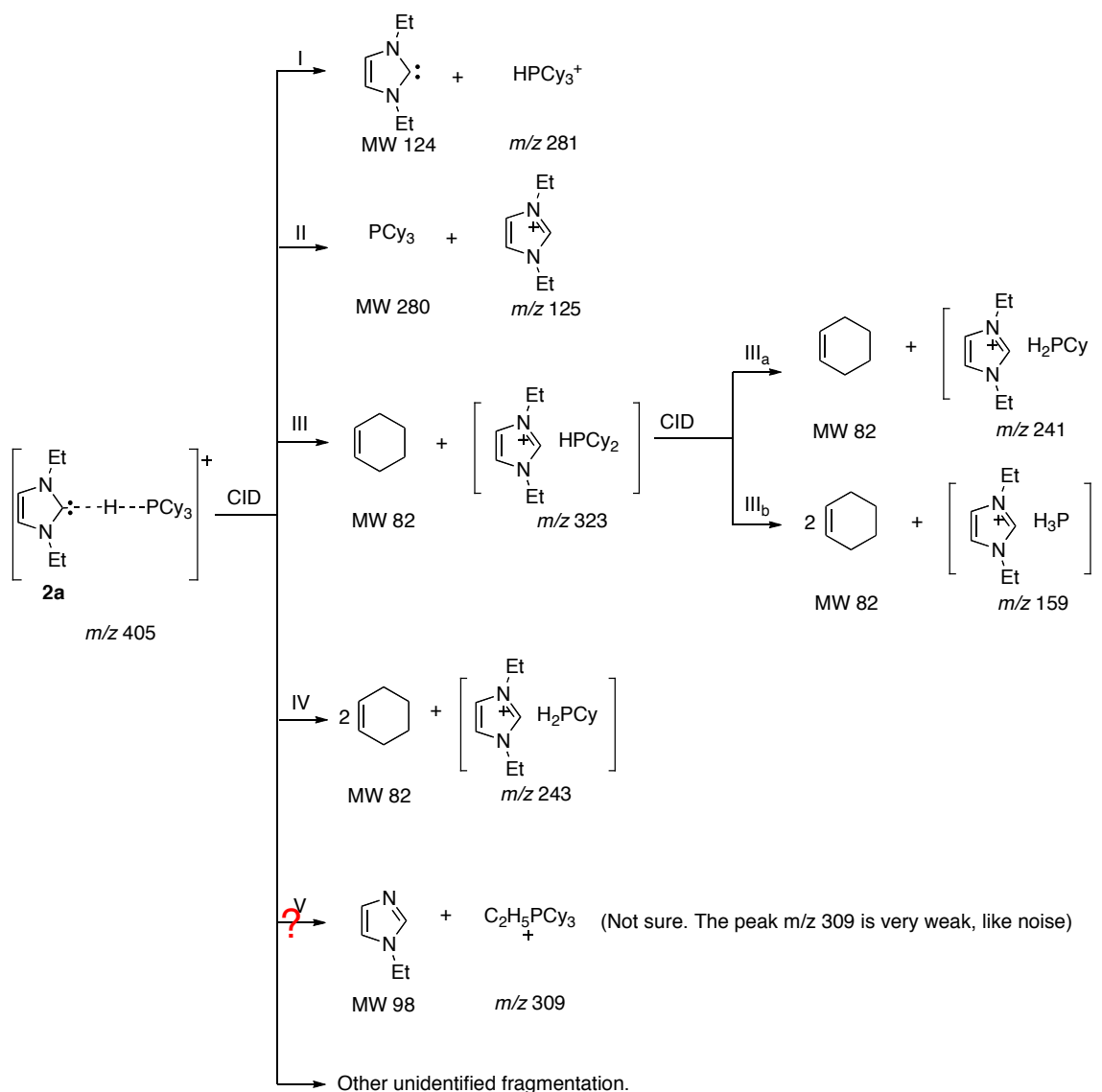
$2a \cdots H \cdots PCy_3^+$: The complex signal m/z 379 was isolated, with CID applied. Four dissociation pathways were found (Scheme 2.5). As with the dissociation of unsaturated carbene $1a \cdots H \cdots PCy_3^+$ (the parent ion in Scheme 2.1) analog, the major dissociation path corresponds to the formation of protonated phosphine. If methyl substitution happened in this case (analogous to pathway III in Scheme 2.1), we would expect a peak of m/z 295 in the secondary MS spectrum. However, no substitution pathway was observed during the dissociation. The peak of m/z 297 in the spectrum indicated elimination of Cy group from PCy_3 . Two types of elimination were observed in this case. In pathway III, $2a \cdots H \cdots PCy_3^+$

lost one Cy group, forming the complex $2\mathbf{a} \cdots \text{H} \cdots \text{PCy}_2^+$ complex (m/z 297). When CID was applied on this $2\mathbf{a} \cdots \text{H} \cdots \text{PCy}_2^+$ fragment, it might keep losing one or two Cy group (pathway III_a and III_b in Scheme 2.5), or followed the normal hydrogen bond breaking (pathway III_c and III_d in Scheme 2.5). In pathway IV, the complex lost cyclohexene and carbene, and cyclohexene may fragment from phosphine if more energy was deposited. It was hard to differentiate if the two neutral fragments left at the same time or sequentially as the combination of III and III_c.

$1\mathbf{b} \cdots \text{H} \cdots \text{PCy}_3^+$: The complex signal m/z 405 was isolated, with CID applied. More than four dissociation paths were observed. (Scheme 2.6) The hydrogen bond breakages were observed, but no longer the major paths (Path I and Path II). Instead, the elimination (Path III) became the major one. The elimination of two Cy groups (path IV, producing $1\mathbf{b} \cdots \text{H} \cdots \text{H}_2\text{PCy}^+$, fragment m/z 243) was also observed. The substitution (Path V) fragment signal m/z 309 was very weak, indicating the rare occurrence if any. There were two fragments m/z 306 and m/z 375 that could not be assigned.

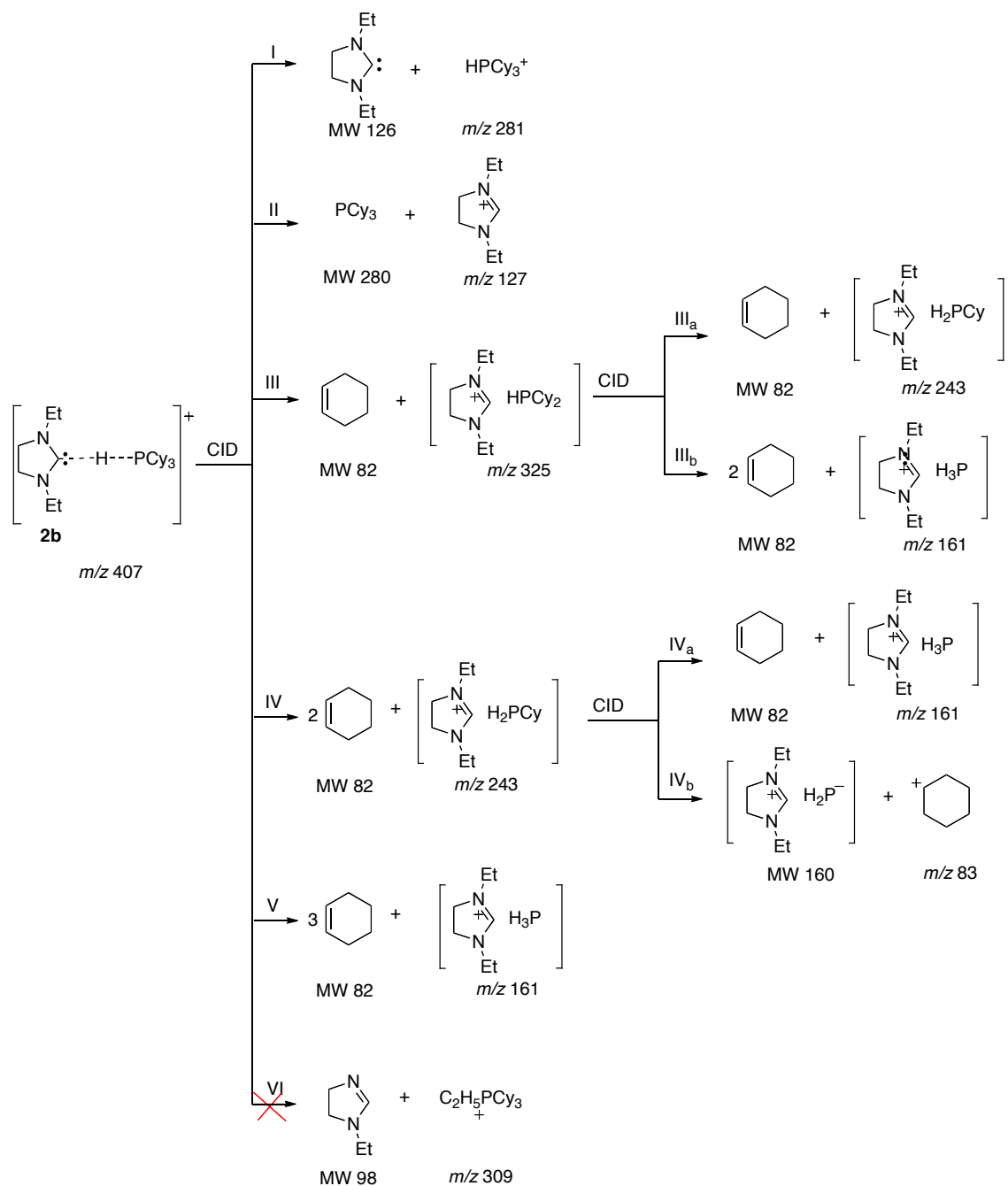


Scheme 2.5 Possible dissociation pathways for CID of $2a \cdots \text{H} \cdots \text{PCy}_3^+$.



Scheme 2.6 Possible dissociation pathways for CID of $\mathbf{1b} \cdots \text{H} \cdots \text{PCy}_3^+$

$\mathbf{2b} \cdots \text{H} \cdots \text{PCy}_3^+$: The complex signal m/z 407 was isolated, with CID applied. Five dissociation paths were observed. (Scheme 2.7) The dissociation paths are similar to that of $\mathbf{2a} \cdots \text{H} \cdots \text{PCy}_3^+$: no substitution pattern was observed (Path VI) while richer elimination was shown.



Scheme 2.7 Possible dissociation pathways for CID of **2b**...H...PCy₃⁺

Because of the rich fragmentation in the CID of NHC...H...PCy₃⁺, this experiment cannot be used to compare the proton affinities between PCy₃ and NHCs. But the dissociation patterns are interesting. Two dissociation paths: elimination and substitution

are observed among the four studied $\text{NHC}\cdots\text{H}\cdots\text{PCy}_3^+$ complexes. Substitution is observed in $\mathbf{1a}\cdots\text{H}\cdots\text{PCy}_3^+$ but not in $\mathbf{1b}\cdots\text{H}\cdots\text{PCy}_3^+$, while elimination happens in $\mathbf{2a}\cdots\text{H}\cdots\text{PCy}_3^+$, $\mathbf{2b}\cdots\text{H}\cdots\text{PCy}_3^+$, and $\mathbf{1b}\cdots\text{H}\cdots\text{PCy}_3^+$. It is hard to conclude that unsaturated $\text{NHC}\cdots\text{H}\cdots\text{PCy}_3^+$ complexes undergo the substitution path and saturated $\text{NHC}\cdots\text{H}\cdots\text{PCy}_3^+$ complexes undergo the elimination path or the opposite. However, if considering the PA trend of these carbenes: $\mathbf{2b} > \mathbf{1b} > \mathbf{2a} > \mathbf{1a}$, it seems the more basic NHC favors elimination in $\text{NHC}\cdots\text{H}\cdots\text{PCy}_3^+$ dissociation.

2.4. Conclusion

We studied a series of saturated and unsaturated NHCs. The PAs of NHCs are measured. Generally, the imidazolinyldene is slightly more basic than its unsaturated counterpart: the imidazolyldene with the same substituents. The $\text{NHC}\cdots\text{H}\cdots\text{PCy}_3^+$ dissociation patterns under CID are investigated. We found that two dissociation paths in addition to the breakage of hydrogen bonds: 1) substitution of PCy_3 by the alkyl group on the NHC and 2) elimination of Cy group on PCy_3 . More basic NHCs favor the elimination.

Note: Major parts of the this chapter have been published: Tian, Y.; Lee, J. K. " Gas Phase Studies of N-Heterocyclic Carbene-Catalyzed Condensation Reactions," *J. Org. Chem.* **2015**, 80, 6831

Reprinted (adapted) with permission from Tian, Y.; Lee, J. K. " Gas Phase Studies of N-Heterocyclic Carbene-Catalyzed Condensation Reactions," *J. Org. Chem.* **2015**, 80, 6831. Copyright 2015 American Chemical Society (see the end of this dissertation for the permission)

Chapter 3 Gas Phase Stetter Reaction catalyzed by Charged Handle Thiazolium Catalysts

3.1. Introduction

A particularly intriguing class of reactions in organic synthesis involves the reversal of the polarity of a functional group (*Umpolung*).⁴⁹ The classic example is the benzoin condensation, first reported by Wöhler and Liebig in 1832 with a proposed mechanism in 1903 by Lapworth; cyanide catalyzes the dimerization of two benzaldehyde units.⁵⁰ In 1943, Ukai and coworkers discovered that thiazolium salts can also catalyze the condensation.⁵¹ Several years later, Breslow proposed the deprotonated thiazolium - the thiazolylidene (which can also be thought of as a thiazolium zwitterion) - as the catalytic species.⁵¹⁻⁵⁴ His proposed mechanism (Figure 3.1) involves deprotonation of the thiazolium to yield thiazolylidene/thiazolium zwitterion, which nucleophilically adds to a benzaldehyde, followed by a proton transfer to form the "Breslow intermediate," which possesses the *Umpolung* reactivity (the aldehyde becomes nucleophilic rather than electrophilic). The Breslow intermediate then adds to a second

benzaldehyde. This reaction, as well as its related counterpart, the Stetter reaction (in which the second addition involves an enone), has seen a renaissance in the last decade, with enantioselective versions catalyzed by a variety of *N*-heterocyclic carbenes (NHCs; thiazolylidenes, imidazolylidenes, and triazolylidenes).⁵⁵⁻⁷¹

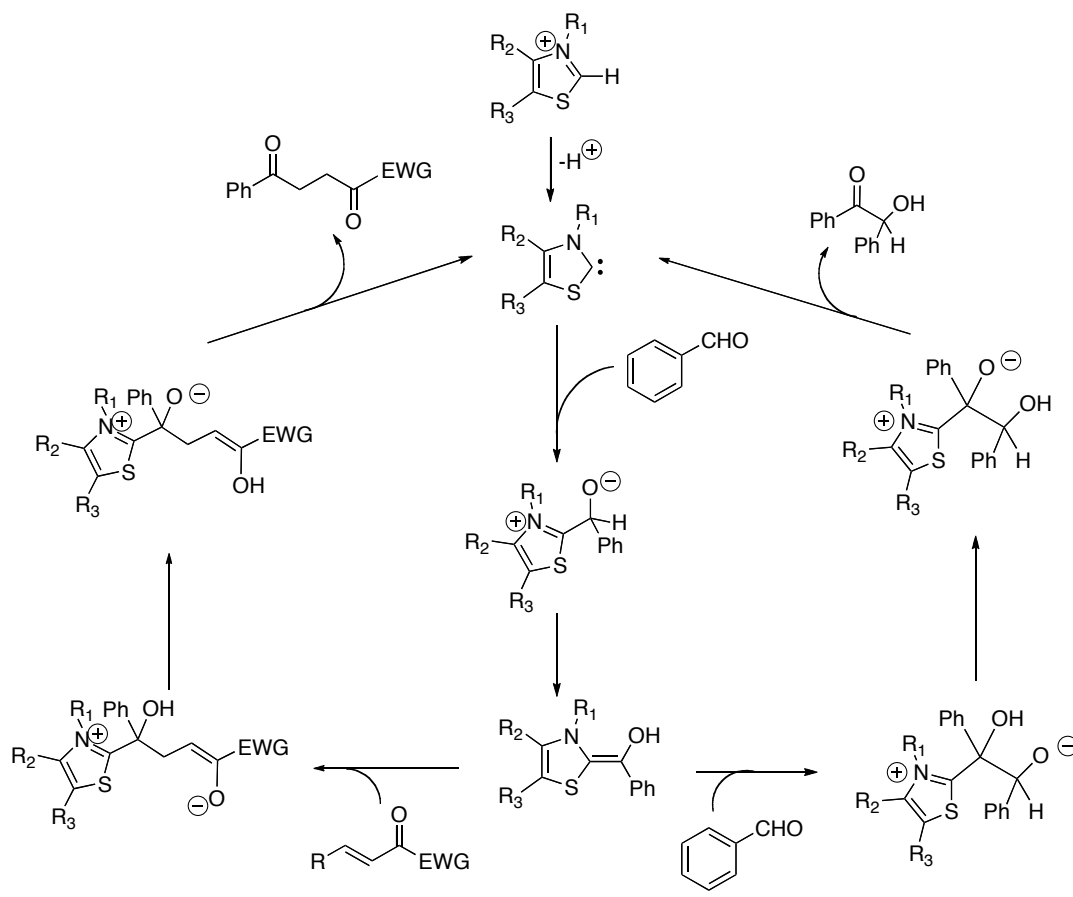


Figure 3.1 Breslow mechanism of benzoin condensation (right) and the mechanism of Stetter reaction (left) proposed according to Breslow mechanism

The Breslow mechanism is commonly accepted for the benzoin condensation. Many attempts over the years had been made to isolate the Breslow intermediate, which had proven to be elusive until 2012, when both a nitrogen analogue and the intermediate itself were observed and characterized spectroscopically; studies on nucleophilicity of related deoxy and methoxy analogues have also been conducted.⁷²⁻⁷⁶ Mechanisms

involving a thiazolylidene dimer (Lemal and Castells, Figure 3.2) have also been suggested; data both in support of and against such mechanisms exist.⁷⁷⁻⁸⁹ Much less mechanistic work exists for the Stetter reaction. The mechanism is generally assumed to be similar to that of the benzoin, as they share the same first step (NHC addition to aldehyde), although possibly with different concertedness and rate determining steps.⁹⁰⁻⁹³

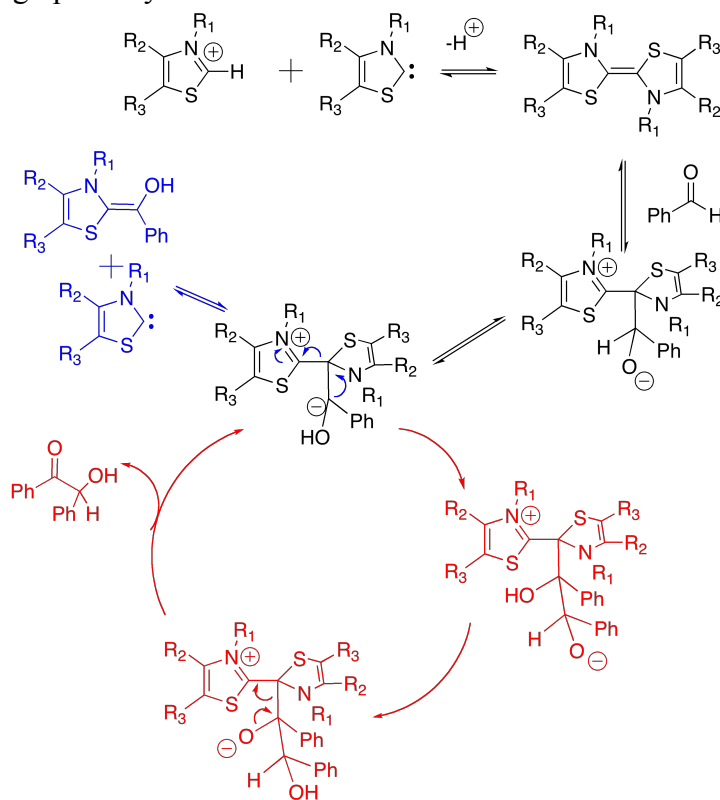


Figure 3.2 Dimer mechanisms of Benzoin condensation. Blue: proposed by Lemal; Red: proposed by Castells.

Because of the ever-growing prevalence and synthetic utility of reactions catalyzed by thiazoylidenes, we sought to explore the potential of studying the *gas-phase* counterpart of this reaction, in the absence of solvent. Because the intermediates are not charged, the reaction is potentially difficult to track using mass spectrometry. The solution phase reaction has been studied using ESI-MS, first by Glorius and coworkers, who examined an imidazolylidene-catalyzed conjugate *Umpolung* reaction to form a

lactone.⁹⁴ They took advantage of the protonation of intermediates in the electrospray process, enabling the use of positive ion mass spectrometry for detection. We also examined the solution phase reaction, but using negative ion mass spectrometry; in our case, we synthesized a novel thiazolium with a sulfonate charge tag.⁹⁵ This synthesized compound was used to catalyze the benzoin condensation in solution, and intermediates were detected using negative ion ESI-MS. In this present work, by contrast, we seek to examine these condensation reactions in the gas phase, for the first time. The two prior mass spectrometric studies of these types of reactions have involved conducting the reactions in solution and using ESI-MS to track reaction progress. By contrast, we are attempting the reactions directly in the gas phase. Such studies are potentially useful, since 1) intrinsic reactivity in the absence of solvent can be useful for understanding the role of solvent in the analogous condensed phase reactions, and 2) the observation of intermediate may help to unveil the mechanism of these reactions.

3.2. Experimental section

3.2.1 Gas phase reaction monitoring

Most substrates are commercially available and were used as received. The sulfonate-tagged thiazolium and benzoyltrimethylsilane are both known compounds and were synthesized according to literature procedure.^{95,96} As described in Chapter 1, the experiments were performed on our modified LCQ instrument. Neutral substrates were added via leak valves, with the helium gas flow. A 0.1 mM solution of the synthesized thiazolium in methanol with 0.1% ammonium hydroxide was injected using ESI. An electrospray needle voltage of 2.7 kV and a flow rate of 20 μ L/min were used, with a capillary temperature of 190 °C. Charged species were isolated from fullscan and allow

up to 10,000 ms to react with neutral substrates. The generated new species were isolated again to perform further reaction or CID. Spectra were an average of ten scans.

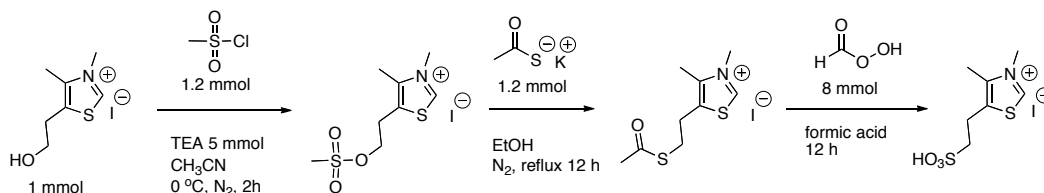
3.2.2 Calculation

Calculations are conducted at B3LYP/6-31+G(d) using Gaussian09.⁴⁴ The geometries are fully optimized and frequencies are calculated. No scaling factor is applied. All the values reported are ΔH at 298 K.

3.3. Results and discussion

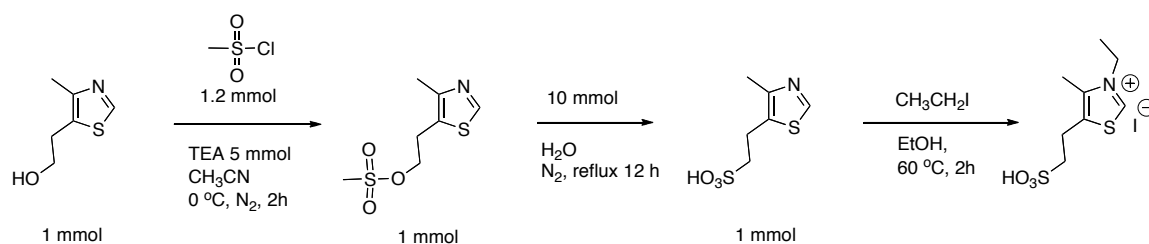
3.3.1 Preparation of charge handle thiazolium pre-catalyst

3,4-dimethyl-5-(2-sulfoethyl)thiazolium iodide (precursor of **1a**): 5-(2-Hydroxyethyl)-3,4-dimethylthiazolium iodide (1 mmol) and methanesulfonyl chloride (1.2 mmol) were dissolved in acetonitrile under protection of N₂. Cool the mixture to 0 °C in ice/water bath and add 5mmol triethylamine. After 2 h stirring, filter the mixture and take the filtrate. Remove the solvent and dissolve the residue and 1.2 mmol potassium ethanethioate in 15mL ethanol. After 12-hour reflux under N₂ protection, filter the mixture while hot and take the filtrate. Remove the solvent and dissolve the residue in 1 mL formic acid and Cool the mixture to 0 °C in ice-water bath. Add the mixture of hydrogen peroxide (8 mmol) and formic acid (1 mmol) dropwise. Stir for 12 hours at room temperature. The final product is purified by HPLC. (Scheme 3.1)



Scheme 3.1 Synthesis of 3,4-dimethyl-5-(2-sulfoethyl)thiazolium iodide (precursor of **1a**)

3-ethyl-4-methyl-5-(2-sulfoethyl)thiazolium iodide (precursor of **1b**): 4-Methyl-5-(2-hydroxyethyl)thiazole (1 mmol) and methanesulfonyl chloride (1.2 mmol) were dissolved in acetonitrile under protection of N₂. Cool the mixture to 0 °C in ice-water bath and add 5mmol triethylamine. Stir for 2 h and purify the product by silica gel column. Dissolve 4-methyl-5-(2-methanesulfonate)thiazole (1 mmol) and sodium sulfite(10 mmol) in 5 mL water, reflux the mixture for 3h and purify the product by silica gel column. Dissolve 4-methyl-5-(2-sulfonyl)thiazole (1 mmol) and ethyl iodide(1.5 mmol) in 1.5 mL ethanol. Stir the mixture at 60 °C for 72 h. The final product was purified by alumina column. (Scheme 3.2)



Scheme 3.2 Synthesis of 3-ethyl-4-methyl-5-(2-sulfoethyl)thiazolium iodide (precursor of **1b**)

3.3.2 Formation of Breslow intermediate

Three different charged handle thiazolium catalysts and two carbonyl substrates (Figure 3.3) were used to probe the first step addition. The sulfonate serves as a nonreactive moiety that, since charged, can be detected using mass spectrometry.

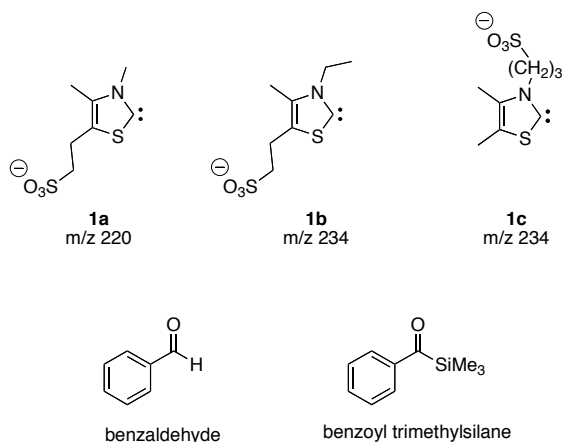
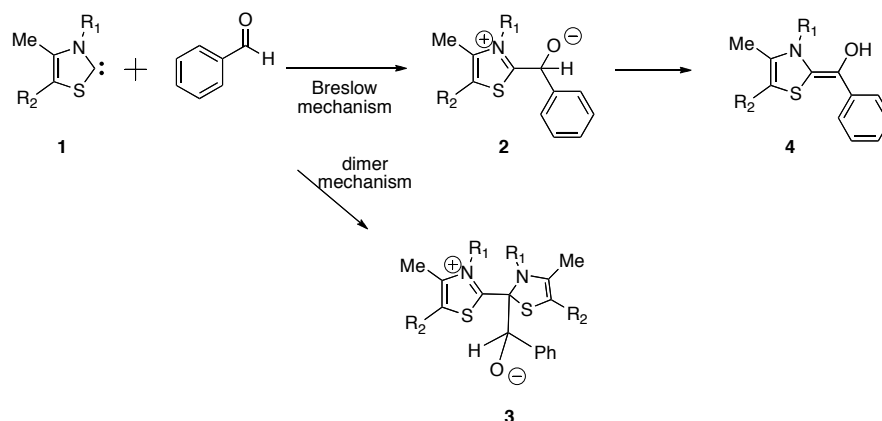


Figure 3.3 Charge handle thiazolyliidines and carbonyl substrates used in this study



Scheme 3.3 Possible first step addition reaction paths of thiazoyliidene catalysts plus benzaldehyde

The charge-tagged catalysts were introduced into the ion trap and then isolated. First we introduced benzaldehyde to ascertain whether the catalyst would add to the aldehyde *in vacuo*. The desired umpolung reactions are shown in Scheme 3.3. Among the possible species, catalyst **1**, tetrahedral intermediate **2** and **3**, Breslow intermediate **4** are charged, thus can be observed in the spectra if generated. Notice that the catalyst **1** and its dimer have the same mass-to-charge ratio and similar structure, thus can hardly be differentiated. **2** and **4** also have the same mass-to-charge ratio, but the structural

difference makes it possible to be differentiated by their fragmentation patterns. The results are summarized in Table 3.1.

Table 3.1 Observations of thiazoylidene catalysts plus benzaldehyde

Entry	Catalyst	2 or 4	3
1	1a	m/z 326 n ^a	m/z 273 n ^a
2	1b	m/z 340 n ^a	m/z 287 n ^a
3	1c	m/z 340 n ^a	m/z 287 n ^a

^a No such ion is observed.

The gas phase addition of the catalysts and benzaldehyde yields no reaction. There is always the possibility that the entire catalytic cycle is taking place, with short-lived charged intermediates, and neutrals that we cannot observe. If the entire reaction in Scheme 3.3 takes place, we would simply regenerate the catalyst, m/z 220 or m/z 234. This is a possibility that we can never discount; however, we thought that perhaps another reason we may not detect **2** - **4** in this gas phase reaction could be due to the difficult proton transfer to form **4** from **2** or **3**. The formation of the Breslow intermediate **4** from the oxyanion requires a 1,2 proton shift. By orbital symmetry rules, one would expect an intramolecular, direct 1,2 proton shift to be highly unfavorable.^{90,97,98} If the solvent is protic, then presumably the solvent can shuttle the proton.^{53,99} However, the solvent is often aprotic, leading to other proposals as to how this proton transfer is effected. Hawkes and Yates studied the Stetter reaction mechanism and proposed that the proton transfer would occur intermolecularly, with another molecule of **2** doing the "shuttling".⁹⁰ Using calculations, Gronert also suggested intermolecular protonation by a second molecule, but rather than **2**, he suggested the *N*-alkyl group of the thiazolium catalyst.^{100,101} A later experimental study by Rovis and coworkers established that for

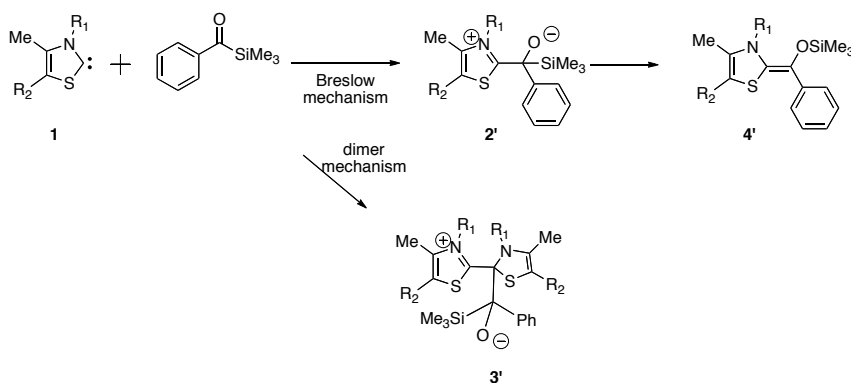
their reaction in toluene, the proton transfer is likely effected by an ether substituent on their substrate.⁹¹

Our reaction is in the gas phase, where there is no solvent to aid in the proton transfer. Reaction with a second molecule of the catalyst is unlikely; the catalysts are both negatively charged, and also, the low relative concentration of catalyst ions disfavors collision and reaction. Rovis and coworkers showed proton transfer with a substituent on the substrate, but our substrates are much simpler and this is not a possibility. We therefore hypothesized that under our conditions, in the absence of solvent, the initial tetrahedral intermediate would not be particularly stable, and that formation of the Breslow intermediate was not possible because of the unfavorable 1,2-proton transfer.

We were drawn to the fact that the 1,2 shift should be facile for a silyl group, which had been shown by Brook several decades ago (thus resulting in an eponymously named rearrangement).¹⁰² Heathcock first invoked the possibility of this pathway for an *Umpolung* reaction in 1981, in his studies of fluoride-catalyzed conversions of acylsilanes to aldehydes and ketones.¹⁰³ Degl'Innocenti followed up on this with fluoride- and cyanide-catalyzed conjugate additions of acylsilanes to enones.¹⁰⁴ In 2003, Linghu and Johnson utilized acylsilanes in the cyanide-catalyzed benzoin condensation, to circumvent the product mixture limitations of the reaction.¹⁰⁵ In the benzoin condensation, the reaction of two different aldehydes results in four possible products. Linghu and Johnson found that coupling an acylsilane and aldehyde resulted in just one product.¹⁰⁶ He later expanded this chemistry to metallophosphite catalysts, with enantioselectivity.¹⁰⁷

In 2004, Scheidt and coworkers reported the successful use of thiazolium salts (as opposed to charged cyanide or fluoride species) as the nucleophilic catalyst precursors in the Stetter reactions of acylsilanes with enones.¹⁰⁸ The Stetter reaction often incurs benzoin side products (with the aldehyde self-condensing) but Scheidt showed that the use of acylsilanes as acyl anion precursors solves this problem, as the sterically congested acylsilane is not a good electrophile.¹⁰⁹

Because the direct, intramolecular 1,2-silyl shift (Brook rearrangement) should be facile, we thought that the use of acylsilanes might allow us to form the silyl version of the Breslow intermediate in the absence of solvent (Scheme 3.4).¹⁰²



Scheme 3.4 Possible first step addition reaction paths of thiazoylidene catalysts plus benzoyltrimethylsilane

The results are summarized in Table 3.2. The reaction of catalyst **1a** with the silyl analog of benzaldehyde (benzoyltrimethylsilane) *does* yield m/z 398, which corresponds to both the initial oxanion **2a'** and the silyl-Breslow intermediate **4'**. Likewise, we find that catalyst **1b** with benzoyltrimethylsilane yields a product with an m/z ratio of 412, which corresponds to the addition product (**2b'** or **4b'**). Interestingly, The N-charged handle catalyst **1c** does not show such reactivity. A possible reason is that the large N-

substituent on **1c** leads to relatively large steric hindrance, which disfavors the nucleophilic attack. In addition, none of the investigated reactions provide charged species corresponding to the intermediates **3** or **3'** in the dimer mechanism, which indicates that our results also support the Breslow mechanism.

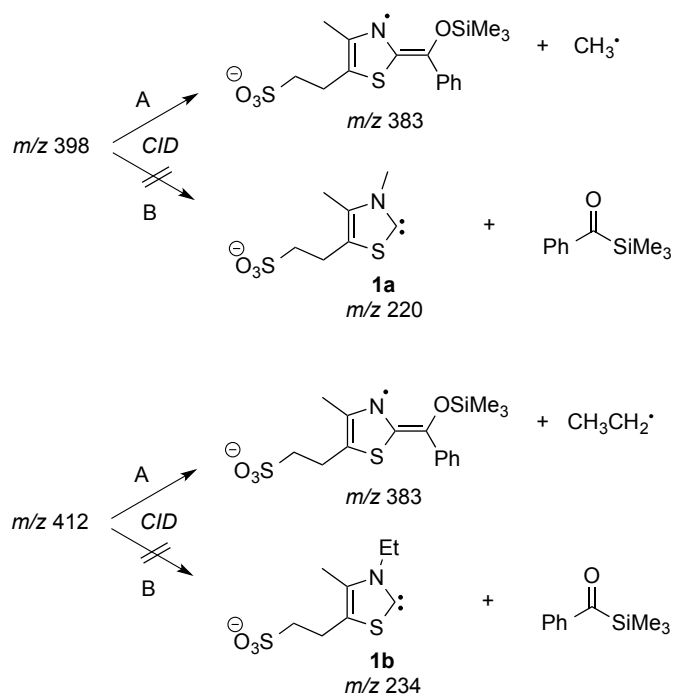
Table 3.2 Observations of thiazoylidene catalysts plus benzoyltrimethylsilane

Entry	Catalyst	2' or 4'	3'
1	1a	m/z 398 y ^b	m/z 309 n ^a
2	1b	m/z 412 y ^a	m/z 323 n ^a
3	1c	m/z 412 n ^a	m/z 323 n ^a

^a No such ion is observed. ^b Such ion is observed.

Our next task is to certain whether we have the oxyanion **2'** or the Breslow-like intermediate **4'**. The observed adduct m/z 398 and m/z 412 were isolated and fragmented by CID. CID of m/z 398 (**2a'** or **4a'**) yields m/z 383, corresponding to the loss of a methyl group. CID of m/z 412 (**2b'** or **4b'**) results a m/z ratio corresponding to the loss of an ethyl group (Scheme 3.5). These results imply that for both m/z 398 and m/z 412, CID results in loss of the *N*-alkyl substituent (Scheme 3.5, Paths A). This result seems to be more consistent with the sila-Breslow intermediate structure **3'**. The oxyanion structure **2'** would presumably dissociate back to catalyst **1** and benzoyltrimethylsilane upon CID (Scheme 3.5, Paths B). A detailed discussion with computational results is in **3.2.4**.

Scheme 3.5



3.3.3 Second step addition

Three aldehydes and three Michael acceptors were tested in the gas phase, (Figure 3.4) adding to the reaction system from leak valve together with benzoyltrimethylsilane. We expected to observe the addition reactions shown in Scheme 3.6. However, no reaction has been observed between the isolated silyl Breslow intermediate and these substrates, given the maximum reaction time 10 s. The results are summarized in Table 3.3.

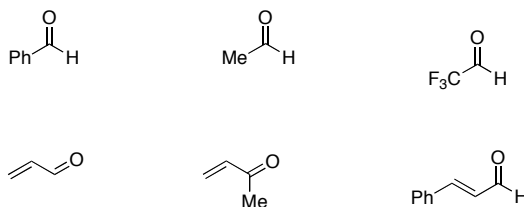
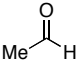
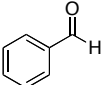
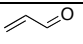
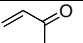
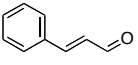
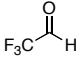
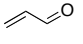
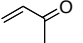
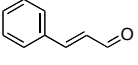
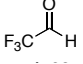


Figure 3.4 Substrates used to test the second step addition

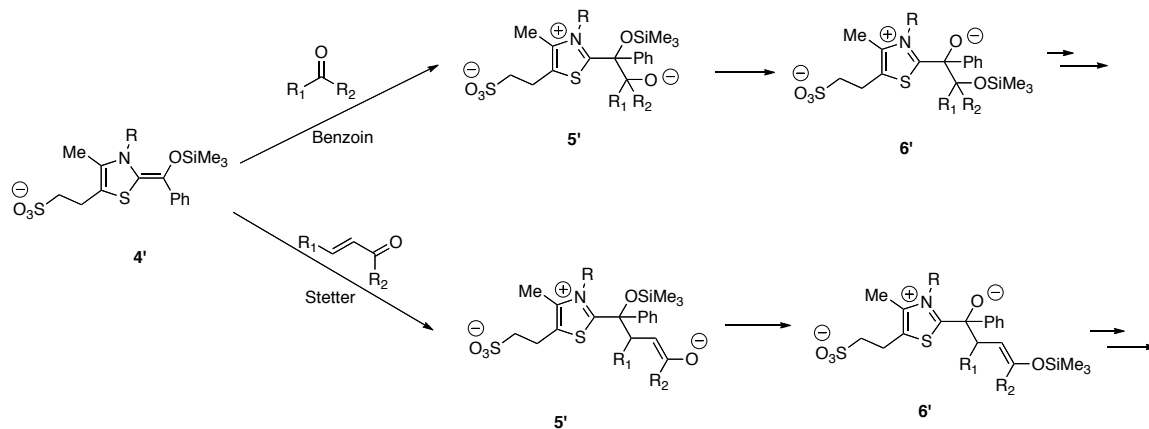
Table 3.3 Silyl Breslow intermediates nucleophilic attack to the Michael acceptors/aldehydes

Breslow intermediate	Michael acceptor/ aldehyde	Adduct
4a' m/z 398	 mw 44	m/z 442 (N)
4a' m/z 398	 mw 106	m/z 504 (N)
4a' m/z 398	 mw 56	m/z 454 (N)
4a' m/z 398	 mw 70	m/z 468 (N)
4a' m/z 398	 mw 132	m/z 530 (N)
4a' m/z 398	 mw 98	m/z 496 (N)
4b' m/z 412	 mw 56	m/z 468 (N)
4b' m/z 412	 mw 70	m/z 482 (N)
4b' m/z 412	 mw 132	m/z 544 (N)
4b' m/z 412	 mw 98	m/z 510 (N)

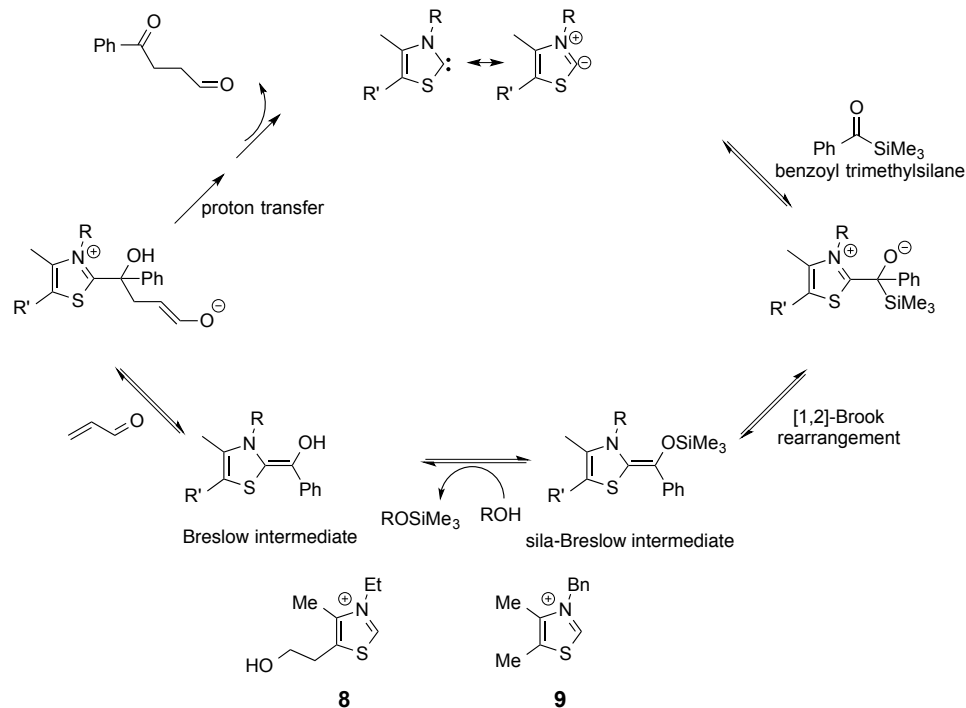
Why does the addition proceed in solution but not in the gas phase? Scheidt and coworkers^{108,109} proposed a mechanism for thiazoylidene catalyzed sila-Stetter reaction, in which the sila-Breslow intermediate is desilylated prior to the enone addition. Scheme 3.7 shows benzoyltrimethylsilane and acrolein as an example. In their work, they either used a catalyst with a hydroxyl moiety **8** or else added isopropanol. Tellingly, use of the catalyst **9** (which lacks the internal hydroxyl) without any isopropanol additive *resulted*

in no catalysis. Scheidt and coworkers therefore hypothesized that desilylation by hydroxyl (whether as a part of the catalyst or as an additive) was imperative for forward reaction. Our results provide further evidence supporting Scheidt's hypothesis that desilylation of the sila-Breslow intermediate precedes enone addition.

Scheme 3.6



Scheme 3.7



Under our gas phase experimental conditions, we did not see evidence of desilylation of the sila-Breslow intermediate. We tried adding isopropanol by vaporizing it with the methyl vinyl ketone, but still saw no reaction (neither desilylation nor reaction of the sila-Breslow intermediate with the enone is observed). In solution, the reaction mixture has the thiazolium pre-catalyst, a base (such as DBU), the acylsilane, enone and an alcohol additive. These conditions allow for the resultant sila-Breslow intermediate to, essentially, act as an alcohol silylating agent. Under our gas phase conditions, the alcohol additive does not appear to effect desilylation. It is known that alkoxides will effect gas phase desilylation, but we have not got a way presently, with our instrument, to effect deprotonation of the alcohol.^{110,111}

3.3.3 Calculation results

To better understand the mechanism of Stetter reaction/Benzoin condensation that might happen in the gas phase, we calculate the energy profile of several model reactions, mainly to study how the catalyst and substrate structure may affect each step the reactions.

3.3.3.1 Neutral thiazolium catalyzed Stetter reaction

First, we examine a simplified system as Scheme 3.8, where a small neutral thiazolium catalyst **1d** attacks benzaldehyde or benzoyltrimethylsilane to form the Breslow intermediate. Then the simplest Michael acceptor acrolein is attacked by the Breslow intermediate. After proton transfer or silyl migration and final regeneration of the catalyst, (transition states are omitted here) the final 1,4-dicarbonyl products are formed. The energy profiles are shown in Figure 3.5.

Scheme 3.8

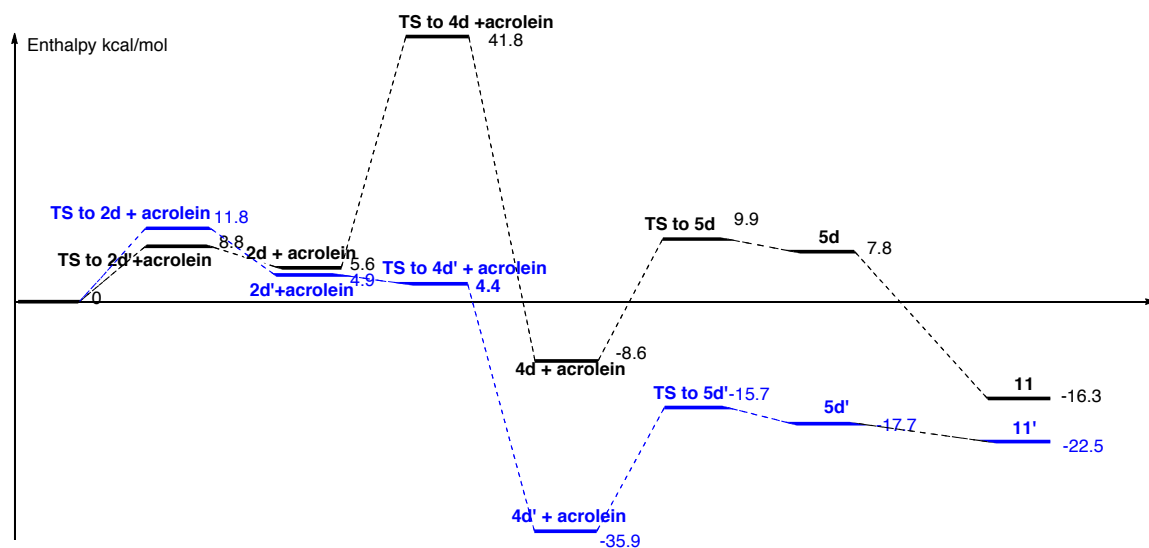
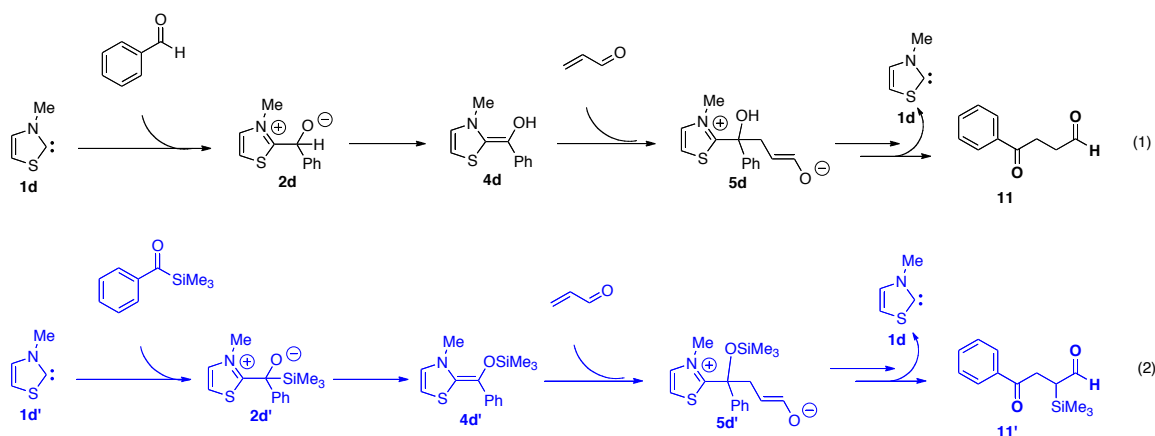


Figure 3.5 The energy profile of the simulated gas phase Stetter reactions shown in Scheme 3.8. Calculations were conducted at B3LYP/6-31+G(d) [ΔH at 298 K in kcal mol⁻¹].

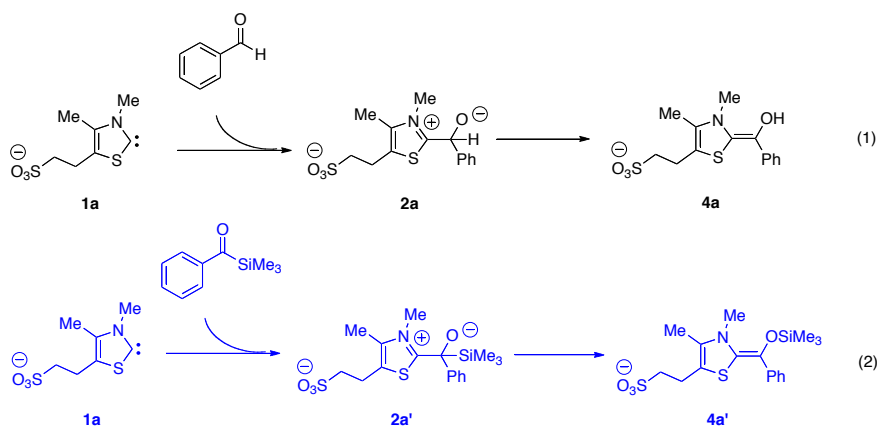
From the energy profile, the overall reaction is exothermic, regardless of the substrates. The formation of first tetrahedron intermediate **2d** and **3d'** is slightly endothermic, with a moderate barrier around 10 kcal/mol. reaction (1) bears a high barrier during the 1,2-proton shift before forming Breslow intermediate, making this

reaction almost impossible. The nearly barrier free 1,2-silyl shift in reaction (2) largely benefits the formation of Breslow intermediate a lot, after the first step addition. This calculation result supports our experimental result that the reactions of thiazoylidenes and benzaldehyde were not observed, while the silyl version is readily to occur.

2.3.3.2. Charged handle thiazolium catalyzed umpolung reaction-first step, formation of Breslow intermediate

With the simplest system calculation results in hand, we then examine the reactions of **1a**. (Scheme 3.9) The energy profiles (Figure 3.6) are similar to the correlating part of their neutral counterparts shown in Figure 3.5. By using charged handle thiazoliums, the formation of the first tetrahedron intermediate **2a** and **2a'** become slightly exothermic, which might be explained by the higher proton affinity (Figure 3.7) of carbene site when the negative charged handle is attached.

Scheme 3.9



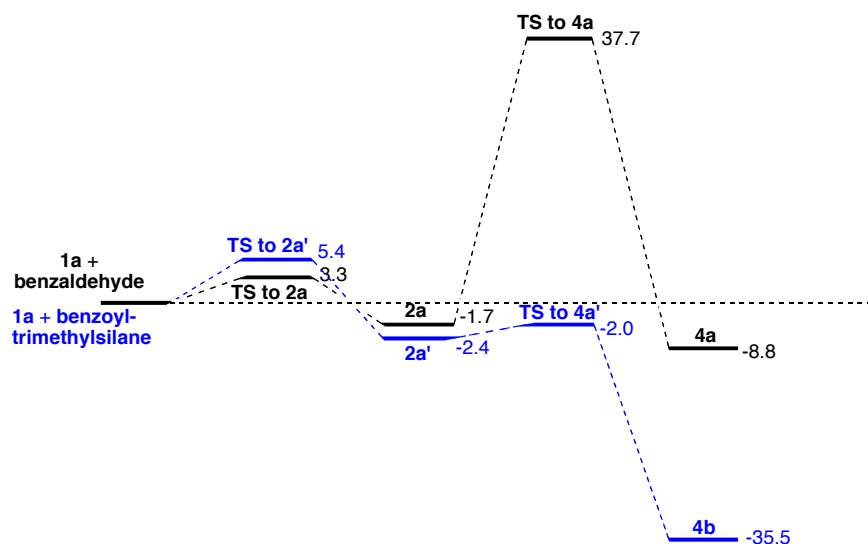


Figure 3.6 The energy profile of the formation of (silyl)Breslow intermediates via **1a**.

(Corresponding to Scheme 3.9) Calculations were conducted at B3LYP/6-31+G(d) [ΔH at 298 K in kcal mol⁻¹].

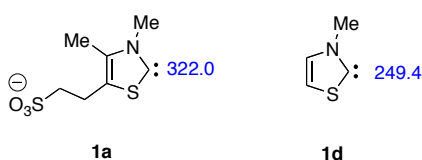


Figure 3.7 Proton affinity of thiazolium carbene site.

2.3.3.3. Charged handle thiazolium catalyzed Stetter reaction-second step addition

We conducted calculations to ascertain whether the sila-Breslow intermediate is less reactive toward enone addition than the non-silylated Breslow intermediate, as discussed in 3.3.2. Take the addition of **4a/4a'** to acrolein as a model, we find that the non-silylated Breslow intermediate has a lower barrier for enone addition than the sila-Breslow intermediate, by 13 kcal/mol. (Figure 3.8) Thus, Scheidt's proposal that desilylation of the sila-Breslow intermediate leads to a more favorable enone addition is supported by our results.

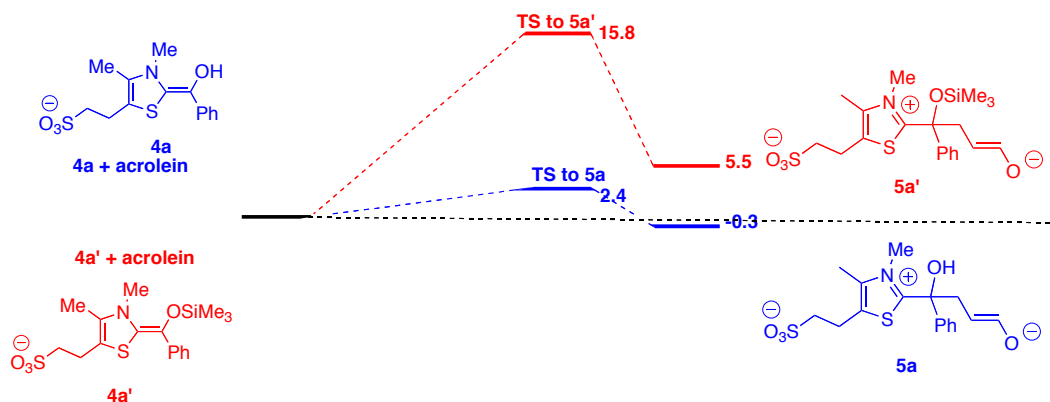
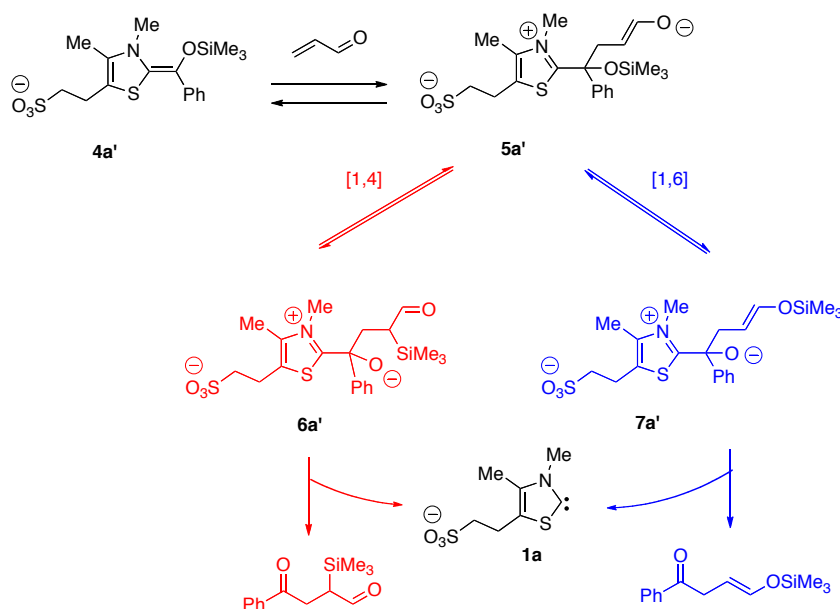


Figure 3.8 The energy profile of second step Michael addition. Red: silyl Stetter reaction. Blue: normal Stetter reaction. Calculations were conducted at B3LYP/6-31+G(d) [ΔH at 298 K in kcal mol⁻¹].

In a further effort to understand the pathways available to us under our gas phase conditions, we calculated the energetics of the possible paths of acrolein addition by **1a**. Acrolein addition results in the intermediate **5a'**. This intermediate could presumably undergo [1,4] O to C silyl migration (Scheme 3.10, red path) or [1,6] O to O silyl migration (Scheme 3.10, blue path).

Scheme 3.10



The profile is shown in Figure 3.9. Enthalpies are shown relative to the separated reactants; we indicate this "starting enthalpy" as "0.0" kcal/mol (indicated by dashed line). In the experiment, we isolate **4a'** in the ion trap, which is thermalized by collisions with the helium bath gas.¹¹² The first step, the formation of the [**4a'**•acrolein] complex, is calculated to be 9.3 kcal/mol exothermic (Figure 4). Subsequent addition would proceed via a TS that is 15.8 kcal/mol above the separated reactants, and therefore 25.1 kcal/mol above the [**3a'**•acrolein] complex. In situations such as this, it is unlikely that any forward reaction would be observed: in a competition between dissociating back to the separated reactants (+9.3 kcal/mol) versus addition (+25.1 kcal/mol), dissociation is the most likely path. Entropy also favors dissociation; this has been studied extensively in the gas phase, particularly for substitution reactions.¹¹³⁻¹¹⁵ In Figure 3.9, we show both [1,4] O to C (in red) and [1,6] O to O silyl migration (in blue). The pathway involving [1,4] O to C silyl migration is overall endothermic (red path), while the path for the [1,6] O to O silyl transfer (blue path) is exothermic by -1.5 kcal/mol. However, the reaction probably never proceeds beyond the first TS (labeled "TS"). Thus the calculations support the experimental observations, showing absence of reaction.

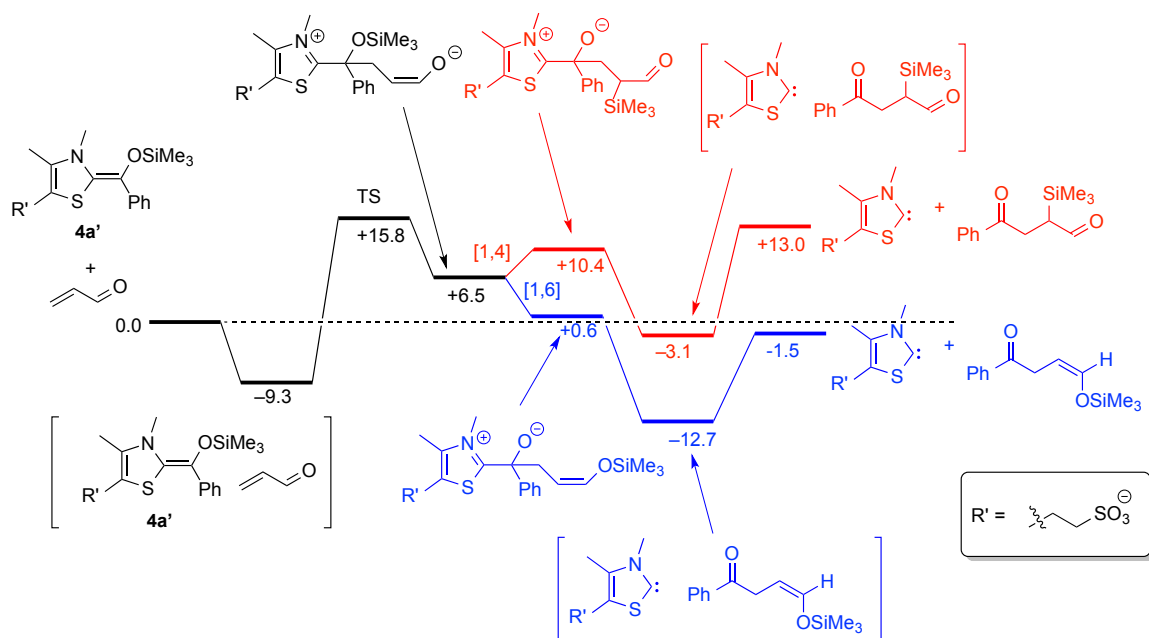
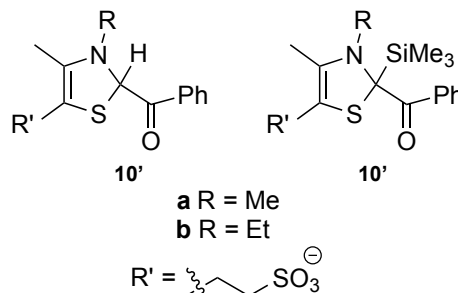


Figure 3.9 Possible pathways for the sila-Stetter. [1,4] O to C trimethylsilyl migration is in red and [1,6] O to O trimethylsilyl migration is in blue. Transition structures for the [1,4] and [1,6] migrations were not calculated. Calculations were conducted at B3LYP/6-31+G(d) [ΔH at 298 K in kcal mol⁻¹].

2.3.3.4. Possible structures of the adduct from benzoyltrimethylsilane and thiazoylidene

One possibility we considered is that rather than an oxyanion **2'** or Breslow intermediate **4'** structure, we have the ketone structure **10'**, which would also not be prone to further reaction. In a 2010 condensed phase study attempting to isolate the Breslow intermediate, Berkessel and coworkers found instead a ketone structure.^{74,116} Subsequent gas phase calculations by us confirmed the greater stability of ketone **10a** over the Breslow intermediate **4a** (by 7 kcal/mol).⁹⁵ To assess the possibility of a ketone structure, we calculated the relative stability of the sila-analog **10a'** as compared to its isomer, the corresponding Breslow intermediate **4a'**. We find that the ketone structure **10a'** is 23 kcal/mol *less* stable than the Breslow intermediate **4a'**. That is, unlike the proton analog **10a**, **10a'** is *not* more stable than the corresponding Breslow intermediate.

The sila-Breslow intermediate **3a'** is therefore the most stable calculated structure for m/z 398 and the lack of subsequent reaction may in fact be due to the unfavorability of the second addition.



3.4. Conclusion

We report herein the first study of the gas-phase *Umpolung* reaction of *N*-heterocyclic carbenes with carbonyl compounds. Although these types of reactions occur readily in solution, they do not appear to do so in the gas phase. Our experiments provide evidence to support the computational prediction that the first step to form the Breslow intermediate requires "shuttling" of the proton; a direct 1,2-proton transfer is not allowed. We overcome this issue by using an acylsilane. Direct 1,2-silyl transfer (Brook rearrangement) is allowed, and computations predict a low barrier to form the sila-Breslow intermediate. Our experimental results are consistent with sila-Breslow intermediate formation. Attempts to effect the Stetter reaction by adding enones are unsuccessful. Our computational and experimental results support Scheidt's hypothesis that desilylation of the sila-Breslow intermediate must occur for reaction to proceed. With this initial study in hand, we can now focus on developing methods, including instrument and experimental modifications, to examine further these types of NHC-catalyzed reactions in the gas phase.

Note: Major parts of the this chapter have been published: Teator, A J.; Tian, Y.; Chen, M.; Lee, J. K.; and Bielawski, C. W. " An Isolable, Photoswitchable N-Heterocyclic Carbene: On-Demand Reversible Ammonia Activation", *Angew. Chem. Int. Ed.* **2015**, 54, 1-6

Reprinted (adapted) with permission from Teator, A J.; Tian, Y.; Chen, M.; Lee, J. K.; and Bielawski, C. W. " An Isolable, Photoswitchable N-Heterocyclic Carbene: On-Demand Reversible Ammonia Activation", *Angew. Chem. Int. Ed.* **2015**, 54, 1-6
Copyright © 2015 WILEY-VCH Verlag GmbH & Co. KGaA, Weinheim (see the end of this dissertation for the permission)

Chapter 4 Computational Study of Photoswitchable Carbenes

4.1 Introduction

An attractive class of ligands for incorporating light-responsive groups is the *N*-heterocyclic carbenes (NHCs) as they have been used to support a broad range of organometallics and organocatalysts.¹¹⁷⁻¹²¹ As the activity and selectivity displayed by NHC-based catalysts are intrinsically linked to the electronic properties of the supporting NHCs, structural modulation of the ligands has been intensely pursued.¹²²⁻¹²⁵

Recently a photoswitchable NHC scaffold was developed by incorporating a photochromic¹²⁶ dithienylethene (DTE)¹²⁷⁻¹³¹ moiety into an imidazolyliene backbone, and found that the corresponding carbene functioned as a photoswitchable organocatalyst that facilitated transesterifications and transamidations¹³² as well as ring-opening polymerizations.¹³³ Similarly, a rhodium catalyst bearing the same DTE functionalized NHC was found to catalyze alkene and alkyne hydroborations.¹³⁴ All of these catalysts

were effectively switched between “off” (inactive, ring closed) and “on” (active, ring open) states by irradiation with UV or visible light, respectively. (Figure 4.1)

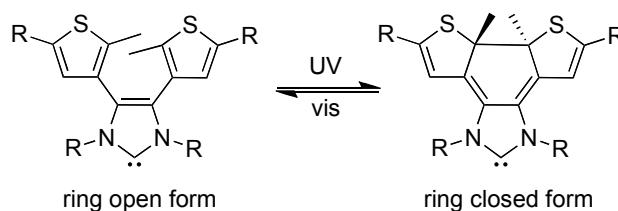


Figure 4.1 Photoswitchable carbene switching between two forms by UV or visible light

This invoked our interest in the role of the ring structure: how could the ring structure modulate the reactivity of the carbene site? Or, how could the ring structure affect the electronic property of the carbenic carbon? We therefore took advantage of computational methods to study the electronic structure of the two different states of the photoswitchable carbene.

4.2. Computational Methods

All calculations were performed using density functional theory as implemented in Gaussian09.⁴⁴ Geometries were fully optimized at the B3LYP/6-31G(d) level of theory and frequencies were calculated; no scaling factor was applied.¹³⁵⁻¹³⁹ The optimized structures have no negative frequencies. The temperature for the calculations was 298 K. For the ¹³C NMR resonances of the carbenic carbon for 1o and 1c, the methodology of Tantillo and Rablen was used;¹⁴⁰⁻¹⁴⁴ chemical shifts were calculated using scaling factors of -0.9679 (slope) and 190.427 (intercept). The NMR calculations (Gauge-Independent Atomic Orbital (GIAO)) were performed as a single point at the B3LYP/6-31+G(d,p) level of theory in benzene.^{145,146} The integral equation formalism variant of the

polarizable continuum model, using radii and non-electrostatic terms for Truhlar and coworkers' SMD solvation model, was utilized.¹⁴⁷⁻¹⁴⁹

4.3. Results and discussion

Two model carbenes studied herein are shown in Figure 4.2. **Me_o** and **Ar_o** are ring open carbenes; **Me_c** and **Ar_c** are the corresponding ring closed form.

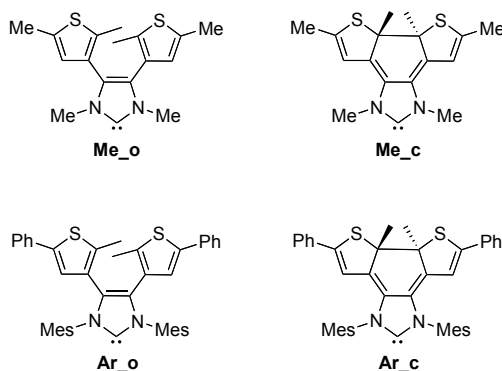


Figure 4.2 model photoswitchable carbene studied herein

4.3.1 ^{13}C NMR of photoswitchable carbenes

The ^{13}C NMR resonances of the carbene nuclei for **Ar_o** and **Ar_c** in C_6D_6 were calculated to be 224 ppm and 252 ppm, respectively. The more deshielded carbene nuclei on **Ar_c** indicates the more electrophilic nature of this carbene.

4.3.2 Molecular orbitals of photoswitchable carbenes

Calculated HOMO/LUMO coefficients on carbenic carbon are listed in Table 4.1. HOMO/LUMO visualization is shown in Figure 4.3 and Figure 4.4.

As compared to the ring-opened structure, the corresponding ring-closed structure always has a smaller HOMO coefficient (absolute value) on carbenic carbon. From the visualization of the HOMO of the carbenes, it is quite obvious that the electron density

shifts away from the carbenic carbon upon ring-closure. As expected, the ring-closed structure has less electron density at the carbene center, comparing to the ring-opened structure.

Comparing to the ring-opened structure, the corresponding ring-closed structure always has a Larger LUMO coefficient (absolute value) on carbenic carbon. From the visualization of the LUMO of the carbenes, the rich component of orbital is on the carbenic carbon in ring-closed form. It probably indicates that the ring-closed form has better ability to accept electrons.

Table 4.1 HOMO/LUMO Coefficient of Carbenic Carbon

Structures	MO Coefficient of Carbenic Carbon	
	HOMO	LUMO
Me_o	0.57733 (3s) ^a	0.03076 (2py), 0.04724 (3s), 0.01826 (3py) ^a
	1.65502 (sum) ^b	0.11923 (sum) ^b
Me_c	0.01236 (4dxz) ^a	-0.19794 (2pz) ^a , -0.17790 (3pz) ^a
	0.02421 (sum) ^b	0.41330 (sum) ^b
Ar_o	-0.15539 (2pz) ^a	0.01275 (2py) ^a
	0.28524 (sum) ^b	0.03314 (sum) ^b
Ar_c	0.01092 (4dxz) ^a	-0.16186 (2pz), -0.13770 (3pz) ^a
	0.02054 (sum) ^b	0.31453 (sum) ^b

^a The largest coefficient(s) among the atomic orbitals of the carbenic carbon are presented here. Since the other atomic orbitals have substantially smaller coefficients, the largest coefficient(s) among the atomic orbitals is used to represent the contribution of the carbenic carbon to the HOMO/LUMO of the molecule. The name of the atomic orbital that has the largest coefficient is in the parenthesis.

^b The sum of absolute values of HOMO/LUMO coefficients on carbenic carbon.

As discussed in Chapter 1, one of the key steps of NHC catalyzed reactions is the nucleophilic attack to the carbonyl group. Thus, the more electrophilic ring-closed structures have no reactivity in these reactions.

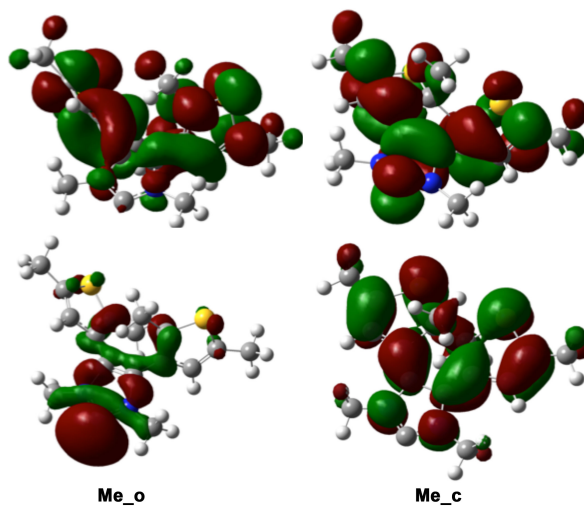


Figure 4.3 HOMO (bottom) and LUMO (top) visualization of Me_o and ring-closed analogue Me_c. Molecular orbitals were generated with an isovalue of 0.02.

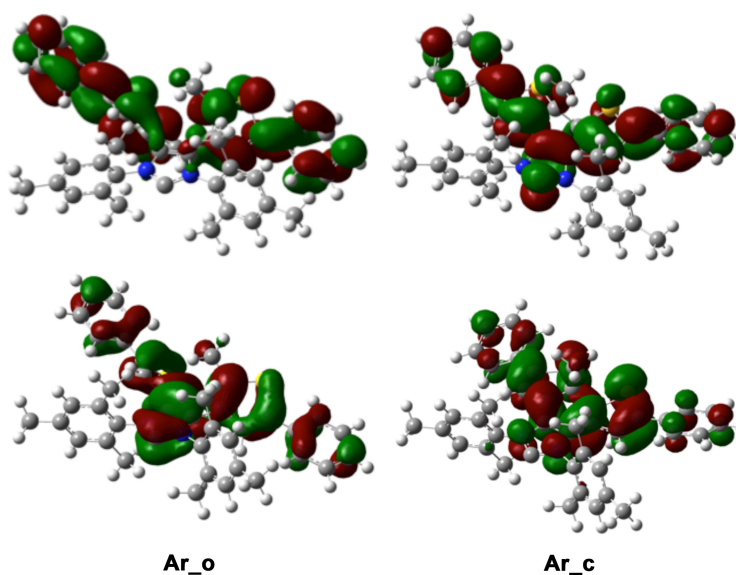


Figure 4.4 HOMO (bottom) and LUMO (top) visualization of Ar_o and ring-closed analogue Ar_c. Molecular orbitals were generated with an isovalue of 0.02.

4.4. Conclusion

We compared the electronic structure of two different forms of the photoswitchable carbenes by calculating the ^{13}C NMR of carbenic carbon and the MO of the molecules. The ring closure shifts electron density away from the carbene center, thus deactivates the NHC in catalysis. This study helps reveal the electronic structure – reactivity relationship of NHCs.

Note: Major parts of the this chapter have been published: Michelson, A. Z.; Rozenberg, A.; Tian, Y.; Sun, X.; Davis, J.; Francis, A. W.; O'Shea, V. L.; Halasyam, M.; Manlove, A. H.; David, S. S.; Lee, J. K. "Gas-Phase Studies of Substrates for the DNA Mismatch Repair Enzyme MutY," *J. Am. Chem. Soc.*, **2012**, 134, 19839-19850.

Reprinted (adapted) with permission from Michelson, A. Z.; Rozenberg, A.; Tian, Y.; Sun, X.; Davis, J.; Francis, A. W.; O'Shea, V. L.; Halasyam, M.; Manlove, A. H.; David, S. S.; Lee, J. K. "Gas-Phase Studies of Substrates for the DNA Mismatch Repair Enzyme MutY," *J. Am. Chem. Soc.*, **2012**, 134, 19839-19850. Copyright 2012 American Chemical Society (see the end of this dissertation for the permission)

Chapter 5 Gas Phase Studies of Adenine Analogs: Implications for Adenine Removal by MutY

5.1. Introduction

As discussed in the first chapter, cells have multi mechanisms to repair different types of DNA damage. 8-oxoguanine (OG) is one of most common lesions caused by oxidation of guanine (G).¹⁵⁰⁻¹⁵² In DNA replication, OG may pair up with adenine (A)¹⁵³ instead of cytosine (C) (Table 5.1), therefore causing the G:C → T:A transversion mutation.

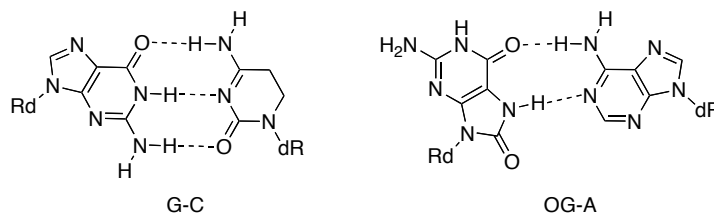


Figure 5.1 The normal G:C base pair and the mismatch OC:A base pair

In *E. coli*, multi enzymes are responsible for OG damage repair, among which MutY is unusual: instead of working on OG itself, it catalyzes the removal of A from OG:A mismatch, but leaves the normal base pair T:A untouched.^{34,154,155}

It was shown in kinetic isotope effect study that the nucleobase scission is S_N1 type,¹⁵⁶⁻¹⁵⁸ in which the leaving group ability of nucleobase (in particular, the N9 acidity) plays an important role in the scission rate as well as the MutY mechanism.

Therefore, we studied the thermochemical properties of a series of synthetic adenine analogues as MutY substrates¹⁵⁹⁻¹⁶¹ computationally and experimentally in the gas phase, hoping to reveal the MutY mechanism. Figure 5.2 shows the structures studied herein. 7-Deazaadenine (Z, **1**) and 1-deazaadenine (Z1, **2**) are missing nitrogen at the N7 and N1 positions, respectively (as compared to the parent adenine), to test the effect of nitrogens,^{159,161} and were designed to test the importance of the nitrogen at those positions. Substrates **B** (**3**) and **Q** (**4**) are nonpolar isosteres of adenine.¹⁶⁰

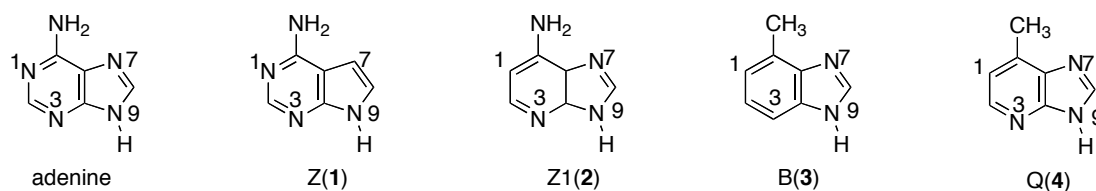


Figure 5.2 Adenine and synthetic analogs studied herein

5.2. Experimental section

All the chemicals were commercially available and were used as received.

5.2.1 Bracketing method

Proton affinities and acidities of MutY substrates were measured by bracketing method described as before, via a Finnigan 2001 duel cell Fourier Transform Ion Cyclotron Resonance Mass Spectrometer (FT-ICR MS).

5.2.2 Cook's kinetic method

Cook's kinetic method was also used to measure the proton affinities and acidities of the substrates on the LCQ instrument. Typically, a 1 mM substrate/reference solution in methanol was used to generate the proton-bound substrate-reference heterodimers. The dimers were introduced into LCQ via ESI, and then dissociated by collision-induced dissociation (CID). The dimers were activated for 30 ms, and the dissociation products were detected. The intensities of products were recorded to provide their relative abundance. A total of 20 scans were averaged for each reaction.

5.2.3 Calculations

Calculations are conducted at B3LYP/6-31+G(d) using Gaussian09.⁴⁴ The geometries are fully optimized and frequencies are calculated. No scaling factor is applied. All the values reported are ΔH at 298 K.

5.3. Results

The gas phase proton affinities and acidities of MutY substrates were studied computationally and experimentally.

5.3.1 Calculation of MutY substrates proton affinities and acidities

The tautomers of each MutY substrate were calculated. For the most stable tautomers and the ones less than 10 kcal/mol above, all acidic and basic sites were calculated. (The calculation was conducted by Dr. Anna Michelson). Figure 5.3 shows the calculated numbers.

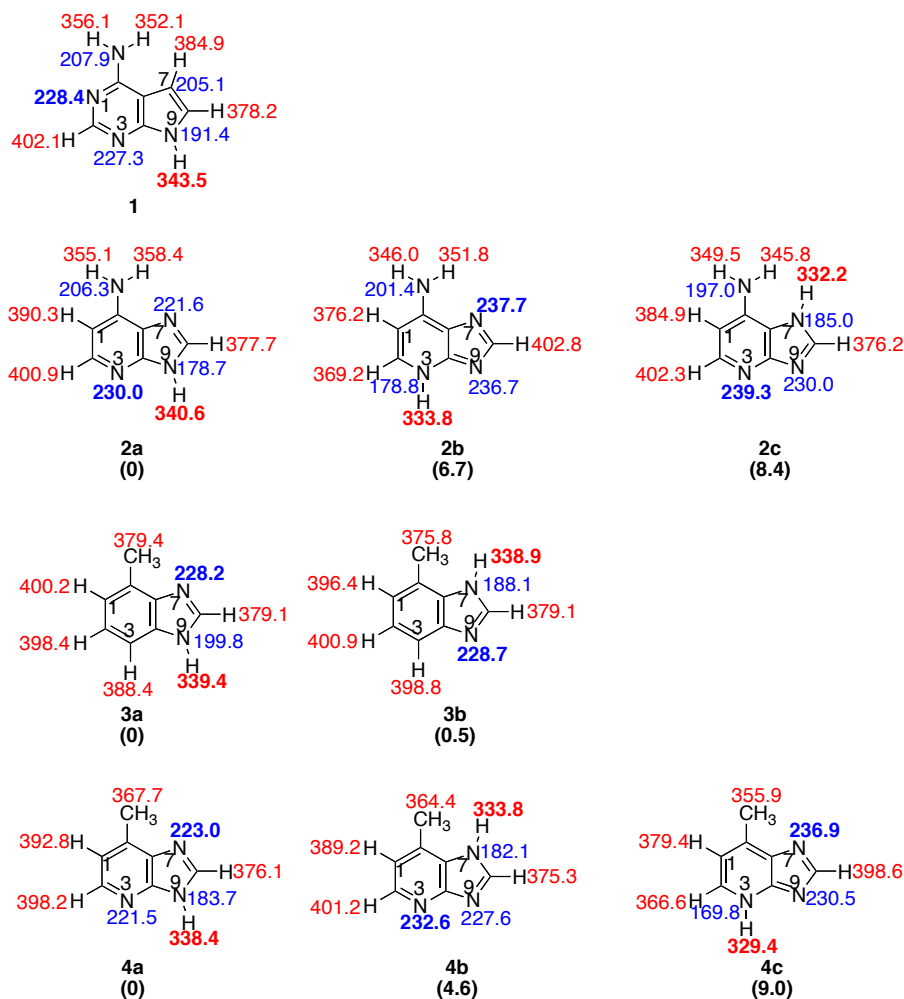


Figure 5.3 The most stable tautomers of MutY substrates and the thermodynamic values.

Proton affinities are labeled in blue; acidities in red. The most basic sites and most acidic sites are in bold.

5.3.2 7-Deazaadenine (Z, 1) measurements

The acidity of Z was measured using acidity bracketing (details in the Methods section). The conjugate base of Z deprotonates butyric acid ($\Delta H_{\text{acid}} = 346.8 \pm 2.0 \text{ kcal mol}^{-1}$); the reaction in the opposite direction (butyrate with Z) also occurs (Table 5.1). We therefore bracket the ΔH_{acid} of Z as $347 \pm 3 \text{ kcal} \cdot \text{mol}^{-1}$.

In bracketing the PA of Z, piperidine ($\text{PA} = 228.0 \pm 2.0 \text{ kcal} \cdot \text{mol}^{-1}$) deprotonates protonated Z; the opposite reaction (Z deprotonating protonated piperidine) also occurs (Table 5.2). Therefore the PA of Z was measured to be $228 \pm 3 \text{ kcal} \cdot \text{mol}^{-1}$.

Table 5.1 Summary of results for acidity bracketing of Z (7-deazaadenine, 1)

<i>Reference compound</i>	ΔH_{acid}^a	<i>Proton transfer</i> ^b	
		<i>Ref. acid</i>	<i>Conj. base</i>
<i>m</i> -cresol	349.5 ± 2.1	—	+
acetic acid	347.4 ± 0.5	—	+
butyric acid	346.8 ± 2.0	+	+
formic acid	346.0 ± 0.5	+	—
methacrylic acid	344.1 ± 2.9	+	—
methyl cyanoacetate	340.80 ± 0.60	+	—

^a Acidities are in $\text{kcal} \cdot \text{mol}^{-1}$.^{162,163} ^b A “+” indicates the occurrence and a “—” indicates the absence of proton transfer.

Table 5.2 Summary of results for proton affinity bracketing of Z (7-deazaadenine, **1**)

<i>Reference compound</i>	<i>PA^a</i>	<i>Proton transfer^b</i>	
		<i>Ref. base</i>	<i>Conj. acid</i>
1-methylpiperidine	232.1±2.0	+	–
1-methylpyrrolidine	230.8±2.0	+	–
piperidine	228.0±2.0	+	+
pyrrolidine	226.6±2.0	–	+
3-picoline	225.5±2.0	–	+

^a PAs are in kcal·mol^{–1}. ¹⁶² ^b A “+” indicates the occurrence and a “–” the absence of proton transfer.

5.3.3 1-Deazaadenine (Z1, **2**) measurements

Efforts to sublime Z1 into the gas phase for acidity and proton affinity bracketing were unsuccessful; we failed to see signal corresponding to the substrate. However, the acidity and proton affinity was successfully measured using an alternative to bracketing: the Cooks kinetic method (details in the Methods). For the acidity measurement, five reference acids were used (2-fluorobenzoic acid, $\Delta H_{\text{acid}} = 338.0 \pm 2.2$ kcal mol^{–1}; 3-hydroxybenzoic acid, $\Delta H_{\text{acid}} = 338.6 \pm 2.1$ kcal mol^{–1}; benzoic acid, $\Delta H_{\text{acid}} = 340.2 \pm 2.2$ kcal mol^{–1}; phenylacetic acid, $\Delta H_{\text{acid}} = 341.5 \pm 2.1$ kcal·mol^{–1}; and glycine, $\Delta H_{\text{acid}} = 342.7 \pm 2.2$ kcal·mol^{–1}), yielding an acidity (ΔH_{acid}) of 341 ± 3 kcal·mol^{–1}. For the PA by measurement, six reference bases were used: guanine (PA = 229.3 ± 2.0 kcal·mol^{–1}), N-methylpyrrolidine (PA = 230.8 ± 2.0 kcal·mol^{–1}), 2,4-lutidine (PA = 230.1 ± 2.0 kcal mol^{–1}), dimethylisopropylamine (PA = 232.0 ± 2.0 kcal·mol^{–1}), N-methylpiperidine (PA

= $232.1 \pm 2.0 \text{ kcal}\cdot\text{mol}^{-1}$), and triethylamine (PA = $234.7 \pm 2.0 \text{ kcal}\cdot\text{mol}^{-1}$). The PA for Z1 was measured to be $232 \pm 3 \text{ kcal}\cdot\text{mol}^{-1}$.

5.3.4 “6-Methylated” 1,3-Deazaadenine (B, 3)

The acidity of B was bracketed as shown in Table 5.3. The reaction of deprotonated B with methyl cyanoacetate ($\Delta H_{\text{acid}} = 340.80 \pm 0.60 \text{ kcal}\cdot\text{mol}^{-1}$) occurs; however, deprotonated methyl cyanoacetate cannot deprotonate B. Deprotonated B cannot deprotonate 2,4-pentadione ($\Delta H_{\text{acid}} = 343.8 \pm 2.1 \text{ kcal}\cdot\text{mol}^{-1}$), but deprotonated 2,4-pentadione does deprotonate B. We therefore bracket the acidity of B to be $343 \pm 3 \text{ kcal}\cdot\text{mol}^{-1}$.

The PA of B was measured using bracketing (Table 5.4). We find that the reaction with piperidine (PA = $228.0 \pm 2.0 \text{ kcal}\cdot\text{mol}^{-1}$) occurs in both directions (piperidine deprotonates protonated B, and B deprotonates protonated piperidine). We therefore measure the PA of B as $228 \pm 3 \text{ kcal}\cdot\text{mol}^{-1}$.

Table 5.3 Summary of Results for Acidity Bracketing of B (3)

<i>Reference compound</i>	ΔH_{acid}^a	<i>Proton transfer</i> ^b	
		<i>Ref. acid</i>	<i>Conj. base</i>
methacrylic acid	344.1 ± 2.9	—	+
2,4-pentanedione	343.8 ± 2.1	—	+
methyl cyanoacetate	340.80 ± 0.60	+	—
trifluoro- <i>m</i> -cresol	339.2 ± 2.1	+	—
malononitrile	335.8 ± 2.1	+	—

^a Acidities are in kcal mol^{-1} .^{162,163} ^b A “+” indicates the occurrence and a “—” indicates the absence of proton transfer.

Table 5.4 Summary of Results for Proton Affinity Bracketing of B (3)

<i>Reference compound</i>	<i>PA^a</i>	<i>Proton transfer^b</i>	
		<i>Ref. base</i>	<i>Conj. acid</i>
1-methylpiperidine	232.1 ± 2.0	+	–
1-methylpyrrolidine	230.8 ± 2.0	+	–
piperidine	228.0 ± 2.0	+	+
pyrrolidine	226.6 ± 2.0	–	+
3-picoline	225.5 ± 2.0	–	+

^a PAs are in kcal mol⁻¹. ¹⁶² ^b A “+” indicates the occurrence and a “–” indicates the absence of proton transfer

5.3.5 “6-Methylated” 1-Deazaadenine (Q, 4) measurement

The acidity of Q was bracketed as shown in Table 5.5. The reaction of deprotonated Q with methyl cyanoacetate ($\Delta H_{\text{acid}} = 340.80 \pm 0.60 \text{ kcal}\cdot\text{mol}^{-1}$) occurs, as does the reverse reaction (deprotonated methyl cyanoacetate with Q). Therefore the acidity of Q was bracketed as $341 \pm 2 \text{ kcal}\cdot\text{mol}^{-1}$.

The proton affinity of Q was bracketed as shown in Table 5.6. The results are somewhat unusual, in that reaction was found to occur in both directions for reference bases with PAs from piperidine ($228.0 \pm 2.0 \text{ kcal}\cdot\text{mol}^{-1}$) to 3-picoline ($225.5 \pm 2.0 \text{ kcal}\cdot\text{mol}^{-1}$).

Table 5.5 Summary of results for acidity bracketing of Q (4)

<i>Reference compound</i>	ΔH_{acid}^a	<i>Proton transfer^b</i>	
		<i>Ref. acid</i>	<i>Conj. base</i>
formic acid	346.0 ± 0.5	—	+
methacrylic acid	344.1 ± 2.9	—	+
2,4-pentanedione	343.8 ± 2.1	—	+
methyl cyanoacetate	340.80 ± 0.60	+	+
trifluoro- <i>m</i> -cresol	339.2 ± 2.1	+	—
2-chloropropanoic acid	337.0 ± 2.1	+	—

^a Acidities are in kcal mol⁻¹.^{162,163} ^bA “+” indicates the occurrence and a “—” indicates the absence of proton transfer.

Table 5.6 Summary of results for proton affinity bracketing of Q (4)

<i>Reference compound</i>	PA^a	<i>Proton transfer^b</i>	
		<i>Ref. base</i>	<i>Conj. acid</i>
1-methylpiperidine	232.1 ± 2.0	+	—
1-methylpyrrolidine	230.8 ± 2.0	+	—
piperidine	228.0 ± 2.0	+	+
pyrrolidine	226.6 ± 2.0	+	+
4-picoline	226.4 ± 2.0	+	+
3-picoline	225.5 ± 2.0	+	+
pyridine	223.8 ± 2.0	—	+
n-octylamine	222.0 ± 2.0	—	+

^a PAs are in kcal mol⁻¹.¹⁶² ^bA “+” indicates the occurrence and a “—” indicates the absence of proton transfer.

5.4. Discussion

The calculated acidity and proton affinity values for all the substrates studied herein are summarized in Table 5.7. Generally, B3LYP/6-31+G(d) appears to provide fairly accurate predictions for the thermochemical values. The one instance where the calculated and experimental data are quite disparate is for the proton affinity of Q: the calculated value for the most stable tautomer is $223.0 \text{ kcal}\cdot\text{mol}^{-1}$, yet the bracketing experiment yields a wide range where proton transfer occurs in both directions (PAs from 225.5 to $228.0 \text{ kcal}\cdot\text{mol}^{-1}$, Table 5.6). This is a fairly significant discrepancy.

Table 5.7 Calculated (B3LYP/6-31+G(d); 298 K) and experimental data

	Substrate	Calculated values	Experimental values ^b
ΔH_{acid}^a	Z (1)	343.5	347
	Z1 (2)	340.6	(341)
	B (3)	339.4	343
	Q (4)	338.4	341
PA^a	Z (1)	228.4	228
	Z1 (2)	230.0	(232)
	B (3)	228.2	228
	Q (4)	223.0	223.8-230.8

^a ΔH_{acid} and PA values are in kcal mol^{-1} . ^bNon-parenthetical experimental value is from bracketing measurement; Cooks kinetic method value is in parentheses. Error is $\pm 3\text{--}4 \text{ kcal}\cdot\text{mol}^{-1}$.

The wide range of proton transfer in both directions for the PA bracketing of Q (Table 5.6) raises the possibility that, under our conditions, we have a mixture of the two most stable Q tautomers (**4a** and **4b**), and the more basic **4b** (calculated PA of $232.6 \text{ kcal}\cdot\text{mol}^{-1}$) influences the experimentally observed value. Although the B3LYP/6-

31+G(d) calculations indicate that **4b** is nearly 5 kcal mol⁻¹ less stable than **4a**, prior studies show that accurate calculations of nucleobase tautomer stabilities can be elusive.¹⁶⁴⁻¹⁶⁸ It is possible that **4b** is less stable than **4a** but perhaps not by as much as the calculations indicating, such that there is some **4b** present in our experiments.

For the PA bracketing experiment, the solid **4** is sublimed into the gas phase via a solids probe (typical pressure in the instrument is 10⁻⁷ – 10⁻⁸ Torr, and the probe is heated to a temperature of roughly 400 K). If only **4a** were present, one would expect a bracketed PA of around 223 kcal mol⁻¹, based on the calculations (Figure 5.3, Table 5.7). The bracketing table would have a “crossover point” near pyridine (Table 5.8).

Table 5.8 *Hypothetical* bracketing table if only **4a** were present

<i>Reference compound</i>	<i>PA^a</i>	<i>Proton transfer^b</i>	
		<i>Ref. base</i>	<i>Conj. acid</i>
1-methylpiperidine	232.1 ± 2.0	+	–
1-methylpyrrolidine	230.8 ± 2.0	+	–
piperidine	228.0 ± 2.0	+	–
pyrrolidine	226.6 ± 2.0	+	–
4-picoline	226.4 ± 2.0	+	–
3-picoline	225.5 ± 2.0	+	–
pyridine	223.8 ± 2.0	–	+
n-octylamine	222.0 ± 2.0	–	+

If only **4b** were present, one would expect a similar table, except the “crossover point” would be near the PA of the most basic site of **4b**, which is calculated to be 232.6 kcal mol⁻¹ (Figure 5.3). Instead, as can be seen in Table 6, there is not a clean crossover

point, but rather a range in which the deprotonation reaction occurs in both directions. We suspect that the reason for this is that both tautomers **4a** and **4b** are present.

In the reactions of a reference base with protonated **4**, if both tautomers were present, then the protonated substrate should be a mixture of **4aH⁺** and **4bH⁺** (Figure 9). Under these conditions, any reference base with a proton affinity greater than or equal to 223.0 kcal·mol⁻¹ should deprotonate **4a**. Consistent with this expectation, we do observe proton transfer for all the reference bases from 3-picoline (PA = 225.5 kcal·mol⁻¹) to 1-methylpiperidine (PA = 232.1 kcal·mol⁻¹, Table 6, “ref base” column). In the opposite direction, the protonated reference bases are allowed to react with **4**. If both **4a** and **4b** were present, we would expect reaction with any protonated reference base with a PA of about 232 kcal mol⁻¹ or less, because **4b** has a calculated PA of 232.6 kcal mol⁻¹ (Figure 5.4). We actually see proton transfer “turn on” at a slightly lower value, 228.0 kcal mol⁻¹ (at piperidine; Table 5.6, “conj acid” column). Still, this value is much higher than the calculated PA of **4a** (223.0 kcal mol⁻¹), pointing to the probable presence of **4b**.

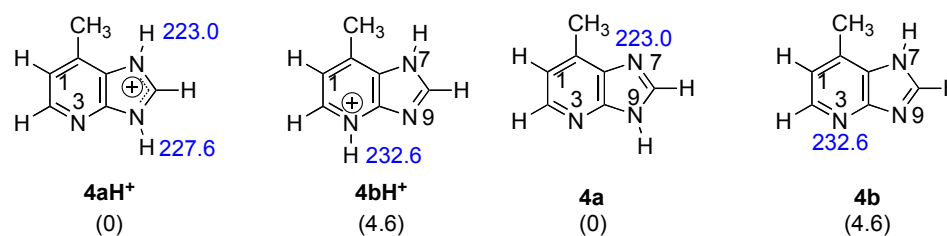


Figure 5.4 Structures of **4a**, **4b**, **4aH⁺**, and **4bH⁺** and calculated proton affinities. Relative stabilities of the two neutral tautomers are shown in parentheses. Calculations were conducted at B3LYP/6-31+G(d) [ΔH at 298 K in kcal mol⁻¹].

We suspect that the proton transfer “turning on” at a slightly lower value than calculated may be due to a mixture in which **4a** predominates, with less of **4b**. In this bracketing experiment, in order to ascertain whether proton transfer occurs, we measured

the kinetics of the proton transfer. We tracked the disappearance of the protonated reference base signal under pseudo-first-order conditions (excess of **4**). We can measure the pressure of **4**, but do not know what percentage of this pressure corresponds to **4b** versus **4a**. Therefore, for those protonated reference bases that only react with **4b**, we measure a rate constant for proton transfer that is less than the actual rate constant, because we can only measure the overall pressure of **4**, but only **4b** reacts. Our PA bracketing results are therefore consistent with a mixture of **4a** and **4b**, with **4a** predominating.

We should also address the bracketed acidity measurement of Q. Tautomer **4a** has a calculated acidity of $338.4 \text{ kcal}\cdot\text{mol}^{-1}$; tautomer **4b**, $333.8 \text{ kcal}\cdot\text{mol}^{-1}$. The measured value is $341 \text{ kcal}\cdot\text{mol}^{-1}$, which implies the presence of tautomer **4a** but not **4b**. However, as we discuss above, we believe both tautomers are present. So why do we measure an acidity consistent with **4a** only?

The deprotonation of both **4a** and **4b** results in the same anion, which is allowed to react with reference acids (Figure 5.5). This anion should be able to deprotonate any reference acid with $\Delta H_{\text{acid}} \approx 338 \text{ kcal mol}^{-1}$ or less. Experimentally, we do see proton transfer “turn on” in this region, starting with methyl cyanoacetate ($\Delta H_{\text{acid}} = 340.8 \text{ kcal mol}^{-1}$, Table 5.5, “ref acid” column).

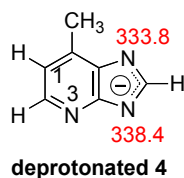


Figure 5.5 Structure of deprotonated **4a** and **4b** and calculated acidities. Calculations were conducted at B3LYP/6-31+G(d) [ΔH at 298 K in kcal mol^{-1}].

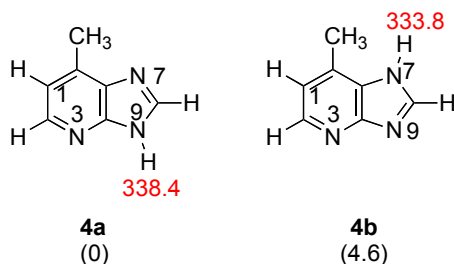


Figure 5.6 Structures of **4a** and **4b** and calculated acidity of the most acidic site.

Relative stabilities of the two neutral tautomers are shown in parentheses. Calculations were conducted at B3LYP/6-31+G(d) [ΔH at 298 K in kcal mol⁻¹].

In the opposite direction, deprotonated reference acids would be allowed to react with **4**, which is presumably a mixture of **4a** and **4b** (Figure 5.6). In this direction, one would expect to see reaction with any deprotonated reference acid whose ΔH_{acid} is 334 kcal mol⁻¹ or higher (since **4b** is present). Instead, however, we do not see proton transfer “turn on” until 340.8 kcal·mol⁻¹ (Table 5.5, “conj base” column). We believe that two factors are at play: one, as we saw with the PA experiments, we have less **4b** present, so reactions with **4b** will appear slower than they are. Second, we cannot preclude basecatalyzed tautomerization of **4b** to **4a** taking place during the bracketing experiment (Figure 5.7; brackets indicate ion–molecule complexes; A⁻ is the deprotonated reference acid). In Figure 5.7, we show the reaction of a deprotonated reference acid A⁻ with **4b**. In this Figure, the reference acid has $\Delta H_{\text{acid}} = 336$ kcal·mol⁻¹, which is a higher value than the ΔH_{acid} of **4b**, so proton transfer occurs to form deprotonated **4**. However, if a subsequent proton transfer takes place (whereby the N9⁻ of deprotonated **4**, whose conjugate acid has an acidity of 338.4 kcal·mol⁻¹, deprotonates AH), then **4a** and A⁻ are formed as products (Figure 5.7). Proton transfer between **4b** and A⁻ has occurred, but since we only track the m/z ratio of A⁻, we would have no way of knowing that proton

transfer occurred. The exothermic scenario shown in Figure 5.7 would look, by mass spectrometry, as if no proton transfer has taken place: one would only see A^- signal when following the reaction progress. This would therefore be marked as a “—” in the last column of Table 5.5, even though proton transfer has occurred. Essentially, therefore, the “—” entries in the rightmost column of Table 5.5 may actually be incorrect. Thus, the bracketed ΔH_{acid} value of $341 \text{ kcal}\cdot\text{mol}^{-1}$ does not necessarily mean that **4b** is not present.

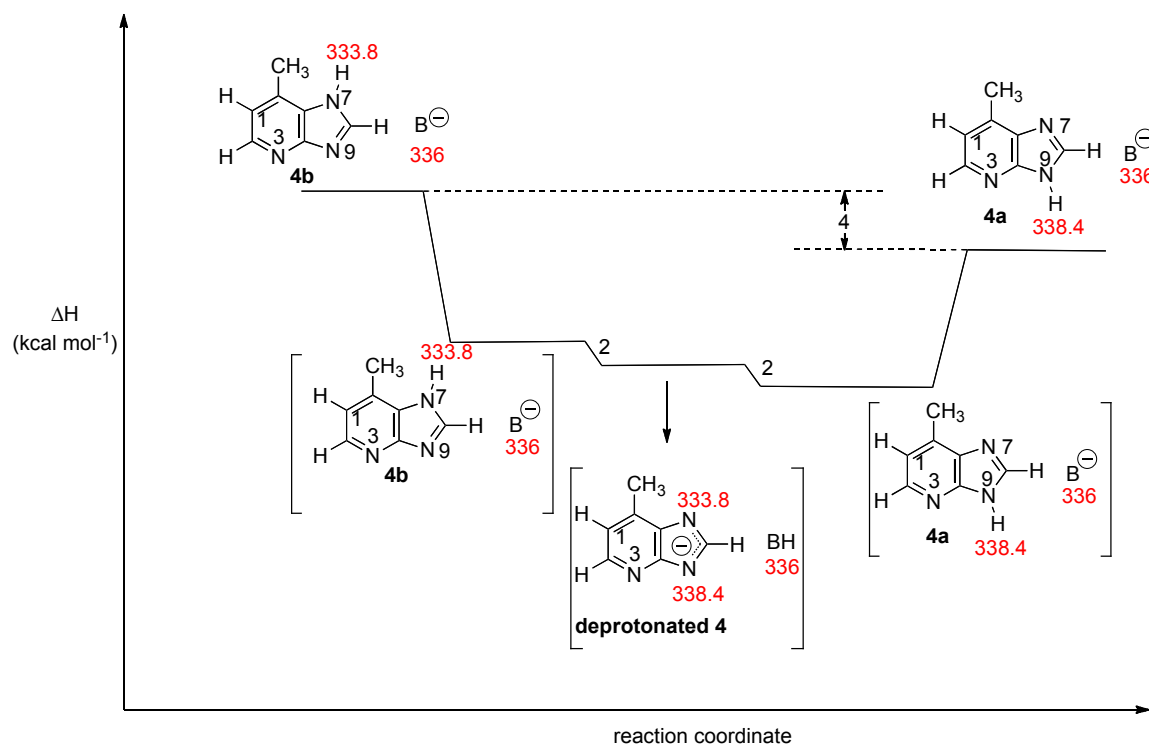


Figure 5.7 Reaction coordinate for the base-catalyzed tautomerization of **4b** to **4a**.

Values in red are B3LYP/6-31+G(d) calculated ΔH_{acid} values (298 K).

Given the wide range of proton transfer in both directions for the PA experiment (Table 5.6) and the ambiguity associated with knowing whether proton transfer occurred in the acidity experiment, we therefore believe that we most likely have a mixture of **4a** and **4b** present under our experimental conditions, with **4a** predominating.

5.5. Conclusions

The unknown thermochemical properties of four adenine analogues have been calculated and measured. Gas-phase measurements benchmark the calculations.

Chapter 6 Identification Of Key Species In the *In-vitro* DNA Transcription via HPLC-MS/MS

6.1. Introduction

In recent decades, it has been found that in bacteria, there are RNAs that are modified by nicotinamide adenine dinucleotide (NAD^+ or NADH , Figure 6.1) at 5' end.^{169,170} The adenosine in NAD^+ , in theory, can be used in transcription. Because the nicotinamide in this structure would block the addition of the structure onto RNA chain, NAD^+/NADH may only be used as an initiating nucleotide. In 2003, Huang reported that bacteriophage T7 RNA polymerase (RNAP) could initiate DNA transcription using NAD *in vitro*.¹⁷¹

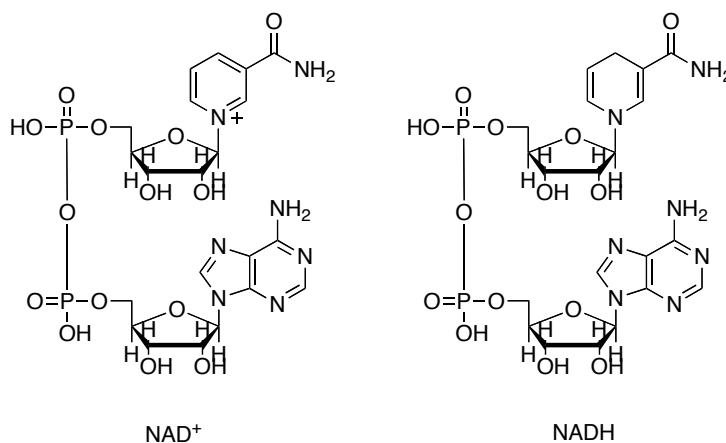


Figure 6.1 Chemical structure of nicotinamide adenine dinucleotide. Left: oxidized form; Right: reduced form.

Our collaborator Dr. Bryce Nickels believed that *E coli* RNAP, a RNAP bearing more hindered active site than T7 RNAP, could also initiate DNA transcription using NAD^+/NADH *in vitro*. Therefore, they carried out a set of *in vitro* experiments. (Table 6.1) They found that by mixing DNA template, *E coli* RNAP, radiolabeled NAD^+ , and

CTP under proper conditions, they found a new band in gel electrophoresis. In contrast, the mixtures in absence of NAD^+ , CTP or *E coli* RNAP showed no such band. They believe that a cytidine 5'-monophosphate was linked to NAD^+ , forming a short RNA sequence NAD^+pC . (Figure 6.2) The problem is how to prove the structure. Because NAD^+pC is neither commercially available nor fully characterized, no standard compound can be used to compare with that of the new band. In addition, the experiments were performed on micromole level, which means very limited amount of sample could be handled. They are searching for a method to analyze the key species in the reactions, hoping to extract the structure information that can support NAD^+pC .

Table 6.1 *in vitro* reactions to test the NAD^+ initiation hypothesis

Trial	DNA template	Reactants			Product New band in gel electrophoresis
		<i>E coli</i> RNAP	NAD^+	CTP	
1(exp.)	✓	✓	✓	✓	✓
2(ctrl.)	✓	✓	✓		
3(ctrl.)	✓	✓		✓	
4(ctrl.)	✓		✓	✓	

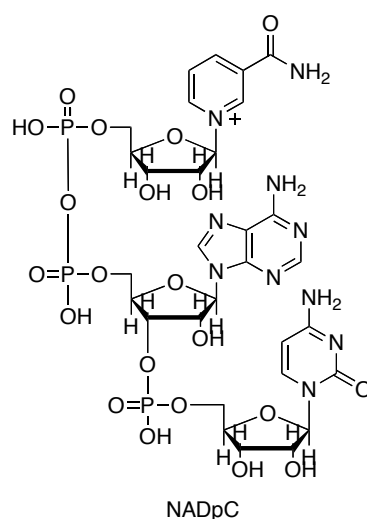


Figure 6.2 Chemical structure of NAD^+pC

Liquid chromatography–mass spectrometry (LC-MS) provides a powerful tool for analyzing the complicated systems. LC physically separates the components from the mixture and provides the characteristic retention time of each component. Mass spectrometry is widely used to analyze biomolecules. “Soft ionization” methods such as ESI and MALDI produce mass spectra with little or no fragment content, which identify the analyte by its mass-to-charge ratio. Due to the high degeneracy of molecular formula of large biomolecules, mass-to-charge ratio cannot be used as a single factor to identify the structure. The tandem mass spectrometry method produces the characteristic fragmentation pattern of the analyte, solving this problem.

In this project, we used a quadrupole ion trap mass spectrometer coupled with ESI to study the fragmentation pattern of NAD^+ and CTP, and developed a LC-MS method to separate and identify the species NAD^+ , CTP and possible NAD^+pC in the reaction mixtures.

6.2 Experimental section

6.2.1 experiment materials and instrumental specification

NAD^+ and cytidine triphosphate (CTP) were used as purchased. Ammonium hydroxide (28.0 to 30.0 w/w %) was purchased from Fisher. Ammonium formate (99%), water (HPLC grade) and methanol (HPLC grade) were purchased from Sigma-Aldrich. The in vitro NAD^+ initiated RNA transcription reaction mixture (experimental samples and control samples) were prepared by Dr. Jeremy Bird in our collaborator Dr. Bryce Nickels Lab.

Compound fragmentation patterns were generated using a Thermo Finnigan LTQ mass spectrometer. LC-UV analysis was performed using Waters 2695 HPLC with a

Waters 2996 photodiode array detector. LC-MS/MS analysis was performed using a Thermo Surveyor HPLC with a Thermo Finnigan LTQ mass spectrometer.

6.2.2 sample preparation protocol (from Dr. Jeremy Bird)

10 nM DNA template was mixed with 50 nM Core RNAP and 250 nM $\sigma 70$ in abortive initiation buffer (AIB) [10 mM Tris HCl pH 8.0, 40 mM KCl, 10 mM $MgCl_2$, 0.1 mM EDTA, 1 mM DTT, 0.1 mg/ml BSA, 2% glycerol] and incubated at 37°C for 15 min to form open complexes. 2 mM NAD^+ and 10 mM CTP were then mixed with the complexes. This mixture was incubated for 1 hour at 37°C to create NAD^+pC product and passed through a Nanosep Centrifugal Device. Control samples were prepared according to the same procedures but with CTP, NAD , or Core RNAP and $\sigma 70$ omitted, respectively. ***6.2.3 sample analysis protocol***

NAD^+ and CTP dissociation patterns were studied using Thermo Finnigan LTQ mass spectrometer. In this study, NAD^+ and CTP were dissolved in 1:1 mobile phase A: mobile phase B to make a 0.5×10^{-4} M solution and injected directly from ESI with flow rate 10 μ L/min. (Table 6.2) NAD^+ standard, CTP standard, and *in vitro* reaction samples were analyzed by 1) LC-UV and 2) LC-MS/MS. We used an YMC ODS-A s5 120Å column. The samples were separated using a LC method shown in Table 6.2.

Table 6.2 HPLC method used in separating samples

Mobile phase A: 5mM ammonium formate in water pH = 7.9
 Mobile phase B: MeOH
 Flow rate: 0.3mL/min
 Gradient:

	A/%	B/%
0min	100	0
5min	100	0
15min	30	70
23min	0	100
28min	0	100
28.1min	100	0
40min	100	0

The effluent was analyzed using 1) UV detector at 260 nm (data collected by MassLynx software) and 2) in-line mass spectrometry, which was equipped with an electrospray ionization interface (ESI). In MS detection, NAD⁺ and CTP standards were first tested using both positive and negative ionization modes. Negative ionization mode was finally chosen with MS/MS detection. Mass spectrometry analysis was carried out using selected reaction monitoring (SRM) mode with an isolation width set at 3 m/z. ESI-MS/MS conditions were optimized for the specific analytes. A typical condition is in Table 6.3. Data collection was performed by XCalibur software.

Table 6.3 Typical ESI-MS/MS condition used in this project

Capillary temperature	200 °C	Multipole 00 offset	1.5 V
Sheath gas flow	40	Multipole 0 offset	4.5 V
Aux gas flow	0	Gate lens offset	68 V
Source voltage	5k V	Multipole 1 offset	19 V
Capillary voltage	-49 V	Multipole RF amplitude	690 Vp-p
Tube lens	-108 V	Front lens	4.5 V

6.3 Results and discussion

6.3.1 Fragmentation of NAD^+ and CTP

Due to the possible difference in MS sensitivity for NAD^+ and CTP, we first tested NAD^+ and CTP in both positive and negative ionization modes. Table 6.3 summarizes the comparison of signal intensities for the two species. Both NAD^+ and CTP showed high sensitivity in negative mode, while NAD^+ was only visible in positive mode. Another possible species, also the desired product of the *in vitro* transcription reaction, is NAD^+pC . We assumed that the properties of NAD^+pC might be similar to that of NAD^+ . Therefore, in the later LC-MS/MS analysis, negative mode was applied for the analysis of NAD^+ , CTP and NAD^+pC .

Table 6.4 Intensities of NAD^+ and CTP in different ion modes

Sample	Ionization mode	Charge number	Ion intensity
NAD^+	negative	1	1.5×10^{-5}
	positive	1	2.5×10^{-5}
CTP	negative	1	1.6×10^{-5}
		2	1.6×10^{-5}
	positive	NA	$< 10^3$

The fragmentation patterns of NAD^+ in both ionization modes were studied. (Figure 6.3 and Figure 6.4) The loss of neutral nicotinamide is the major dissociation pathway.

Figure 6.5 shows the fragmentation pattern of $(CTP-H)^-$. Under CID, the loss of phosphoric acid is the major dissociation pathway that produces a negative-charge fragment of mass-to-charge ratio 384.

NAD_644_20% #1-10 RT: 0.01-0.22 AV: 10 NL: 2.36E5
T: + c Full ms2 664.00@cid20.00 [180.00-800.00]

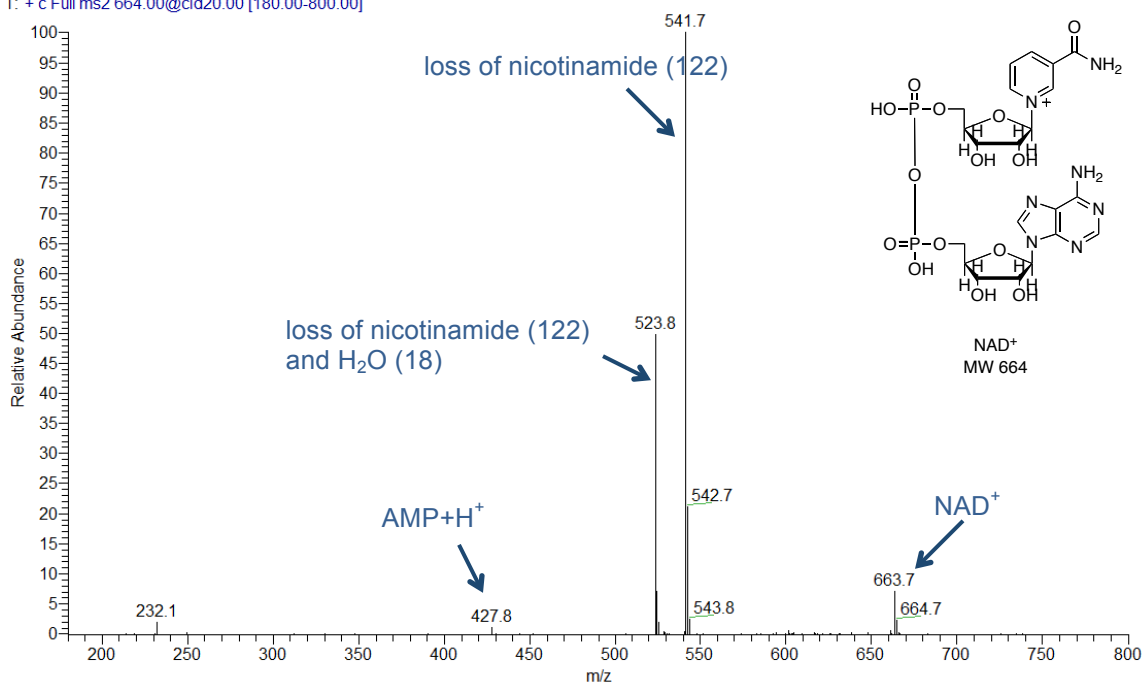


Figure 6.3 Fragmentation of NAD⁺ in positive mode.

nad neg662 w3 10% #3-10 RT: 0.01-0.04 AV: 8 NL: 1.48E5
T: ITMS - c ESI Full ms2 662.00@cid10.00 [130.00-1000.00]

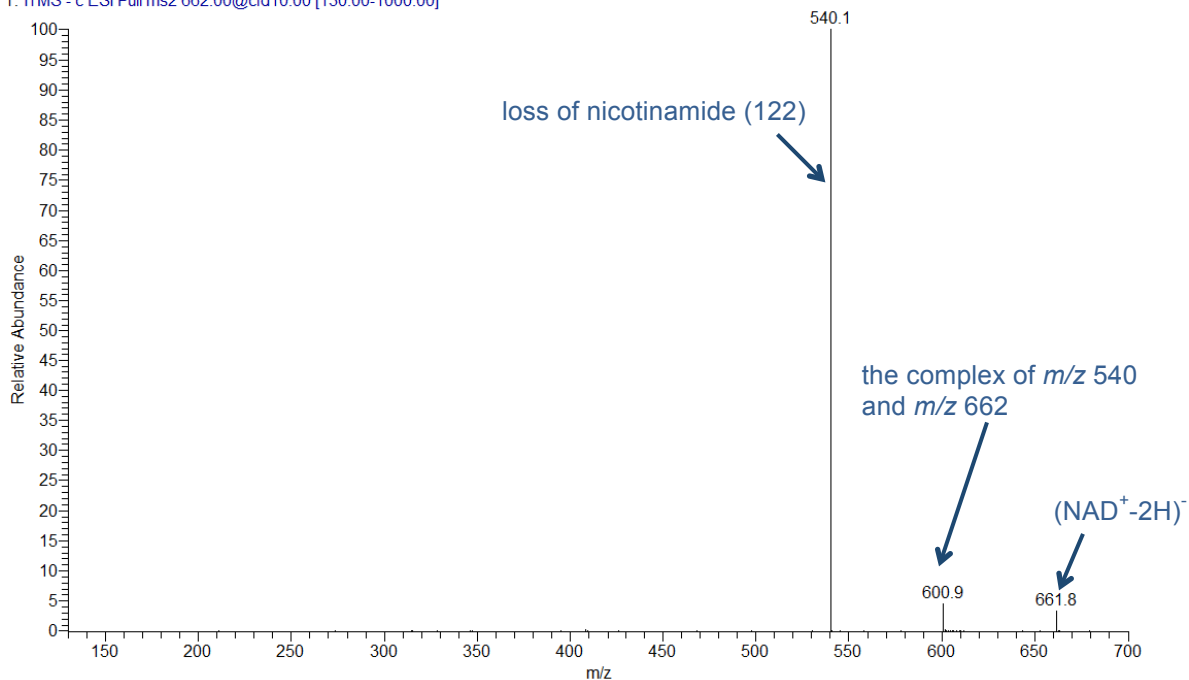


Figure 6.4 Fragmentation of (NAD⁺-2H)⁻ in negative mode.

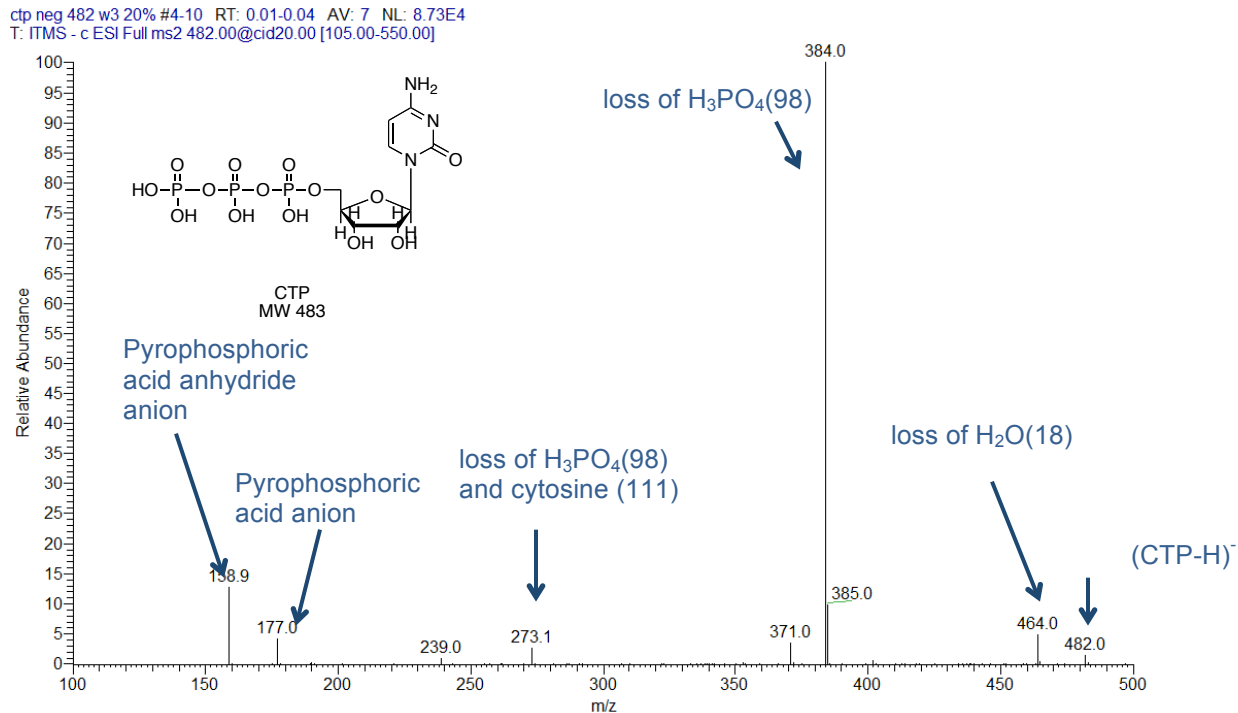


Figure 6.5 Fragmentation of (CTP-H)⁻ in positive mode

6.3.2 LC-UV analysis of CTP standard, NAD standard, and transcription reaction samples

The LC method was developed using NAD⁺ and CTP standards. Figure 6.6 shows the LC-UV chromatograms of NAD⁺ and CTP standards (1nmol injection, respectively). NAD⁺ elutes at 11.5 min, and CTP elutes at 1.6 min. Four samples were also analyzed using the same LC method. The samples were injected without dilution. The injection volume is 20uL (NAD⁺ 40 nmole, CTP 0.2 nmole) for each sample. Samples 1, 2 and 4 show NAD⁺ peak around 11 min. Samples 1, 3 and 4 show small CTP peak around 5 min. No clue of NAD⁺pC was found in the chromatograms. (Figure 6.7)

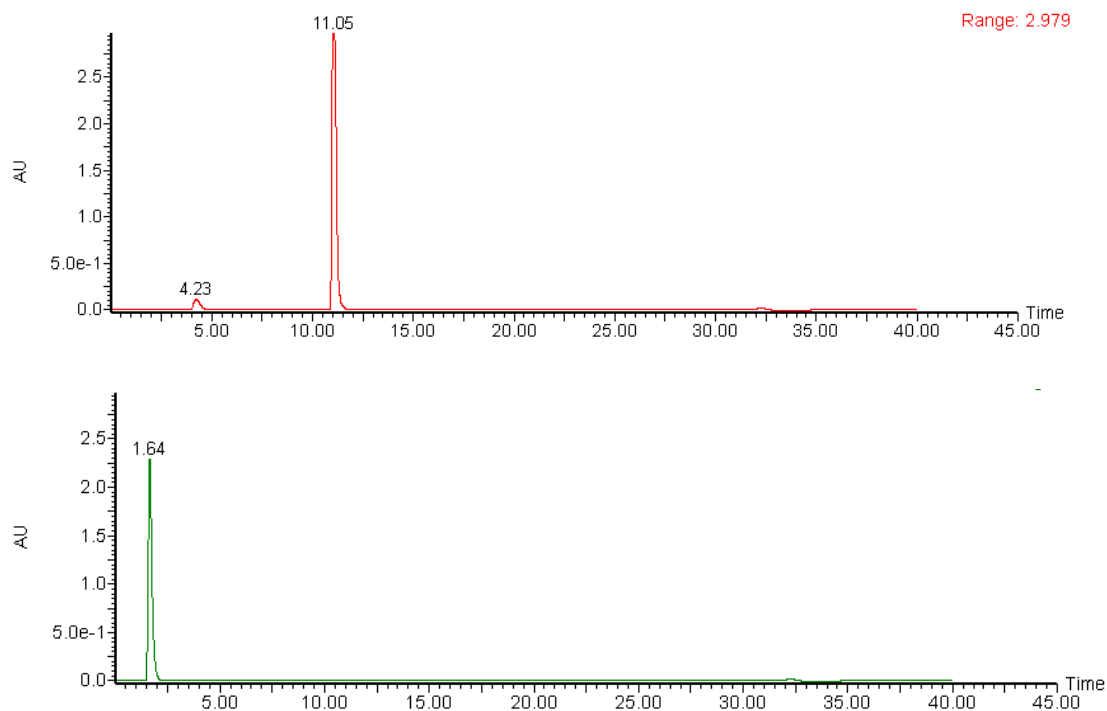


Figure 6.6 LC-UV chromatograms of NAD^+ (top) and CTP (bottom) standards.

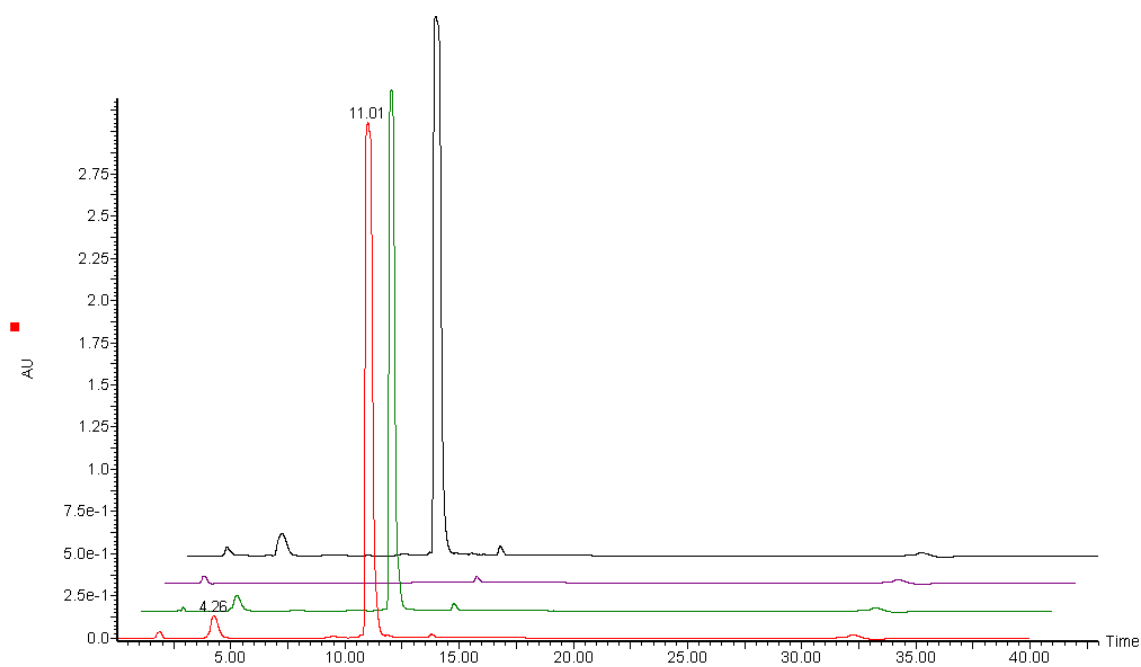


Figure 6.7 LC-UV chromatograms of four samples. Red: Sample 1. experimental; Green: Sample 2. control (no NAD^+); Purple: Sample 3. control (no CTP); Black: Sample 4. control (no RNA polymerase)

6.3.3 LC-MS/MS of CTP standard, NAD standard, and transcription reaction samples

A NAD⁺/CTP standards mixture was analyzed by LC-MS/MS to validate the LC-MS/MS method. According to the fragmentation analysis in 6.3.1, we decided to analyze 1) CTP by isolating the single charged anion m/z 482 and detecting its fragment m/z 384 under CID = 25% 2) NAD⁺ by isolating the single charged anion m/z 662 and detecting its fragment m/z 540 under CID = 20%. We searched for the possible NAD⁺pC by isolating the single charged anion m/z 967 (NAD⁺pC-2H⁺) and examine its fragmentation pattern under CID = 20%. In our condition, NAD⁺ elutes around 10.5 min and CTP elutes around 1.4 min, consistent to the LC-UV result. In NAD⁺ and CTP standards, no anion with m/z 967 was observed.

We also used different levels of injections to test the instrument sensitivity for our method. 40, 20, 10, 5 and 1 pmol of analysts (NAD⁺ or CTP, respectively) were injected. The 1 pmol injection of CTP has signal-to-noise ratio about 10-20, approaching to the detection limit. The 1 pmol injection of NAD⁺ had signal-to-noise ratio over 500. The injection vs peak area linearity is shown in Figure 6.8.

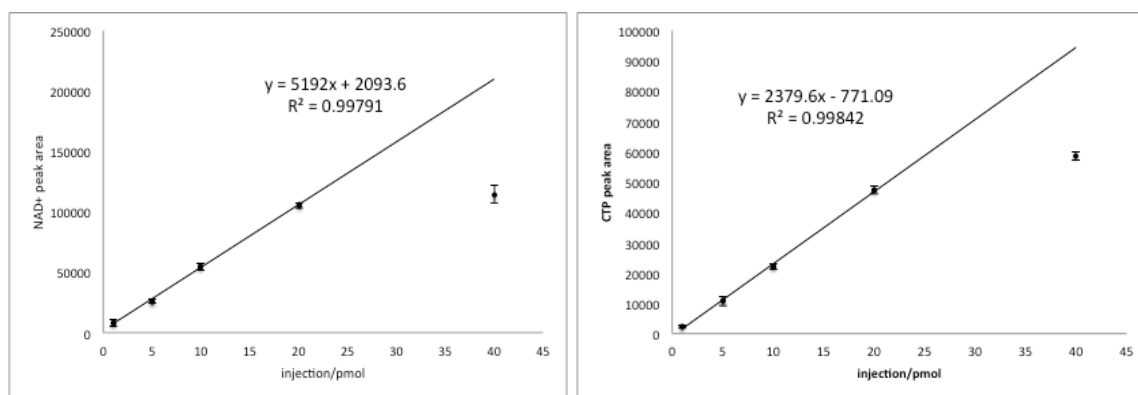


Figure 6.8 The injection vs. peak area linearity for NAD⁺ (left) and CTP (right). The trend lines were generated without the outlier (40 pmol injection).

Both NAD^+ and CTP have linear MS response from 1 to 20 pmol injection. The 40 pmol injection is off the line. It may be because of the saturation of instrument under high injection level, or the sample preparation error.

All four samples were $100\times$ diluted before injection. A peak of m/z 967 (NAD^+pC losing two protons) was detected in the Sample 1 (experimental) chromatogram, eluting at around 11 min, overlapped by the peak of NAD^+ . The full scan of its fragmentation is as shown in Figure 6.9. The major fragment m/z 845 may correspond to the loss of neutral nicotinamide. Minor fragments m/z 540 and m/z 662 also indicate the parent m/z 967 contains NAD^+ unit. Therefore we identified the structure corresponding to NAD^+pC peak by isolating m/z 967 and detecting its fragment m/z 845 under $\text{CID} = 20\%$ for all four samples. This peak did not appear in any of the control samples. Both the fragmentation pattern and chromatogram of m/z 967 support the NAD^+pC structure.

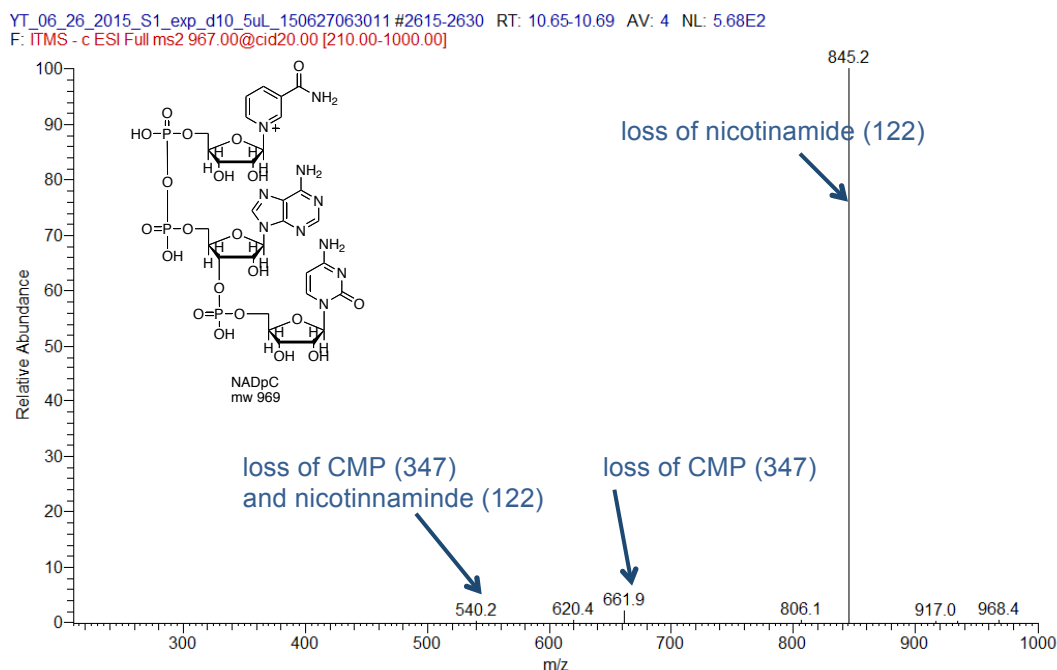


Figure 6.9 CID of m/z 967 detected in sample 1(experimental).

NAD^+ and CTP were also analyzed for all four samples. The typical chromatograms of 20uL injections are shown as Figure 6.10 to Figure 6.13. NAD^+ and CTP chromatograms also match the sample compositions. Notice that in Figure 6.12, there is a small NAD^+ peak in sample 3, (control, no NAD^+) of which the intensity is around only 100 counts. The intensity of NAD^+ peak in sample 3 is much lower than that in sample 1, 2 and 4, where NAD^+ was added. The appearance of NAD^+ peak in sample 3 might be due to the high concentration of NAD^+ in other samples that slightly contaminated the injection line.

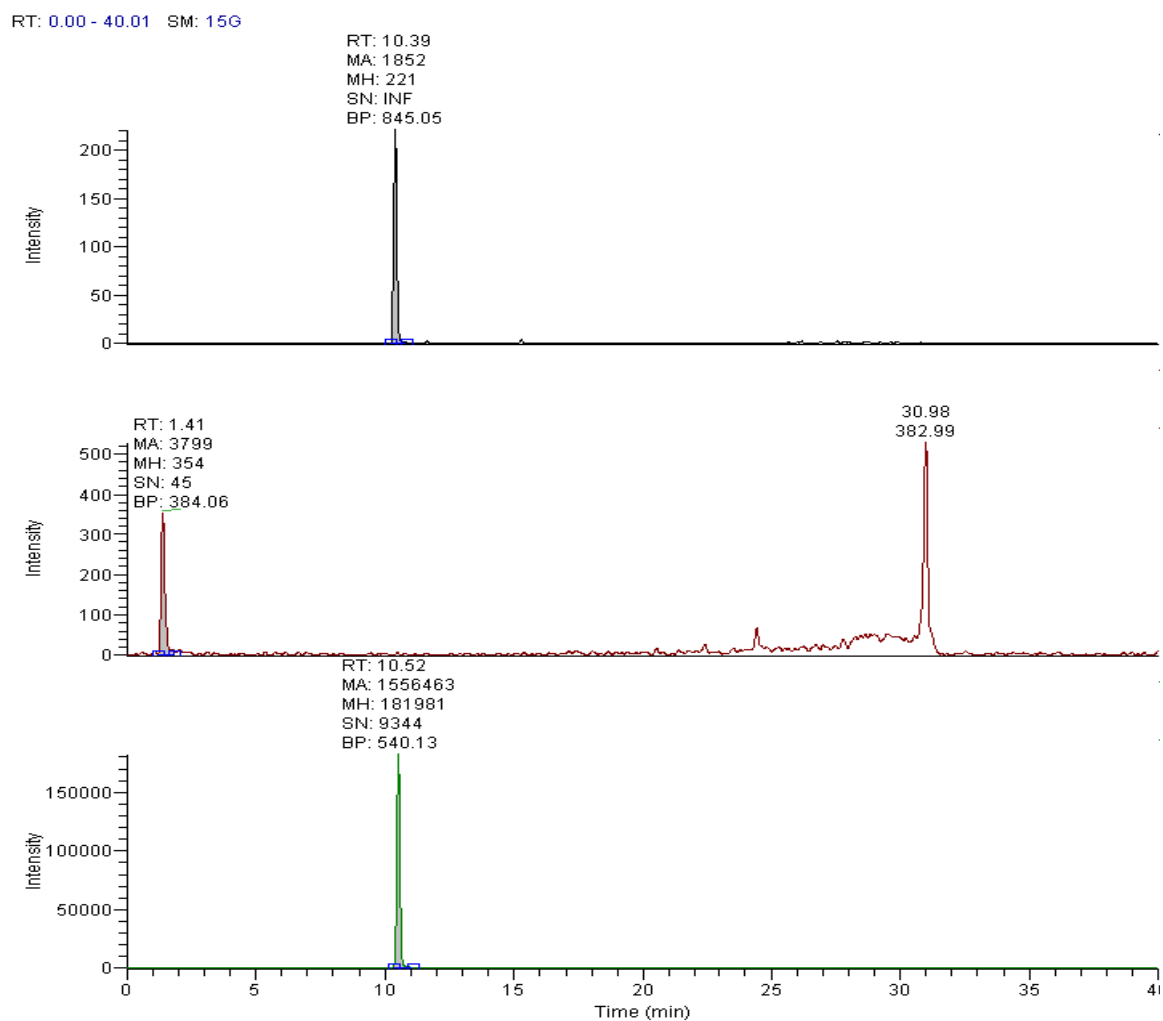


Figure 6.10 LC-MS/MS chromatograms of sample 1 (experimental). Top: analysis of NAD⁺pC, isolating m/z 967, detecting m/z 845; Middle: analysis of CTP, isolating m/z 482, detecting m/z 384; Bottom: analysis of NAD⁺pC, isolating m/z 662, detecting m/z

540

RT: 0.00 - 40.01 SM: 15G

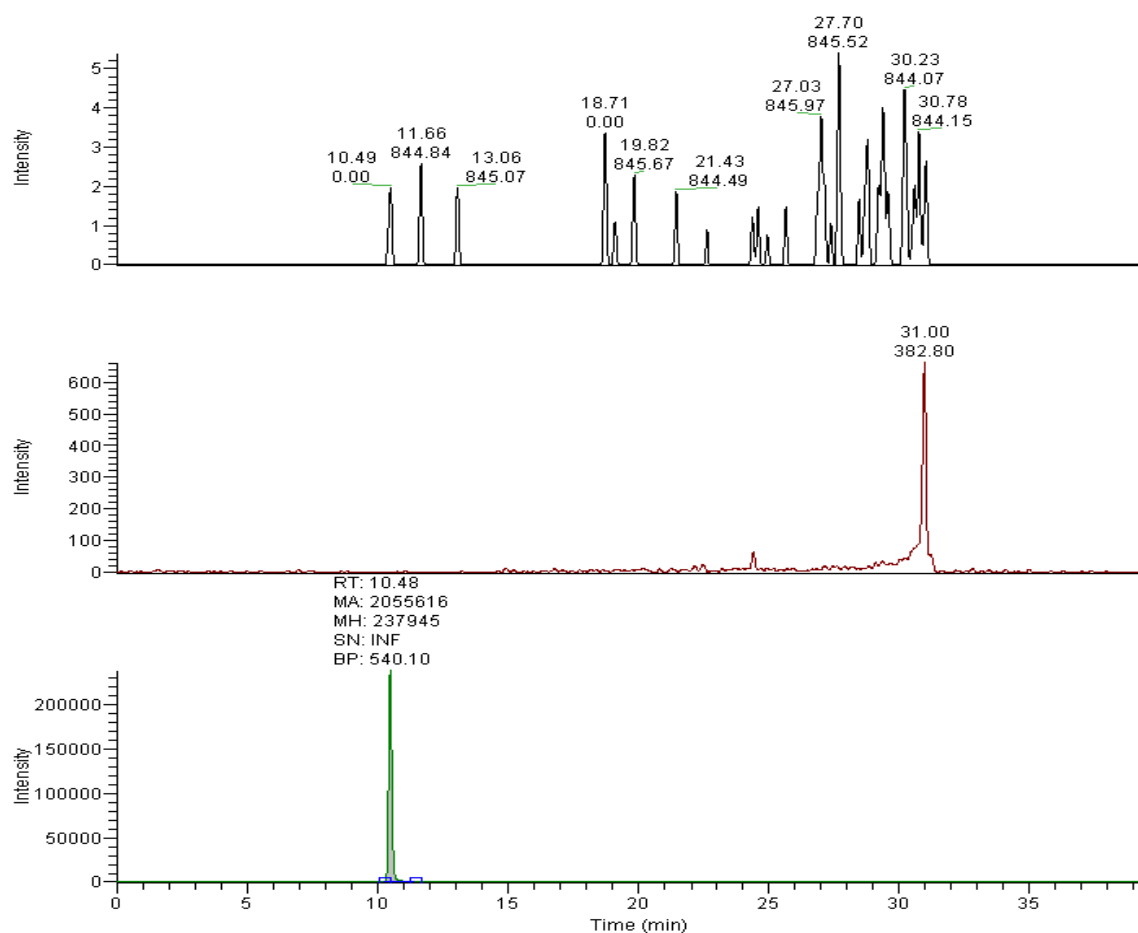


Figure 6.11 LC-MS/MS chromatograms of sample 2 (control, no CTP). Top: analysis of NAD^+pC , isolating m/z 967, detecting m/z 845; Middle: analysis of CTP, isolating m/z 482, detecting m/z 384; Bottom: analysis of NAD^+pC , isolating m/z 662, detecting m/z

540.

RT: 0.00 - 40.00 SM: 15G

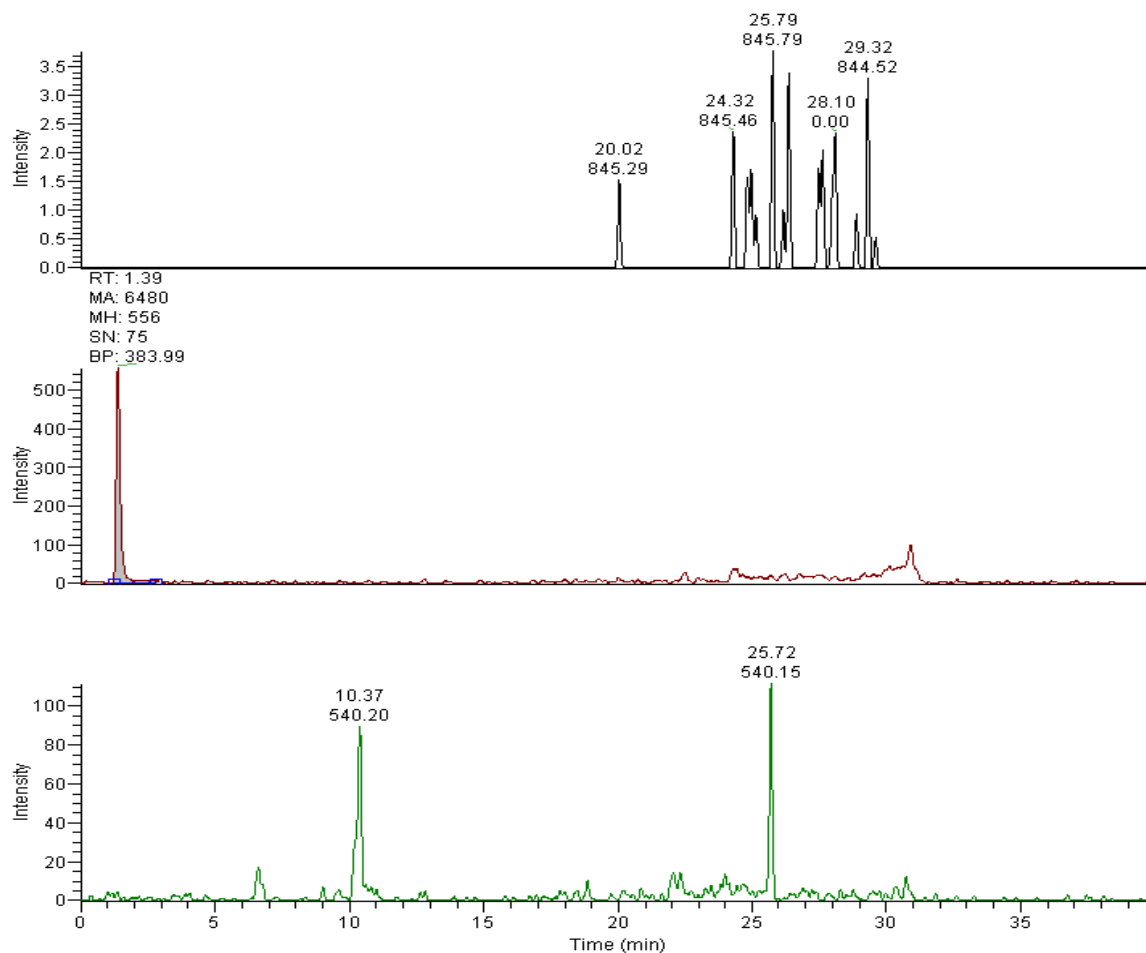


Figure 6.12 LC-MS/MS chromatograms of sample 3 (control, no NAD⁺). Top: analysis of NAD⁺pC, isolating m/z 967, detecting m/z 845; Middle: analysis of CTP, isolating m/z 482, detecting m/z 384; Bottom: analysis of NAD⁺pC, isolating m/z 662, detecting m/z 540.

RT: 0.00 - 40.01 SM: 15G

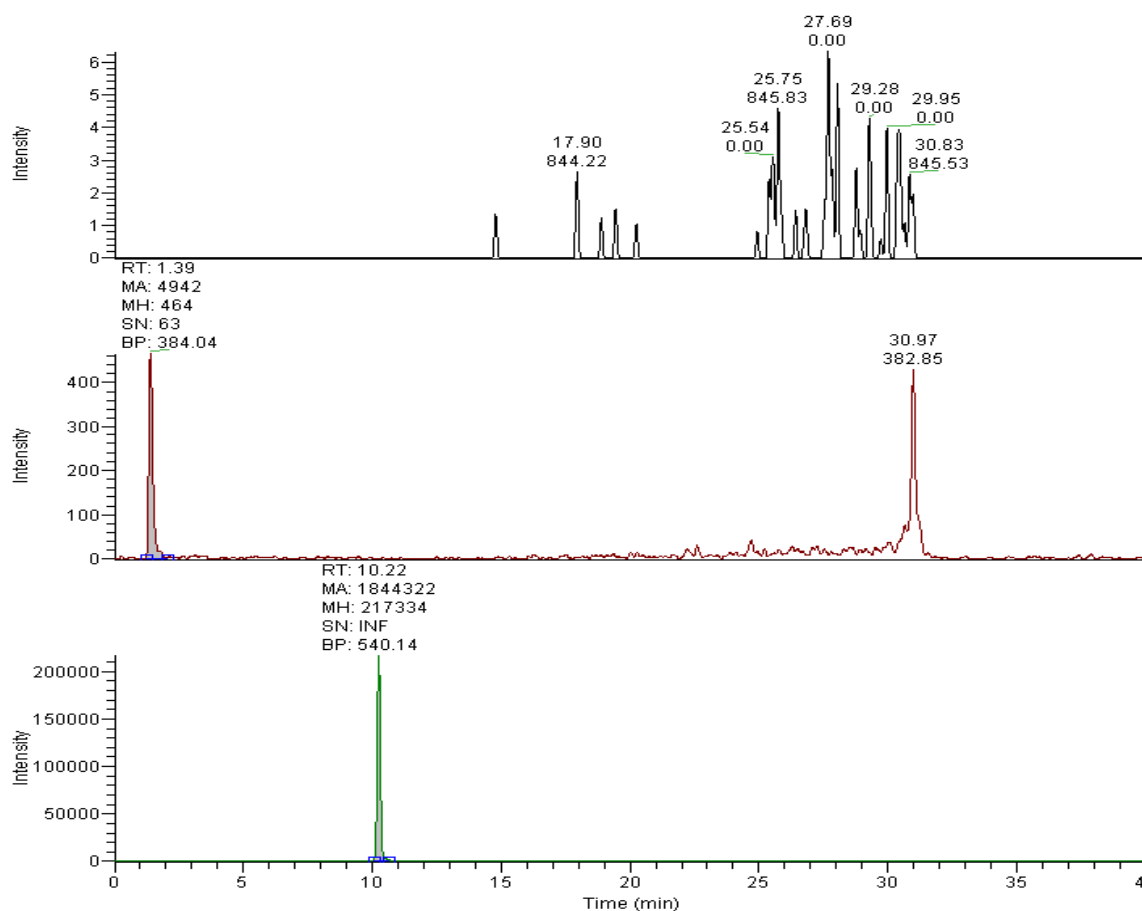


Figure 6.13 LC-MS/MS chromatograms of sample 4 (control, no RNA polymerase).

Top: analysis of NAD⁺pC, isolating m/z 967, detecting m/z 845; Middle: analysis of CTP, isolating m/z 482, detecting m/z 384; Bottom: analysis of NAD⁺pC, isolating m/z 662, detecting m/z 540.

6.4 Conclusion

A LC-ms/ms method was developed for analysis of key species in an in vitro transcription reaction mixture. The detection of m/z 967 in the experimental sample and its fragmentation pattern supports the NAD⁺pC structure, thus supports the hypothesis of NAD⁺ initiating DNA transcription catalyzed by *E. coli* RNA polymerase.

References

- (1) Moon, J. H.; Yoon, S.; Bae, Y. J.; Kim, M. S. *Mass Spectrom. Rev.* **2015**, 34, 94.
- (2) Palii, S. P.; John Wiley & Sons Ltd.: 2014, p 65.
- (3) Nibbering, N. M. M. *Int. J. Mass Spectrom.* **2015**, 377, 10.
- (4) Chen, C.-C.; Lin, P.-C. *Anal. Methods* **2015**, 7, 6947.
- (5) Richardson, D. E.; Plattner, D. A.; Elsevier Ltd.: 2007; Vol. 1, p 801.
- (6) Croft, N. P.; Purcell, A. W.; Tschärke, D. C. *Mol. Immunol.* **2015**, Ahead of Print.
- (7) Arduengo, A. J., III; Harlow, R. L.; Kline, M. J. *Am. Chem. Soc.* **1991**, 113, 361.
- (8) Hopkinson, M. N.; Richter, C.; Schedler, M.; Glorius, F. *Nature (London, U. K.)* **2014**, 510, 485.
- (9) Naumann, S.; Dove, A. P. *Polym. Chem.* **2015**, 6, 3185.
- (10) Lin, I. J. B.; Vasam, C. S. *Can. J. Chem.* **2005**, 83, 812.
- (11) **Jones, M. J. M., Robert A.** In *Reactive Intermediate Chemistry*; Moss, R. A. P., Matthew. S.; Jones, Maitland Jr., Ed.; Wiley: New York, 2004.
- (12) Haynes, M. T., II; Jackson, E. P.; Montgomery, J.; Wiley-VCH Verlag GmbH & Co. KGaA: 2014, p 371.
- (13) Hoyos, M.; Guest, D.; Navarro, O.; Wiley-VCH Verlag GmbH & Co. KGaA: 2014, p 85.
- (14) Lazreg, F.; Cazin, C. S. J.; Wiley-VCH Verlag GmbH & Co. KGaA: 2014, p 199.
- (15) Lazreg, F.; Cazin, C. S. J.; Wiley-VCH Verlag GmbH & Co. KGaA: 2014, p 173.
- (16) Patil, S. A.; Patil, S. A.; Patil, R.; Keri, R. S.; Budagumpi, S.; Balakrishna, G. R.; Tacke, M. *Future Med. Chem.* **2015**, 7, 1305.
- (17) Sen, S.; Schowner, R.; Buchmeiser, M. R. *Monatsh. Chem.* **2015**, 146, 1037.
- (18) Tsurusaki, A. *Yuki Gosei Kagaku Kyokaishi* **2015**, 73, 82.
- (19) Yetra, S. R.; Patra, A.; Biju, A. T. *Synthesis* **2015**, 47, 1357.
- (20) Cavallo, L.; Correa, A.; Costabile, C.; Jacobsen, H. J. *Organomet. Chem.* **2005**, 690, 5407.
- (21) Credendino, R.; Poater, A.; Ragone, F.; Cavallo, L. *Catal. Sci. Technol.* **2011**, 1, 1287.
- (22) Kumar, A.; Ghosh, P. *Eur. J. Inorg. Chem.* **2012**, 2012, 3955.
- (23) Fuerstner, A.; Ackermann, L.; Gabor, B.; Goddard, R.; Lehmann, C. W.; Mynott, R.; Stelzer, F.; Thiel, O. R. *Chem. - Eur. J.* **2001**, 7, 3236.
- (24) Scholl, M.; Trnka, T. M.; Morgan, J. P.; Grubbs, R. H. *Tetrahedron Lett.* **1999**, 40, 2247.
- (25) Vougioukalakis, G. C.; Grubbs, R. H. *Chem. Rev. (Washington, DC, U. S.)* **2010**, 110, 1746.
- (26) Grossmann, A.; Enders, D. *Angew. Chem., Int. Ed.* **2012**, 51, 314.
- (27) Holbrey, J. D.; Reichert, W. M.; Tkatchenko, I.; Bouajila, E.; Walter, O.; Tommasi, I.; Rogers, R. D. *Chem. Commun. (Cambridge, U. K.)* **2003**, 28.

- (28) Zhang, Y.; Chan, J. Y. G. *Energy Environ. Sci.* **2010**, *3*, 408.
- (29) Zhou, F.; Liang, Y.; Liu, W. *Chem. Soc. Rev.* **2009**, *38*, 2590.
- (30) Evans, K. O. *Colloids Surf., A* **2006**, *274*, 11.
- (31) Lindahl, T. *Proc. Natl. Acad. Sci. U. S. A.* **1974**, *71*, 3649.
- (32) Drohat, A. C.; Maiti, A. *Org. Biomol. Chem.* **2014**, *12*, 8367.
- (33) Prakash, A.; Doublié, S.; Wallace, S. S. *Prog. Mol. Biol. Transl. Sci.* **2012**, *110*, 71.
- (34) David, S. S.; Williams, S. D. *Chem. Rev. (Washington, D. C.)* **1998**, *98*, 1221.
- (35) Goldman, S. R.; Ebright, R. H.; Nickels, B. E. *Science (Washington, DC, U. S.)* **2009**, *324*, 927.
- (36) Kebarle, P.; Tang, L. *Analytical Chemistry* **1993**, *65*, 972A.
- (37) Chen, H.; Justes, D. R.; Cooks, R. G. *Org. Lett.* **2005**, *7*, 3949.
- (38) Bartmess, J. E.; Georgiadis, R. M. *Vacuum* **1983**, *33*, 149.
- (39) Barker, R. A.; Ridge, D. P. *J. Chem. Phys.* **1976**, *64*, 4411.
- (40) Miller, K. J.; Savchik, J. *J. Am. Chem. Soc.* **1979**, *101*, 7206.
- (41) Celli, F.; Weddle, G.; Ridge, D. P. *J. Chem. Phys.* **1980**, *73*, 801.
- (42) Su, T.; Chesnavich, W. J. *J. Chem. Phys.* **1982**, *76*, 5183.
- (43) Cooks, R. G.; Kruger, T. L. *J. Am. Chem. Soc.* **1977**, *99*, 1279.
- (44) Frisch, M. J. T., G. W.; Schlegel, H. B.; Scuseria, G. E.; Robb, M. A.; Cheeseman, J. R.; Scalmani, G.; Barone, V.; Mennucci, B.; Petersson, G. A.; Nakatsuji, H.; Caricato, M.; Li, X.; Hratchian, H. P.; Izmaylov, A. F.; Bloino, J.; Zheng, G.; Sonnenberg, J. L.; Hada, M.; Ehara, M.; Toyota, K.; Fukuda, R.; Hasegawa, J.; Ishida, M.; Nakajima, T.; Honda, Y.; Kitao, O.; Nakai, H.; Vreven, T.; Montgomery, J., J. A.; Peralta, J. E.; Ogliaro, F.; Bearpark, M.; Heyd, J. J.; Brothers, E.; Kudin, K. N.; Staroverov, V. N.; Kobayashi, R.; Normand, J.; Raghavachari, K.; Rendell, A.; Burant, J. C.; Iyengar, S. S.; Tomasi, J.; Cossi, M.; Rega, N.; Millam, J. M.; Klene, M.; Knox, J. E.; Cross, J. B.; Bakken, V.; Adamo, C.; Jaramillo, J.; Gomperts, R.; Stratmann, R. E.; Yazyev, O.; Austin, A. J.; Cammi, R.; Pomelli, C.; Ochterski, J. W.; Martin, R. L.; Morokuma, K.; Zakrzewski, V. G.; Voth, G. A.; Salvador, P.; Dannenberg, J. J.; Dapprich, S.; Daniels, A. D.; Farkas, Ö.; Foresman, J. B.; Ortiz, J. V.; Cioslowski, J.; Fox, D. J. In *Gaussian, Inc., Wallingford CT*, 2009.
- (45) Krokan, H. E.; Bjoraas, M. *Cold Spring Harbor Perspect. Biol.* **2013**, *5*, a012583/1.
- (46) Aidouni, A.; Bendahou, S.; Demonceau, A.; Delaude, L. *J. Comb. Chem.* **2008**, *10*, 886.
- (47) Archer, R. H.; Zones, S. I.; Davis, M. E. *Microporous Mesoporous Mater.* **2010**, *130*, 255.
- (48) Liu, M.; Chen, M.; Zhang, S.; Yang, I.; Buckley, B.; Lee, J. K. *J. Phys. Org. Chem.* **2011**, *24*, 929.
- (49) Seebach, D. *Angew. Chem. Int. Ed.* **1979**, *18*, 239.
- (50) Wohler, F.; Liebig, J. *Ann. Pharm.* **1832**, *3*, 249.
- (51) Ukai, T.; Tanaka, S.; Dokawa, S. *J. Pharm. Soc. Jpn.* **1943**, *63*, 296.
- (52) Lapworth, A. *J. Chem. Soc.* **1903**, *83*, 995.
- (53) Breslow, R. *J. Am. Chem. Soc.* **1958**, *80*, 3719.
- (54) Mizuhara, S.; Handler, P. *J. Am. Chem. Soc.* **1954**, *76*, 571.

- (55) Stetter, H. *Angewandte Chemie* **1976**, 88, 695.
- (56) Stetter, H.; Raemsch, R. Y.; Kuhlmann, H. *Synthesis* **1976**, 11, 733.
- (57) Stetter, H.; Kuhlmann, H. *Organic Reactions* **1991**, 40, 407.
- (58) Enders, D.; Breuer, K.; Teles, J. H. *Helv. Chim. Acta* **1996**, 79, 1217.
- (59) de Alaniz, J. R.; Rovis, T. *Synlett* **2009**, 8, 1189.
- (60) Christmann, M. *Angew. Chem. Int. Ed.* **2005**, 44, 2632.
- (61) Enders, D.; Niemeier, O.; Henseler, A. *Chem. Rev.* **2007**, 107, 5606.
- (62) Moore, J. L.; Rovis, T. *Top. Curr. Chem.* **2009**, 291, 77.
- (63) Enders, D.; Han, J.; Henseler, A. *Chem. Comm.* **2008**, 3989.
- (64) Liu, Q.; Perreault, S.; Rovis, T. *J. Am. Chem. Soc.* **2008**, 130, 14066.
- (65) DiRocco, D. A.; Oberg, K. M.; Dalton, D. M.; Rovis, T. *J. Am. Chem. Soc.* **2009**, 131, 10872.
- (66) Um, J. M.; DiRocco, D. A.; Noey, E. L.; Rovis, T.; Houk, K. N. *J. Am. Chem. Soc.* **2011**, 133, 11249.
- (67) DiRocco, D. A.; Rovis, T. *J. Am. Chem. Soc.* **2011**, 133, 10402.
- (68) DiRocco, D. A.; Noey, E. L.; Houk, K. N.; Rovis, T. *Angew. Chem. Int. Ed.* **2012**, 51, 2391.
- (69) Jousseau, T.; Wurz, N. E.; Glorius, F. *Angew. Chem. Int. Ed.* **2011**, 50, 1410.
- (70) Fang, X.; Chen, X.; Lv, H.; Chi, Y. R. *Angew. Chem. Int. Ed.* **2011**, 50, 11782.
- (71) Holmes, J. M.; Gravel, M. In *Comprehensive Organic Synthesis II*; Molander, G. A., Knochel, P., Eds.; Elsevier: 2014.
- (72) DiRocco, D. A.; Oberg, K. M.; Rovis, T. *J. Am. Chem. Soc.* **2012**, 134, 6143.
- (73) Berkessel, A.; Elfert, S.; Yatham, V. R.; Neudörfl, J.-M.; Schlrer, N. E.; Teles, J. H. *Angew. Chem. Int. Ed.* **2012**, 51, 12370.
- (74) Berkessel, A.; Elfert, S.; Etzenbach-Effers, K.; Teles, J. H. *Angew. Chem. Int. Ed.* **2010**, 49, 7120.
- (75) Maji, B.; Mayr, H. *Angew. Chem. Int. Ed.* **2012**, 51, 10408.
- (76) Maji, B.; Horn, M.; Mayr, H. *Angew. Chem. Int. Ed.* **2012**, 51, 6231.
- (77) Lemal, D. M.; Lovald, R. A.; Kawano, K. I. *J. Am. Chem. Soc.* **1964**, 86, 2518.
- (78) Chen, Y.-T.; Barletta, G. L.; Haghjoo, K.; Cheng, J. T.; Jordan, F. *J. Org. Chem.* **1994**, 59, 7714.
- (79) Castells, J.; Lopez-Calahorra, F.; Domingo, L. *J. Org. Chem.* **1988**, 53, 4433.
- (80) Castells, J.; Domingo, L.; Lopez-Calahorra, F.; Marti, J. *Tetrahedron Lett.* **1993**, 34, 517.
- (81) Chen, Y.-T.; Jordan, F. *J. Org. Chem.* **1991**, 56, 5029.
- (82) Castells, J.; Lopez-Calahorra, F.; Geijo, F.; Perez-Dolz, R.; Bassedas, M. *J. Heterocycl. Chem.* **1986**, 23, 715.
- (83) Breslow, R.; Kim, R. *Tetrahedron Lett.* **1994**, 35, 699.
- (84) Lopez-Calahorra, F.; Rubires, R. *Tetrahedron* **1995**, 51, 9713.
- (85) Breslow, R.; Schmuck, C. *Tetrahedron Lett.* **1996**, 37, 8241.

- (86) Ma, Y.; Wei, S.; Lan, J.; Wang, J.; Xie, R.; You, J. *J. Org. Chem.* **2008**, *73*, 8256.
- (87) Sakaki, S.; Musashi, Y.; Ohkubo, K. *J. Am. Chem. Soc.* **1993**, *115*, 1515.
- (88) van den Berg, H. J.; Challa, G. *J. Mol. Cat.* **1989**, *51*, 1.
- (89) Metzger, J.; Larive, H.; Dennilaule, R.; Baralle, R.; Gauret, C. *Bull. Soc. Chim. Fr.* **1964**, 2857.
- (90) Hawkes, K. J.; Yates, B. F. *Eur. J. Org. Chem.* **2008**, 5563.
- (91) Moore, J. L.; Silvestri, A. P.; Read de Alaniz, J.; DiRocco, D. A.; Rovis, T. *Org. Lett.* **2011**, *13*, 1742.
- (92) Collett, C. J.; Massey, R. S.; Maguire, O. R.; Batsanov, A. S.; O'Donoghue, A. C.; Smith, A. D. *Chem. Sci.* **2013**, *4*, 1514.
- (93) Mahatthananchai, J.; Bode, J. W. *Chem. Sci.* **2012**, *3*, 192.
- (94) Schrader, W.; Handayani, P. P.; Burstein, C.; Glorius, F. *Chem. Comm.* **2007**, 716.
- (95) Zeng, H.; Wang, K.; Tian, Y.; Niu, Y.; Greene, L.; Hu, Z.; Lee, J. K. *Int. J. Mass Spectrom.* **2014**, *369*, 92.
- (96) Picard, J. P.; Calas, R.; Dunogues, J.; Duffaut, N.; Gervai, J.; Lapouyade, P. *J. Org. Chem.* **2007**, *44*, 420.
- (97) Goldfuss, B.; Schumacher, M. *J. Mol. Model.* **2006**, *12*, 591.
- (98) Kemp, D. S. *J. Org. Chem.* **1971**, *36*, 202.
- (99) White, M. J.; Leeper, F. J. *J. Org. Chem.* **2001**, *66*, 5124.
- (100) , Gronert's mechanism also involved a spiroepoxide intermediate (formed from **2**).
- (101) Gronert, S. *Org. Lett.* **2007**, *9*, 3065.
- (102) Brook, A. G. *Acc. Chem. Res.* **1974**, *7*, 77.
- (103) Schinzer, D.; Heathcock, C. H. *Tetrahedron Lett.* **1981**, *22*, 1881.
- (104) Degl'Innocenti, A.; Ricci, A.; Mordini, A.; Reginato, G.; Colotta, V. *Gazz. Chim. Ital.* **1987**, *117*, 645.
- (105) Linghu, X.; Johnson, J. S. *Angew. Chem. Int. Ed.* **2003**, *42*, 2534.
- (106) Linghu, X.; Bausch, C. C.; Johnson, J. S. *J. Am. Chem. Soc.* **2005**, *127*, 1833.
- (107) Linghu, X.; Potnick, J. R.; Johnson, J. S. *J. Am. Chem. Soc.* **2004**, *126*, 3070.
- (108) Mattson, A. E.; Bharadwaj, A. R.; Scheidt, K. A. *J. Am. Chem. Soc.* **2004**, *126*, 2314.
- (109) Mattson, A. E.; Bharadwaj, A. R.; Zuhl, A. M.; Scheidt, K. A. *J. Org. Chem.* **2006**, *71*, 5715.
- (110) Squires, R. R.; DePuy, C. H. *Org. Mass Spectrom.* **1982**, *17*, 187.
- (111) DePuy, C. H.; Damrauer, R.; Bowie, J. H.; Sheldon, J. C. *Acc. Chem. Res.* **1987**, *20*, 127.
- (112) Gronert, S. *J. Am. Soc. Mass Spectrom.* **1998**, *9*, 845.
- (113) DePuy, C. H.; Bierbaum, V. M. *Acc. Chem. Res.* **1981**, *14*, 146.
- (114) Olmstead, W. N.; Brauman, J. I. *J. Am. Chem. Soc.* **1977**, *99*, 4219.
- (115) Gronert, S. *Chem. Rev.* **2001**, *101*, 329.
- (116) Holloczki, O.; Kelemen, Z.; Nyulaszi, L. *J. Org. Chem.* **2012**, *77*, 6014–6022.

- (117) Corberan, R.; Mas-Marza, E.; Peris, E. *Eur. J. Inorg. Chem.* **2009**, 1700.
- (118) Fortman, G. C.; Nolan, S. P. *Chem. Soc. Rev.* **2011**, 40, 5151.
- (119) Hahn, F. E.; Jahnke, M. C. *Angew. Chem., Int. Ed.* **2008**, 47, 3122.
- (120) Herrmann, W. A. *Angew. Chem., Int. Ed.* **2002**, 41, 1290.
- (121) Ingleson, M. J.; Layfield, R. A. *Chem. Commun. (Cambridge, U. K.)* **2012**, 48, 3579.
- (122) Benhamou, L.; Vujkovic, N.; Cesar, V.; Gornitzka, H.; Lugan, N.; Lavigne, G. *Organometallics* **2010**, 29, 2616.
- (123) Fuerstner, A.; Alcarazo, M.; Krause, H.; Lehmann, C. W. *J. Am. Chem. Soc.* **2007**, 129, 12676.
- (124) Khramov, D. M.; Rosen, E. L.; Er, J. A. V.; Vu, P. D.; Lynch, V. M.; Bielawski, C. W. *Tetrahedron* **2008**, 64, 6853.
- (125) Szadkowska, A.; Zukowska, K.; Pazio, A. E.; Wozniak, K.; Kadyrov, R.; Grela, K. *Organometallics* **2011**, 30, 1130.
- (126) Irie, M. *Chem. Rev. (Washington, D. C.)* **2000**, 100, 1683.
- (127) Fernandez-Acebes, A.; Lehn, J.-M. *Chem. - Eur. J.* **1999**, 5, 3285.
- (128) Irie, M. *Chem. Rev. (Washington, D. C.)* **2000**, 100, 1685.
- (129) Irie, M.; Sakemura, K.; Okinaka, M.; Uchida, K. *J. Org. Chem.* **1995**, 60, 8305.
- (130) Lee, S.; You, Y.; Ohkubo, K.; Fukuzumi, S.; Nam, W. *Chem. Sci.* **2014**, 5, 1463.
- (131) Tsuji, Y.; Hoffmann, R. *Angew. Chem., Int. Ed.* **2014**, 53, 4093.
- (132) Neilson, B. M.; Bielawski, C. W. *J. Am. Chem. Soc.* **2012**, 134, 12693.
- (133) Neilson, B. M.; Bielawski, C. W. *Chem. Commun. (Cambridge, U. K.)* **2013**, 49, 5453.
- (134) Neilson, B. M.; Bielawski, C. W. *Organometallics* **2013**, 32, 3121.
- (135) Becke, A. D. *J. Chem. Phys.* **1993**, 98, 5648.
- (136) Becke, A. D. *J. Chem. Phys.* **1993**, 98, 1372.
- (137) Kohn, W.; Becke, A. D.; Parr, R. G. *J. Phys. Chem.* **1996**, 100, 12974.
- (138) Lee, C.; Yang, W.; Parr, R. G. *Phys. Rev. B: Condens. Matter* **1988**, 37, 785.
- (139) Stephens, P. J.; Devlin, F. J.; Chabalowski, C. F.; Frisch, M. J. *J. Phys. Chem.* **1994**, 98, 11623.
- (140) Jain, R.; Bally, T.; Rablen, P. R. *J. Org. Chem.* **2009**, 74, 4017.
- (141) Lodewyk, M. W.; Siebert, M. R.; Tantillo, D. J. *Chem. Rev. (Washington, DC, U. S.)* **2012**, 112, 1839.
- (142) Lodewyk, M. W.; Soldi, C.; Jones, P. B.; Olmstead, M. M.; Rita, J.; Shaw, J. T.; Tantillo, D. J. *J. Am. Chem. Soc.* **2012**, 134, 18550.
- (143) Lodewyk, M. W.; Tantillo, D. J. *J. Nat. Prod.* **2011**, 74, 1339.
- (144) Rablen, P. R.; Pearlman, S. A.; Finkbiner, J. *J. Phys. Chem. A* **1999**, 103, 7357.
- (145) Ditchfield, R. *Mol. Phys.* **1974**, 27, 789.
- (146) Wolinski, K.; Hinton, J. F.; Pulay, P. *J. Am. Chem. Soc.* **1990**, 112, 8251.
- (147) Marenich, A. V.; Cramer, C. J.; Truhlar, D. G. *J. Phys. Chem. B* **2009**, 113, 6378.
- (148) Miertus, S.; Scrocco, E.; Tomasi, J. *Chem. Phys.* **1981**, 55, 117.

- (149) Pascual-Ahuir, J. L.; Silla, E.; Tunon, I. *J. Comput. Chem.* **1994**, *15*, 1127.
- (150) Shigenaga, M. K.; Park, J. W.; Cundy, K. C.; Gimeno, C. J.; Ames, B. N. *Methods Enzymol.* **1990**, *186*, 521.
- (151) Dizdaroglu, M. *Biochemistry* **1985**, *24*, 4476.
- (152) Burrows, C. J.; Muller, J. G. *Chem. Rev. (Washington, D. C.)* **1998**, *98*, 1109.
- (153) McAuley-Hecht, K. E.; Leonard, G. A.; Gibson, N. J.; Thomson, J. B.; Watson, W. P.; Hunter, W. N.; Brown, T. *Biochemistry* **1994**, *33*, 10266.
- (154) Michaels, M. L.; Miller, J. H. *J. Bacteriol.* **1992**, *174*, 6321.
- (155) Michaels, M. L.; Cruz, C.; Grollman, A. P.; Miller, J. H. *Proc. Natl. Acad. Sci. U. S. A.* **1992**, *89*, 7022.
- (156) Fromme, J. C.; Banerjee, A.; Huang, S. J.; Verdine, G. L. *Nature (London, U. K.)* **2004**, *427*, 652.
- (157) Lee, S.; Verdine, G. L. *Proc. Natl. Acad. Sci. U. S. A.* **2009**, *106*, 18497.
- (158) McCann, J. A. B.; Berti, P. J. *J. Am. Chem. Soc.* **2008**, *130*, 5789.
- (159) Chepanoske, C. L.; Langelier, C. R.; Chmiel, N. H.; David, S. S. *Org. Lett.* **2000**, *2*, 1341.
- (160) Francis, A. W.; Helquist, S. A.; Kool, E. T.; David, S. S. *J. Am. Chem. Soc.* **2003**, *125*, 16235.
- (161) Porello, S. L.; Williams, S. D.; Kuhn, H.; Michaels, M. L.; David, S. S. *J. Am. Chem. Soc.* **1996**, *118*, 10684.
- (162) **NIST Chemistry WebBook, NIST Standard Reference Database Number 69; retrieved in 2011. Linstrom, P. J.; Mallard, W. G., Eds.; National Institute of Standards and Technology: Gaithersburg, MD 20899, <http://webbook.nist.gov>.**
- (163) Eyet, N.; Villano, S. M.; Bierbaum, V. M. *Int. J. Mass Spectrom.* **2009**, *283*, 26.
- (164) Colominas, C.; Luque, F. J.; Orozco, M. *J. Am. Chem. Soc.* **1996**, *118*, 6811.
- (165) Plekan, O.; Feyer, V.; Richter, R.; Coreno, M.; Vall-Iloera, G.; Prince, K. C.; Trofimov, A. B.; Zaytseva, I. L.; Moskovskaya, T. E.; Gromov, E. V.; Schirmer, J. *J. Phys. Chem. A* **2009**, *113*, 9376.
- (166) Shukla, M. K.; Leszczynski, J. *Chem. Phys. Lett.* **2006**, *429*, 261.
- (167) Trygubenko, S. A.; Bogdan, T. V.; Rueda, M.; Orozco, M.; Luque, F. J.; Sponer, J.; Slavicek, P.; Hobza, P. *Phys. Chem. Chem. Phys.* **2002**, *4*, 4192.
- (168) Wolken, J. K.; Yao, C.; Turecek, F.; Polce, M. J.; Wesdemiotis, C. *Int. J. Mass Spectrom.* **2007**, *267*, 30.
- (169) Cahova, H.; Winz, M.-L.; Hoefer, K.; Nuebel, G.; Jaeschke, A. *Nature (London, U. K.)* **2015**, *519*, 374.
- (170) Chen, Y. G.; Kowtoniuk, W. E.; Agarwal, I.; Shen, Y.; Liu, D. R. *Nat. Chem. Biol.* **2009**, *5*, 879.
- (171) Huang, F. *Nucleic Acids Res.* **2003**, *31*, e8/1.



RightsLink®

Home

Create Account

Help



ACS Publications
Most Trusted. Most Cited. Most Read.

Title: Gas Phase Studies of N-Heterocyclic Carbene-Catalyzed Condensation Reactions
Author: Yuan Tian, Jeehiun K. Lee
Publication: The Journal of Organic Chemistry
Publisher: American Chemical Society
Date: Jun 1, 2015
Copyright © 2015, American Chemical Society

LOGIN
If you're a **copyright.com** user, you can login to RightsLink using your copyright.com credentials. Already a **RightsLink** user or want to [learn more?](#)

PERMISSION/LICENSE IS GRANTED FOR YOUR ORDER AT NO CHARGE

This type of permission/license, instead of the standard Terms & Conditions, is sent to you because no fee is being charged for your order. Please note the following:

- Permission is granted for your request in both print and electronic formats, and translations.
- If figures and/or tables were requested, they may be adapted or used in part.
- Please print this page for your records and send a copy of it to your publisher/graduate school.
- Appropriate credit for the requested material should be given as follows: "Reprinted (adapted) with permission from (COMPLETE REFERENCE CITATION). Copyright (YEAR) American Chemical Society." Insert appropriate information in place of the capitalized words.
- One-time permission is granted only for the use specified in your request. No additional uses are granted (such as derivative works or other editions). For any other uses, please submit a new request.

BACK

CLOSE WINDOW

Copyright © 2015 [Copyright Clearance Center, Inc.](#) All Rights Reserved. [Privacy statement](#). [Terms and Conditions](#). Comments? We would like to hear from you. E-mail us at customercare@copyright.com

**JOHN WILEY AND SONS LICENSE
TERMS AND CONDITIONS**

Sep 01, 2015

This Agreement between Yuan Tian ("You") and John Wiley and Sons ("John Wiley and Sons") consists of your license details and the terms and conditions provided by John Wiley and Sons and Copyright Clearance Center.

License Number	3700280867026
License date	Sep 01, 2015
Licensed Content Publisher	John Wiley and Sons
Licensed Content Publication	Angewandte Chemie International Edition
Licensed Content Title	An Isolable, Photoswitchable N-Heterocyclic Carbene: On-Demand Reversible Ammonia Activation
Licensed Content Author	Aaron J. Teator, Yuan Tian, Mu Chen, Jeehiun K. Lee, Christopher W. Bielawski
Licensed Content Date	Aug 14, 2015
Pages	1
Type of use	Dissertation/Thesis
Requestor type	Author of this Wiley article
Format	Print and electronic
Portion	Full article
Will you be translating?	Yes, including English rights
Number of languages	1
Languages	english
Title of your thesis / dissertation	THEORETICAL AND MASS SPECTROMETRIC STUDIES OF N-HETEROCYCLIC COMPOUNDS AND THEIR ROLES IN REACTIONS
Expected completion date	Sep 2015
Expected size (number of pages)	110
Requestor Location	Yuan Tian 5225 Deborah Dr PISCATAWAY, NJ 08854 United States Attn: Yuan Tian
Billing Type	Invoice
Billing Address	Yuan Tian 5225 Deborah Dr PISCATAWAY, NJ 08854



United States
Attn: Yuan Tian

Total

0.00 USD

[Terms and Conditions](#)

TERMS AND CONDITIONS

This copyrighted material is owned by or exclusively licensed to John Wiley & Sons, Inc. or one of its group companies (each a "Wiley Company") or handled on behalf of a society with which a Wiley Company has exclusive publishing rights in relation to a particular work (collectively "WILEY"). By clicking accept in connection with completing this licensing transaction, you agree that the following terms and conditions apply to this transaction (along with the billing and payment terms and conditions established by the Copyright Clearance Center Inc., ("CCC's Billing and Payment terms and conditions"), at the time that you opened your Rightslink account (these are available at any time at <http://myaccount.copyright.com>).

Terms and Conditions

- The materials you have requested permission to reproduce or reuse (the "Wiley Materials") are protected by copyright.
- You are hereby granted a personal, non-exclusive, non-sub licensable (on a stand-alone basis), non-transferable, worldwide, limited license to reproduce the Wiley Materials for the purpose specified in the licensing process. This license is for a one-time use only and limited to any maximum distribution number specified in the license. The first instance of republication or reuse granted by this licence must be completed within two years of the date of the grant of this licence (although copies prepared before the end date may be distributed thereafter). The Wiley Materials shall not be used in any other manner or for any other purpose, beyond what is granted in the license. Permission is granted subject to an appropriate acknowledgement given to the author, title of the material/book/journal and the publisher. You shall also duplicate the copyright notice that appears in the Wiley publication in your use of the Wiley Material. Permission is also granted on the understanding that nowhere in the text is a previously published source acknowledged for all or part of this Wiley Material. Any third party content is expressly excluded from this permission.
- With respect to the Wiley Materials, all rights are reserved. Except as expressly granted by the terms of the license, no part of the Wiley Materials may be copied, modified, adapted (except for minor reformatting required by the new Publication), translated, reproduced, transferred or distributed, in any form or by any means, and no derivative works may be made based on the Wiley Materials without the prior permission of the respective copyright owner. You may not alter, remove or suppress in any manner any copyright, trademark or other notices displayed by the Wiley Materials. You may not license, rent, sell, loan, lease, pledge, offer as security, transfer or assign the Wiley Materials on a stand-alone basis, or any of the rights granted to you hereunder to any other person.
- The Wiley Materials and all of the intellectual property rights therein shall at all times remain the exclusive property of John Wiley & Sons Inc, the Wiley Companies, or

their respective licensors, and your interest therein is only that of having possession of and the right to reproduce the Wiley Materials pursuant to Section 2 herein during the continuance of this Agreement. You agree that you own no right, title or interest in or to the Wiley Materials or any of the intellectual property rights therein. You shall have no rights hereunder other than the license as provided for above in Section 2. No right, license or interest to any trademark, trade name, service mark or other branding ("Marks") of WILEY or its licensors is granted hereunder, and you agree that you shall not assert any such right, license or interest with respect thereto.

- NEITHER WILEY NOR ITS LICENSORS MAKES ANY WARRANTY OR REPRESENTATION OF ANY KIND TO YOU OR ANY THIRD PARTY, EXPRESS, IMPLIED OR STATUTORY, WITH RESPECT TO THE MATERIALS OR THE ACCURACY OF ANY INFORMATION CONTAINED IN THE MATERIALS, INCLUDING, WITHOUT LIMITATION, ANY IMPLIED WARRANTY OF MERCHANTABILITY, ACCURACY, SATISFACTORY QUALITY, FITNESS FOR A PARTICULAR PURPOSE, USABILITY, INTEGRATION OR NON-INFRINGEMENT AND ALL SUCH WARRANTIES ARE HEREBY EXCLUDED BY WILEY AND ITS LICENSORS AND WAIVED BY YOU
- WILEY shall have the right to terminate this Agreement immediately upon breach of this Agreement by you.
- You shall indemnify, defend and hold harmless WILEY, its Licensors and their respective directors, officers, agents and employees, from and against any actual or threatened claims, demands, causes of action or proceedings arising from any breach of this Agreement by you.
- IN NO EVENT SHALL WILEY OR ITS LICENSORS BE LIABLE TO YOU OR ANY OTHER PARTY OR ANY OTHER PERSON OR ENTITY FOR ANY SPECIAL, CONSEQUENTIAL, INCIDENTAL, INDIRECT, EXEMPLARY OR PUNITIVE DAMAGES, HOWEVER CAUSED, ARISING OUT OF OR IN CONNECTION WITH THE DOWNLOADING, PROVISIONING, VIEWING OR USE OF THE MATERIALS REGARDLESS OF THE FORM OF ACTION, WHETHER FOR BREACH OF CONTRACT, BREACH OF WARRANTY, TORT, NEGLIGENCE, INFRINGEMENT OR OTHERWISE (INCLUDING, WITHOUT LIMITATION, DAMAGES BASED ON LOSS OF PROFITS, DATA, FILES, USE, BUSINESS OPPORTUNITY OR CLAIMS OF THIRD PARTIES), AND WHETHER OR NOT THE PARTY HAS BEEN ADVISED OF THE POSSIBILITY OF SUCH DAMAGES. THIS LIMITATION SHALL APPLY NOTWITHSTANDING ANY FAILURE OF ESSENTIAL PURPOSE OF ANY LIMITED REMEDY PROVIDED HEREIN.
- Should any provision of this Agreement be held by a court of competent jurisdiction to be illegal, invalid, or unenforceable, that provision shall be deemed amended to achieve as nearly as possible the same economic effect as the original provision, and the legality, validity and enforceability of the remaining provisions of this Agreement shall not be affected or impaired thereby.
- The failure of either party to enforce any term or condition of this Agreement shall not constitute a waiver of either party's right to enforce each and every term and condition

of this Agreement. No breach under this agreement shall be deemed waived or excused by either party unless such waiver or consent is in writing signed by the party granting such waiver or consent. The waiver by or consent of a party to a breach of any provision of this Agreement shall not operate or be construed as a waiver of or consent to any other or subsequent breach by such other party.

- This Agreement may not be assigned (including by operation of law or otherwise) by you without WILEY's prior written consent.
- Any fee required for this permission shall be non-refundable after thirty (30) days from receipt by the CCC.
- These terms and conditions together with CCC's Billing and Payment terms and conditions (which are incorporated herein) form the entire agreement between you and WILEY concerning this licensing transaction and (in the absence of fraud) supersedes all prior agreements and representations of the parties, oral or written. This Agreement may not be amended except in writing signed by both parties. This Agreement shall be binding upon and inure to the benefit of the parties' successors, legal representatives, and authorized assigns.
- In the event of any conflict between your obligations established by these terms and conditions and those established by CCC's Billing and Payment terms and conditions, these terms and conditions shall prevail.
- WILEY expressly reserves all rights not specifically granted in the combination of (i) the license details provided by you and accepted in the course of this licensing transaction, (ii) these terms and conditions and (iii) CCC's Billing and Payment terms and conditions.
- This Agreement will be void if the Type of Use, Format, Circulation, or Requestor Type was misrepresented during the licensing process.
- This Agreement shall be governed by and construed in accordance with the laws of the State of New York, USA, without regards to such state's conflict of law rules. Any legal action, suit or proceeding arising out of or relating to these Terms and Conditions or the breach thereof shall be instituted in a court of competent jurisdiction in New York County in the State of New York in the United States of America and each party hereby consents and submits to the personal jurisdiction of such court, waives any objection to venue in such court and consents to service of process by registered or certified mail, return receipt requested, at the last known address of such party.

WILEY OPEN ACCESS TERMS AND CONDITIONS

Wiley Publishes Open Access Articles in fully Open Access Journals and in Subscription journals offering Online Open. Although most of the fully Open Access journals publish open access articles under the terms of the Creative Commons Attribution (CC BY) License only, the subscription journals and a few of the Open Access Journals offer a choice of Creative Commons Licenses:: Creative Commons Attribution (CC-BY) license [Creative Commons Attribution Non-Commercial \(CC-BY-NC\) license](#) and [Creative Commons](#)

**JOHN WILEY AND SONS LICENSE
TERMS AND CONDITIONS**

Sep 01, 2015

This Agreement between Yuan Tian ("You") and John Wiley and Sons ("John Wiley and Sons") consists of your license details and the terms and conditions provided by John Wiley and Sons and Copyright Clearance Center.

License Number	3700280867026
License date	Sep 01, 2015
Licensed Content Publisher	John Wiley and Sons
Licensed Content Publication	Angewandte Chemie International Edition
Licensed Content Title	An Isolable, Photoswitchable N-Heterocyclic Carbene: On-Demand Reversible Ammonia Activation
Licensed Content Author	Aaron J. Teator, Yuan Tian, Mu Chen, Jeehiun K. Lee, Christopher W. Bielawski
Licensed Content Date	Aug 14, 2015
Pages	1
Type of use	Dissertation/Thesis
Requestor type	Author of this Wiley article
Format	Print and electronic
Portion	Full article
Will you be translating?	Yes, including English rights
Number of languages	1
Languages	english
Title of your thesis / dissertation	THEORETICAL AND MASS SPECTROMETRIC STUDIES OF N-HETEROCYCLIC COMPOUNDS AND THEIR ROLES IN REACTIONS
Expected completion date	Sep 2015
Expected size (number of pages)	110
Requestor Location	Yuan Tian 5225 Deborah Dr PISCATAWAY, NJ 08854 United States Attn: Yuan Tian
Billing Type	Invoice
Billing Address	Yuan Tian 5225 Deborah Dr PISCATAWAY, NJ 08854

copy, display and redistribute to colleagues Wiley Open Access articles, as well as adapt, translate, text- and data-mine the content subject to the following conditions:

- The authors' moral rights are not compromised. These rights include the right of "paternity" (also known as "attribution" - the right for the author to be identified as such) and "integrity" (the right for the author not to have the work altered in such a way that the author's reputation or integrity may be impugned).
- Where content in the article is identified as belonging to a third party, it is the obligation of the user to ensure that any reuse complies with the copyright policies of the owner of that content.
- If article content is copied, downloaded or otherwise reused for non-commercial research and education purposes, a link to the appropriate bibliographic citation (authors, journal, article title, volume, issue, page numbers, DOI and the link to the definitive published version on **Wiley Online Library**) should be maintained. Copyright notices and disclaimers must not be deleted.
- Any translations, for which a prior translation agreement with Wiley has not been agreed, must prominently display the statement: "This is an unofficial translation of an article that appeared in a Wiley publication. The publisher has not endorsed this translation."

Use by commercial "for-profit" organisations

Use of Wiley Open Access articles for commercial, promotional, or marketing purposes requires further explicit permission from Wiley and will be subject to a fee. Commercial purposes include:

- Copying or downloading of articles, or linking to such articles for further redistribution, sale or licensing;
- Copying, downloading or posting by a site or service that incorporates advertising with such content;
- The inclusion or incorporation of article content in other works or services (other than normal quotations with an appropriate citation) that is then available for sale or licensing, for a fee (for example, a compilation produced for marketing purposes, inclusion in a sales pack)
- Use of article content (other than normal quotations with appropriate citation) by for-profit organisations for promotional purposes
- Linking to article content in e-mails redistributed for promotional, marketing or educational purposes;
- Use for the purposes of monetary reward by means of sale, resale, licence, loan, transfer or other form of commercial exploitation such as marketing products
- Print reprints of Wiley Open Access articles can be purchased from:
corporatesales@wiley.com

Further details can be found on Wiley Online Library
<http://olabout.wiley.com/WileyCDA/Section/id-410895.html>

Other Terms and Conditions:

v1.9

Questions? customercare@copyright.com or +1-855-239-3415 (toll free in the US) or
+1-978-646-2777.



RightsLink®

[Home](#)
[Create Account](#)
[Help](#)


ACS Publications
Most Trusted. Most Cited. Most Read.

Title: Gas-Phase Studies of Substrates for the DNA Mismatch Repair Enzyme MutY

Author: Anna Zhachkina Michelson, Aleksandr Rozenberg, Yuan Tian, et al

Publication: Journal of the American Chemical Society

Publisher: American Chemical Society

Date: Dec 1, 2012

Copyright © 2012, American Chemical Society

LOGIN

If you're a **copyright.com user**, you can login to RightsLink using your copyright.com credentials. Already a **RightsLink user** or want to [learn more?](#)

PERMISSION/LICENSE IS GRANTED FOR YOUR ORDER AT NO CHARGE

This type of permission/license, instead of the standard Terms & Conditions, is sent to you because no fee is being charged for your order. Please note the following:

- Permission is granted for your request in both print and electronic formats, and translations.
- If figures and/or tables were requested, they may be adapted or used in part.
- Please print this page for your records and send a copy of it to your publisher/graduate school.
- Appropriate credit for the requested material should be given as follows: "Reprinted (adapted) with permission from (COMPLETE REFERENCE CITATION). Copyright (YEAR) American Chemical Society." Insert appropriate information in place of the capitalized words.
- One-time permission is granted only for the use specified in your request. No additional uses are granted (such as derivative works or other editions). For any other uses, please submit a new request.

[BACK](#)
[CLOSE WINDOW](#)

Copyright © 2015 [Copyright Clearance Center, Inc.](#) All Rights Reserved. [Privacy statement.](#) [Terms and Conditions.](#) Comments? We would like to hear from you. E-mail us at customercare@copyright.com